DEVELOPMENT OF ALPHA-ARBUTIN AND RESVERATROL-LOADED
DISSOLVING MICRONEEDLES FOR SKIN DEPIGMENTATION

By
Miss Nway Nway AUNG

A Thesis Submitted in Partial Fulfillment of the Requirements
for Doctor of Philosophy (PHARMACEUTICAL TECHNOLOGY)
INTERNATIONAL PROGRAM
Department of PHARMACEUTICAL TECHNOLOGY
Graduate School, Silpakorn University
Academic Year 2020
Copyright of Graduate School, Silpakorn University

การพัฒนาไมโครนีเดิลส์ชนิดละลายบรรจุแอลฟาอาร์บูติน
และเรสเวอราทรอลสำหรับการต้านจุดด่างดำของผิวหนัง

โดย
MissNway Nway Aung

DEVELOPMENT OF ALPHA-ARBUTIN AND RESVERATROL-LOADED DISSOLVING MICRONEEDLES FOR SKIN DEPIGMENTATION

By

Miss Nway Nway AUNG

A Thesis Submitted in Partial Fulfillment of the Requirements
for Doctor of Philosophy (PHARMACEUTICAL TECHNOLOGY)
INTERNATIONAL PROGRAM
Department of PHARMACEUTICAL TECHNOLOGY
Graduate School, Silpakorn University
Academic Year 2020
Copyright of Graduate School, Silpakorn University

Title	Development of alpha-arbutin and resveratrol-loaded dissolving microneedles for skin depigmentation
By	Nway Nway AUNG
Field of Study	(PHARMACEUTICAL TECHNOLOGY) INTERNATIONAL PROGRAM
Advisor	Professor PRANEET OPANASOPIT , Ph.D.

Graduate School Silpakorn University in Partial Fulfillment of the Requirements for the Doctor of Philosophy

....Dean of graduate school
(Associate Professor Jurairat Nunthanid, Ph.D.)

Approved by

....Chair person
(Assistant Professor Worranan Rangsimawong)

....Advisor
(Professor PRANEET OPANASOPIT , Ph.D.)

....Co advisor
(Associate Professor TANASAIT NGAWHIRUNPAT , Ph.D.)

....Co advisor
(Doctor Boonnada Pamornpathomkul , Ph.D.)

....Committee
(Associate Professor SUWANNEE PANOMSUK)
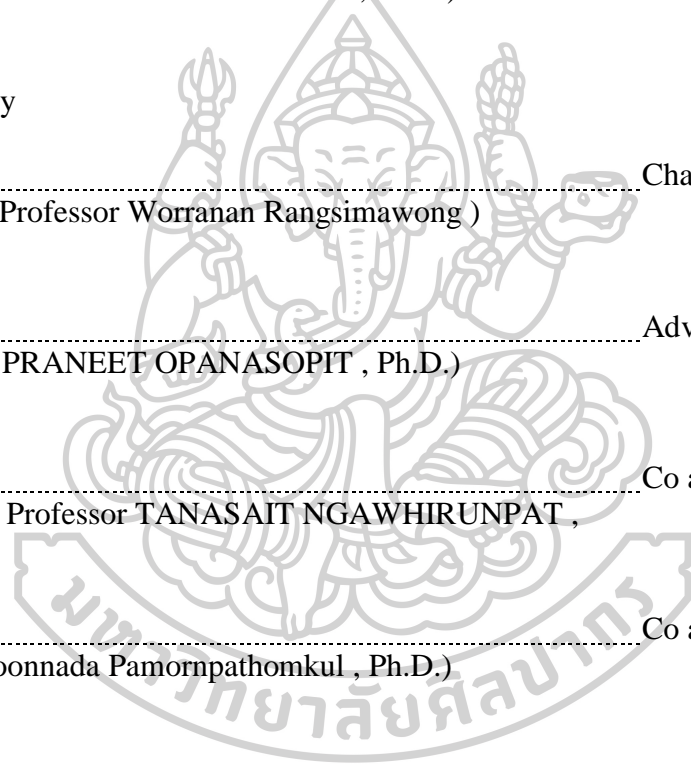
61353804 : Major (PHARMACEUTICAL TECHNOLOGY) INTERNATIONAL PROGRAM
Keyword : alpha-arbutin, resveratrol, dissolving microneedles, skin depigmentation, melanogenesis, inhibit tyrosinase

MISS NWAY NWAY AUNG : DEVELOPMENT OF ALPHA-ARBUTIN AND RESVERATROL-LOADED DISSOLVING MICRONEEDLES FOR SKIN DEPIGMENTATION THESIS ADVISOR : PROFESSOR PRANEET OPANASOPIT, Ph.D.

In this study, polymeric dissolving microneedles (DMNs) were developed to enhance the transdermal delivery of skin depigmentation agents into the melanocytes where melanin is synthesized. Alpha-arbutin (AA) is a well-known skin depigmentation agent due to its tyrosinase inhibition activity, whereas resveratrol (Res) possesses potent antioxidant and melanin inhibition activities. However, poor permeability of AA and poor solubility with chemical instability of Res limit their use in skin applications. Therefore, AA- and/or Res-loaded DMNs were prepared with HPMC/PVP-K90, PAMA/PVA, Eudragit E100/PVP-K90, Eudragit RS100/PVP-K90, and Eudragit RL100/PVP-K90 to overcome these issues. The results revealed that AA and/or Res were successfully incorporated into DMNs, which were characterized and evaluated in $vitro$ and in $vivo$. All needles of 8% AA-loaded DMNs, 5% Res-loaded DMNs, and 10% AA and 2% Res-loaded DMNs were dissolved entirely within 45 min, 30 min, and 15 min, respectively. In $vitro$ skin permeation of 8% AA-loaded HPMC/PVP-K90 DMNs and PAMA/PVA DMNs showed delivery of AA approximately 8.5 and 4.5 times compared with their gel formulations, whereas 3.7 and 2.8 times in comparison to commercial AA cream ($p<0.05$). In the case of 5% Res-loaded Eudragit E/PVP-K90 DMNs and Eudragit RS/PVP-K90 DMNs, Res permeation significantly increased about 3.4 and 3.8 folds compared to their gel formulations ($p<0.05$). The percentage of melanin contents after treatment of AA (2000 µg/mL) or Res (20 µg/mL) was significantly decreased as compared with control group ($p<0.01$). The best synergistic effect on melanogenesis was obtained at the weight ratio of AA and Res at 5:1 which represented the lowest CI value (0.58). Therefore, it was selected for fabricating 10% AA and 2% Res-loaded Eudragit RL/PVP-K90 DMNs. The high cumulative amount of AA (1265.93 µg/cm^2) and Res (45.24 µg/cm^2) was delivered at 24 h following the application of 10% AA and 2% Res-loaded DMNs compared to 10% AA and 2% Res combination cream (85.69 µg/cm^2 of AA delivered and 3.98 µg/cm^2 of Res delivered). In $vivo$ studies also indicated that AA- and/or Res-loaded DMNs provided more AA and/or Res into the mice's skin than commercial cream and combination cream. The mice's skin can reseal naturally without any damage after removing DMNs. Moreover, 10% AA and 2% Res-loaded DMNs remained highly stable in DMNs formulations at 25±2ºC, 60±5% RH for 6 months. In a clinical study, DMNs demonstrated the safety in human. Although using DMNs slightly decreased melanin index for skin depigmentation, there was no significant difference between before and after applied DMNs for 24 h. Accordingly, 10% AA and 2% Res-loaded DMNs were would be a promising platform for cosmetic applications.

ACKNOWLEDGEMENTS

Finally, I would like to give the greatest appreciation to my parents and my family for their understanding, encouragement, and supporting me spiritually throughout my life.

Nway Nway AUNG

TABLE OF CONTENTS

LIST OF TABLES

LIST OF FIGURES

Page

REFERENCES

LIST OF ABBREVIATIONS

%	percentage (s)
℃	degree Celsius
®	registered trademark
~	approximately
<	less than
>	more than
µL	microliter (s)
µm	micrometer (s)
µg	microgram (s)
v/v	volume by volume
w/w	weight by weight
×g	gravity at the Earth's surface
AA	alpha-arbutin
Al_2O_3	Alumina
ANOVA	analysis of variance
AU	arbitrary unit
cm^2	square centimeter
cm^3	cubic centimeter
$CaHPO_4$	calcium phosphate
$CaSO_4$	calcium sulphate
CMC	carboxy methyl cellulose

CO_2	carbon dioxide
COX-2	cyclooxygenase-2
DMEM	dulbecco's modified eagle medium
DMNs	dissolving microneedle (s)
DMSO	dimethyl sulfoxide
DNA	deoxyribonucleic acid
DOPA	3,4-dihydroxyphenylalanine
Eq.	equation
et al.	*et alia* (Latin abbreviation of " andohters", For references with more than two authors
Fa	fraction of effect
FBS	fetal bovine serum
g	gram (s)
h	hour (s)
HA	hyaluronic acid
HPMC	hydroypropyl methylcellulose
IC	inhibition concentration
kDa	kilodalton (s)
L	liter (s)
LE	loading efficiency
LC	loading capacity
min	minute (s)

MITF	microphthalmia transcription factor
mL	milliliter (s)
mRNA	messenger ribonucleic acid
MNs	microneedle (s)
MTT	3-(4,5-Dimethylthiazol-2-yl)-2,5-Diphenyltetrazolium Bromide
MW	molecular weight
nM	nanomolar (s)
NMH	normal human melanocytes
NO	nitric oxide
PAMA	poly(acrylic acid-co-maleic acid)
PBS	phosphate buffered saline
PC	polycarbonate
PCL	polycarprolactone
PGA	polyglycolic acid
PGD2	prostaglandin D2
PGE2	prostaglandin E2
pH	potentia hydrogenii (latin); power of hydrogen
PLA	polylactic acid
PMMA	poly(methylmethacrylate)
pOVA	plasmid ovalbumin
PVA	polyvinyl alcohol

PVP   polyvinylpyrrolidone

Res   Resveratrol

RH   relative humidity

rhGH   recombinant human growth hormone

ROS   reactive oxygen species

rpm   revolutions per minutes or rounds per min

RPMI-1640   Roswell Park Memorial Institute-1640

s   second

SEM   scanning electron microscope

SC   stratum corneum

SCCP   Scientific Committee on Consumer Products

SCCS   Scientific Committee on Consumer Safety

Sir2   silent information regulator 2

SIRT 1   sirtuin 1

TRP 1   tyrosinase-related protein 1

TRP 2   tyrosinase-related protein 2

UV   ultraviolet

ZrO_2 zirconium dioxide

CHAPTER 1

INTRODUCTION

1.1 Statement and significance of the research problem

Skin depigmentation is the lightening of the skin or loss of pigment, which is considered an essential cultural element in the female's beauty society because light skin is associated with privilege, beauty, and the belief that a fair-skinned person is more acceptable. Therefore, women engage in skin lightening to look beautiful, attractive, and increase self-confidence among persons. Nowadays, the prevalence of skin lightening products has increased tremendously among Asian women, and many cosmetic methods are used to obtain a lighter skin complexion. A skin depigmentation agent has drug-like benefits because it can be disturbed in the melanin-producing process of the skin (1). Excess production and accumulation of melanin level on the skin can induce hyperpigmentation disorders such as melasma, age spots, and solar lentigo (2). Besides, the variation in human skin color depends on the functional levels of melanin production (3). Melanin is a nitrogenous light-absorbing polymer that is produced and concentrated in melanosomes within melanocytes located in the basal layer of the skin. In addition, melanin contains pigment cells, which can be found in the hair, eyes, ears, and brain (4). The key enzyme involved in melanogenesis is tyrosinase, a copper containing transmembrane glycoprotein (5, 6). Tyrosinase catalyzes two processes in melanin biosynthesis, the hydroxylation of tyrosine to 3,4-dihydroxyphenylalanine (DOPA) and oxidation of DOPA to DOPA quinone (7, 8). Thus, tyrosinase inhibition has become the most common strategy for skin depigmentation products. Many cosmetic industries have been investigated as the best technology to achieve skin depigmentation using ascorbic acid, tranexamic acid, alpha-arbutin, resveratrol, niacinamide, and kojic acid (9).

Arbutin is a glycosylated hydroquinone moiety found in plants such as bearberry, mulberry, blueberry, and cranberry naturally; Arbutin exists in different forms, including a free, ether, or esterified form. It has been used as a skin-lightening agent for cosmetics in Japan since 1988 due to its diverse functions, including tyrosinase inhibition in melanogenesis and antioxidant (10). Two forms of arbutin, namely alpha-arbutin (4-hydroxyphenyl-α-d-glucopyranoside) and beta-arbutin (4-

hydroxyphenyl-β-d-glucopyranoside), have the same chemical formula structure, but different rotation configurations (11). Among them, alpha-arbutin has a greater affinity to inhibit the tyrosinase at the active site than beta-arbutin (12). Alpha-arbutin (AA) is a known tyrosinase inhibitor in keratinocytes because it has a similar structure to the substrate tyrosinase. AA inhibits tyrosinase activity by interacting with copper at the active site of the enzyme (13). Hence, AA has increased interest in the cosmetic industry due to the lack of significant adverse effects as a hydroquinone, alternative for external use in hyperpigmentation treatment (12). The Scientific Committee on Consumer Safety (SCCS) also confirmed that cosmetic products containing AA are safe for the consumer (14). However, AA has low percutaneous absorption and does not penetrate readily through the skin barrier, stratum corneum (SC), due to its hydrophilic nature. This result has become a limitation of its effective concentration penetrated the stratum basale, where the melanocyte occupies (15).

Resveratrol (3,5,4′-trihydroxy-trans-stilbene) is a natural stilbene and phenol produced by several plants such as grapes, red wine, berries, peanuts, and cocoa (4). Resveratrol has been reported to possess many biological activities such as antioxidation, anticancer, anti-aging, cardioprotection, antiviral, and depigmentation properties (4, 16-21). The antioxidant activity of resveratrol may affect melanogenesis by inhibiting their process in treating pigmentary skin disorders (22). Resveratrol (Res) exists in two isomeric forms, trans-resveratrol and cis-resveratrol. Trans-resveratrol has been observed as a bioactive material for human health when compared with cis-resveratrol. However, trans-resveratrol is highly unstable to UV light and rapidly isomerizes to cis-resveratrol (23, 24). Res contains two phenyl groups which consist of a weak acid and are linked together by a double bond. According to the functional group, Res possesses poor water solubility (25). Although the topical application of Res in skincare products has increased in popularity, Res has limitations such as poor solubility and chemical instability (26). To overcome these limitations, many researchers have been developed the new formulation of Res such as encapsulation, liposomes, nanoparticles, dendrimer nanotechnology, and microneedles (MNs) (24, 27-30).

Recently, a newly microneedle-based drug delivery system has been interested in the pharmaceutical field because MNs can deliver a wide range of molecules, which is

heavier than 500 Da to the skin bypass the SC in a non-invasive and pain-free manner (30). They have gained significant attention as an attractive system for improving the delivery of drugs, vaccines, macromolecules, and cosmetics across the skin barrier (31). MNs comprised micron-sized needles less than 2000 μm in length and are designed to pierce the SC for delivering the compounds into the skin for local or systemic administration (32, 33). MNs are categorized into five types: solid, hollow, coated, dissolving, and hydrogel-forming MNs based on their mechanisms (34, 35). Among them, dissolving MNs (DMNs) has become the most promising tool in current applications to enhance transdermal drug delivery (36). DMNs can control the release kinetics of drugs by adjusting the polymeric composition and modifying the MNs fabrication process (33). Another advantage of DMNs is that it reduces the drug administration process to one step. The DMNs can pierce the skin and are kept inserted until the complete dissolution without a medical professional is needed (37). DMNs are typically fabricated with polymeric materials that encapsulated the drug matrix and are designed to dissolve completely and release the drug when contacted with the skin interstitial fluid after an insertion. DMNs can be made of several materials, such as hyaluronic acid (HA), polyvinyl alcohol (PVA), polyvinylpyrrolidone (PVP), polycaprolactone (PCL), polylactic acid (PLA), polylactic-co-glycolic acid (PLGA), Gantrez® S-97, chitosan, carboxymethyl cellulose (CMC), Eudragit series, starch, and gelatin (38-47). Hydrophilic polymers including hydroxypropyl methylcellulose (HPMC), PVA, PVP-K90, poly(acrylic acid-co-maleic acid) (PAMA), and the hydrophobic property of Eudragit polymers (E100, RS 100, and RL 100) are selected to fabricate DMNs in this study. In the case of HPMC, HPMC is a synthetic modification of the natural polymer, soluble in water, and is widely used in oral, ophthalmic, and topical pharmaceutical formulations in which transdermal polymeric films containing HPMC was developed by many researchers for the delivery of drugs (48). PVA is a synthetic water-soluble polymer, biocompatible, and toxicologically safe employed in many pharmaceutical applications. PVA can also be used in drug-loaded DMNs fabrication by combining with other polymers to increase the hardness of the needles (39, 49). PAMA is used as a crosslinker to form hydrogen bonding with suitable polymers such as PVA due to its carboxylic group (50, 51). PVP-K90 is a non-ionic amorphous polymer widely used

in transdermal drug delivery systems due to the ability to dissolve in both water and oil. In addition, PVP-K90 did not induce skin irritation and sensitization (52). In the case of Eudragit series, Eudragit are the particular biodegradable copolymers obtained from the acrylic esters and methacrylic acid with different degrees of solubility, which depend on their functional groups (R). Different polymers were obtained to achieve the desired drug release profile with various series of Eudragit, such as Eudragit 100, Eudragit RS 100, and Eudragit RL 100 (53).

According to improve depigmentation, there is a synergistic effect on melanin inhibition between the antioxidant defense system and melanogenesis (54). Moreover, skin depigmentation agents are the best candidates for DMNs technology because DMNs can effectively deliver the active compounds to melanocytes where the melanin is synthesized (1). Therefore, this study aimed to develop polymeric DMNs incorporating AA and Res for transdermal drug delivery. For the first time, synergism effects of AA and Res on melanogenesis were investigated, and CompuSyn, a computer modeling software, was used to analyze synergistic activity. AA and Res-loaded DMNs were fabricated using micromolding technology and characterized for their morphology, mechanical strength, skin insertion, dissolution times, loading efficiency, and loading capacity. Afterward, the permeation of AA and Res into the skin was determined using the vertical Franz diffusion cell and animal model. *In vivo* skin resealing ability after removal of DMNs from the skin and stability of each formulation were also evaluated. Furthermore, the clinical assessment of skin melanin, skin erythema, transepidermal water loss (TEWL), skin hydration, skin elasticity, and safety were also evaluated in human volunteers.

1.2 Aims and objectives

1. To evaluate the depigmentation and synergistic inhibitory effects of alpha-arbutin and resveratrol on B16F10 melanoma cells.

2. To develop alpha-arbutin- and/or resveratrol-loaded DMNs for skin depigmentation.

3. To characterize the blank and drug-loaded DMNs for their morphology, mechanical strength, skin penetration, loading efficiency, loading capacity, *in vitro* dissolution times, *in vitro* skin permeation, and stability.

4. To evaluate the *in vivo* dissolution times, *in vivo* skin permeation, and skin resealing in mice.

5. To study the safety and efficacy of alpha-arbutin and resveratrol-loaded DMNs in human volunteers.

1.3 The research hypothesis

1. Alpha-arbutin and resveratrol have a synergistic role in melanin inhibition in B16F10 melanoma cells induced with alpha-melanocyte-stimulating hormone (α-MSH).

2. Alpha-arbutin and/or resveratrol can be loaded into the biodegradable polymers during the fabrication of DMNs.

3. DMNs reveal good appearances and mechanical strengths that can insert into the skin, high loading efficiency, and high loading capacity. In addition, different biodegradable polymers used have influenced the *in vitro* dissolution times and *in vitro* skin permeation of alpha-arbutin and resveratrol.

4. DMNs enhanced the *in vivo* permeation of alpha-arbutin and resveratrol in mice. Moreover, mice's skin can be resealed after the application of DMNs.

5. Alpha-arbutin- and/or resveratrol-loaded DMNs are physically and chemically stable at 5±3°C and 25±2°C with 60±5% RH for 6 months.

CHAPTER 2
LITERATURE REVIEW

2.1 Skin depigmentation

Skin pigmentation means coloring the skin and obtaining its color from a natural pigment cell called melanin. Melanin is synthesized by melanocytes, highly branched dendritic cells, found in the basal epidermis (4). Melanin can be found in the skin, eyes, hair, ears, and its role is to protect the skin damage from ultraviolet radiation (UVR) (55). Skin pigmentation disorders of the skin such as melasma, freckles, solar lentigo, and age spots depend on the over-production and accumulation of melanin (7). The melanogenesis pathway is mainly enhanced by the activation of the critical enzyme called tyrosinase. Tyrosinase is a copper-containing transmembrane glycoprotein enzyme that catalyzes the hydroxylation of the tyrosine to the 3,4-dihydroxyphenylalanine (DOPA) in the first step in melanin synthesis, which is subsequently oxidized into DOPA quinone (4, 8). The products of the melanin synthesis pathway are separated into two basic forms of melanin, including eumelanin (brown or black insoluble) and pheomelanin (red and yellow soluble), as shown in Figure 1 (7, 8, 56). The skin pigmentation changes can be designated into depigmentation (loss of pigment), hypopigmentation (abnormally low amount of melanin), and hyperpigmentation (abnormally high amount of melanin). Several depigmentation agents are currently being researched and used for ages in Asian countries to lighten the skin tone (11). Therefore, the inhibition of the tyrosinase enzyme in melanin production has become the most common target for skin depigmentation.
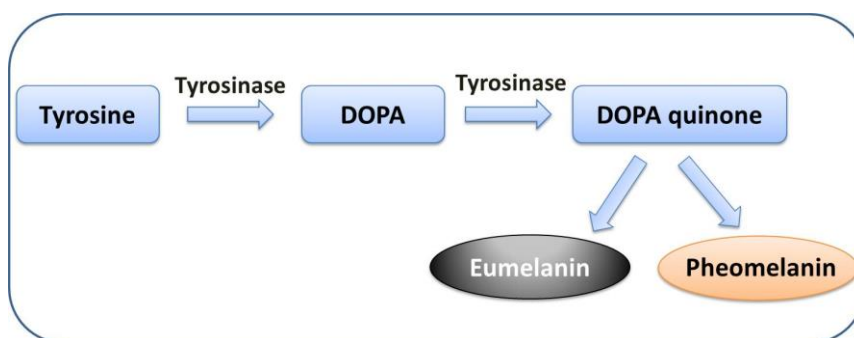
Figure 1. Synthesis of melanin (57)

2.1.1 Mechanism of depigmentation agents

The depigmentation agents exert their effects by regulating melanin synthesis through several mechanisms. The different mechanisms of action of depigmentation agents are (1) inhibition of tyrosinase transcription, (2) inhibition of tyrosinase activity, (3) inhibition of tyrosinase glycosylation, (4) inhibition of plasmin, (5) regulation of tyrosinase degradation, (6) inhibition of melanosome transfer, and (7) acceleration of epidermal turnover and desquamation (7, 8).

2.1.1.1 Inhibition of tyrosinase transcription

The transcription level is the first step of melanin synthesis in which tyrosinase and related melanogenic enzymes such as tyrosinase-related protein 1 (TYRP1) and tyrosinase-related protein 2 (TYRP2) modulated. In this process, the microphthalmia-associated transcription factor (MITF) plays a crucial role in controlling the transcription of tyrosinase, both melanocyte proliferation and melanogenesis (7).

2.1.1.2 Inhibition of tyrosinase activity

In the synthesis of melanin, tyrosinase plays as a rate-limiting enzyme, catalyzing the hydroxylation of amino acid tyrosine to DOPA and oxidation of DOPA to DOPA quinone. In humans, DOPA quinone is converted by a series of complex reactions to melanin formation. Therefore, inhibition of enzyme activity by tyrosinase inhibitors is an essential effort for treating pigmentation (8).

2.1.1.3 Inhibition of tyrosinase glycosylation

A major post-translational modification of melanogenic enzymes is glycosylation by attaching the N-linked glycans of an asparagine residue (N-glycosylation). It is a critical step for the proper maturation of tyrosinase. Therefore, inhibition of N-glycan in the process of melanogenesis enzyme can result in improper polypeptide folding, which inhibits melanogenesis (7).

2.1.1.4 Inhibition of plasmin

The melanin synthesis can activate by an intracellular release of arachidonic acid, a precursor of prostanoid and α-MSH. The level of these two substances is increased as a result of plasma activity. Therefore, the anti-plasmin of tranexamic acid is considered as the main mechanical for depigmentation effect (58).

2.1.1.5 Regulation of tyrosinase degradation

The tyrosinase degradations via the physiologic proteasome leading to alteration of tyrosinase protein content in hyperactive melanocytes. The fatty acid can influence the enzyme's degradation by regulating the target tyrosinase (7, 59).

2.1.1.6 Inhibition of melanosome transfer

Melanosome is a specialized subcellular organelle that produced pigment granules called melanin. The transfer of mature melanosomes from the melanocyte dendrites to surrounding keratinocytes is one of the skin pigmentation mechanisms. Once the melanosome reaches the keratinocyte, the organelles are moved to cover the top of the nucleus to prevent harmful sunlight from enhancing mutations in DNA, leading to skin cancer. Therefore, melanosome transfer is essential for visible pigmentation and photoprotection (4).

2.1.1.7 Acceleration of epidermal turnover and desquamation

Some chemical agents such as linoleic acid and salicylic acid can exfoliate the skin by accelerating epidermal layers' turnover and removing the uppermost layer of keratinocytes containing melanin (7, 8).

2.1.2 Classification of depigmentation agents

Nowadays, a variety of depigmentation agents are used to inhibit melanin synthesis. The depigmentation agents are classified based on their mechanisms of action as listed in Table 1 (56, 59, 60).

Table 1. Classification of depigmentation agents based on their mechanism of actions (6, 59)

Stages of melanogenesis	Mechanism of action	Active compounds
Before melanin synthesis	(a) Tyrosinase transcription	Tretinoin, C_2-ceramide, Glucosamine, N-acetyl glucosamine
	(b) Tyrosinase glycosylation	Calcium D-pantethenin-S-sulphate ($PaSSO_3Ca$)
	(c) Inhibition of plasmin	Tranexamic acid
During melanin synthesis	(a) Tyrosinase inhibition	Hydroquinone, Arbutin, Kojic acid, Azelaic acid, N-acetyl-4-s-cysteaminylphenol (NCPA), Resveratrol, Gentisic acid, 4-n butyl resorcinol, Aloesin, Hydroxystilbene, Licorice extract
	(b) Tyrosinase reduction	Ceramide, Lysophosphatidic acid, Sphingosine-1-phosphate
	(c) Reactive oxygen species (ROS) scavengers antioxidants	Ascorbic acid, α-tocopherol, Thioctic acid, Resveratrol, 6-Hydroxy-3,4-dihydrocoumarin
After melanin synthesis	(a) Tyrosinase degradation	Linoleic acid, Oleic acid, Phospholipase D2
	(b) Inhibition of melanosome transfer	Niacinamide, Lectins, Neoglycoproteins, Centaurecidin
	(c) Skin turnover acceleration	Lactic acid, Liquiritin, Glycolic acid, Retinoic acid, Salicylic acid, Linoleic acid
	(d) Reduction of melanocyte environment	Corticosteroids, Glabiridin

2.1.3 Active ingredients used for skin depigmentation

2.1.3.1 Tretinoin

Tretinoin (Figure 2) is also known as retinoic acid or vitamin A acid. It affects skin pigmentation by inhibiting tyrosinase transcription in the keratinocytes. However, it is not allowed to be used in the cosmetic industry due to its undesirable effects such as erythema and desquamation. The concentrations range from 0.025% to 0.1% of topical tretinoin alone or combined with hydroquinone to treat skin aging and pigmentation prescribed by specialist doctors (6, 11).
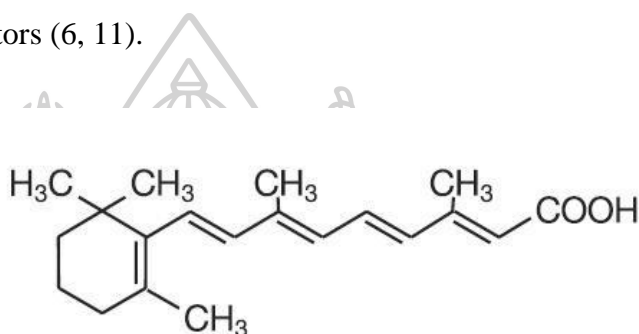
Figure 2. Tretinoin structure (61)

2.1.3.2 Tranexamic acid

Tranexamic acid (Figure 3) is a synthetic derivative of the amino acid lysine used to treat melasma in Asia. Tranexamic acid can inhibit tyrosinase activity by blocking the interaction of melanocytes and keratinocytes through the inhibition of the plasminogen system (62).
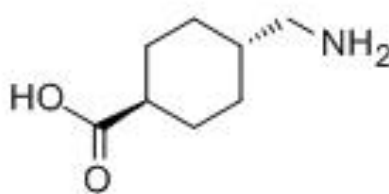
Figure 3. Tranexamic acid structure (63)

2.1.3.3 Hydroquinone (HQ)

Hydroquinone (1,4 dihydroxybenzene) (Figure 4) is a phenolic compound that can be found in tea, coffee, wine, beer, and cigarette smoke (11, 64). It is used for the treatment of melanogenesis and other pigmentation disorders. It has a hydroxyl group at the para position for an electron donor, which is required to use as an alternative substrate of tyrosinase (4). The inhibition of tyrosinase induced the destruction of melanocytes via the free radicals' production. Although it is effectively used as a tyrosinase inhibitor, it can cause toxicity, defiguring effect, and mutagenicity (65). In Europe and Thailand, the cosmetic product including hydoquinone used for skin has been banned (11).

Figure 4. Hydroquinone structure (11)

2.1.3.4 Kojic acid

Kojic acid (5-Hydroxy-2-(hydroxymethyl)-4-pyrone) (Figure 5) is derived from various species of fungi such as Penicillium and Aspergillus (66). It is also known as a tyrosinase inhibitor because it can chelate the copper at the active site of the tyrosinase enzyme to prevent the conversion of DOPA quinone to its corresponding melanins, eumelanin or pheomelanin. Moreover, it has a free radical scavenging activity and is widely used as a topical skin lightening agent in Asia (11, 56). The Scientific Committee on Consumer Products (SCCP) reported that less than 1% of kojic acid containing in preparation is typically safe even though it may be associated with sensitization, contact dermatitis, and erythema (14).
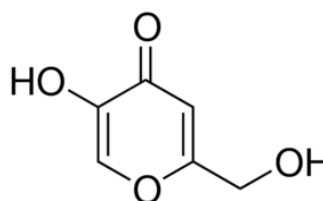
Figure 5. Kojic acid structure (67)

2.1.3.5 Azelaic acid

Azelaic acid (1,7-heptane dicarboxylic acid) (Figure 6) was obtained from *Pityrosporum ovale* (*Malassezia furfur*). Azelaic acid can bind amino and carboxyl groups to prevent the interaction of tyrosine as a competitive and reversible inhibitor of tyrosinase. Moreover, the depigmentation effect is also mediated by inhibiting DNA synthesis and mitochondrial oxidoreductase activity (6).
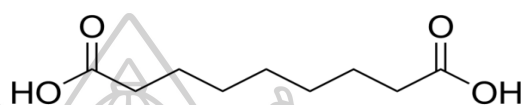
Figure 6. Azelaic acid structure (68)

2.1.3.6 N-acetyl-4-s-cysteaminylphenol

N-acetyl-4-s-cysteaminylphenol (Figure 7) is a phenolic thioether, which has a similar structure to tyrosine. It is used as an alternative tyrosinase substrate for the treatment of epidermal pigmentation such as melasma. Ferguson *et al*. found that N-acetyl-4-s-cysteaminylphenol has an interference action on cell growth and proliferation by undergoing the alkylating free thiol groups of cellular enzymes, which oxidized in melanocytes to form o-quinone (56).
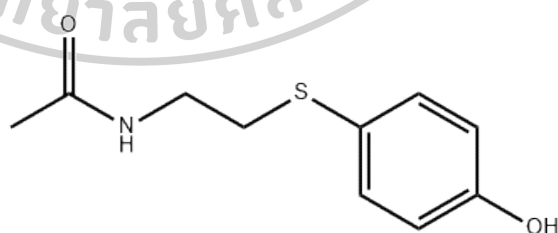
Figure 7. N-acetyl-4-s- cysteaminylphenol structure (69)

2.1.3.7 Aloesin

      Aloesin (2-acetonyl-8β-D-glucopyranosyl-7-hydroxy-5ethylchrome) (Figure 8) is a natural hydroxymethyl chromone compound derived from aloe vera plants and has been used for centuries in cosmetic and medical uses. Aloesin has been used to inhibit the hydroxylation of tyrosine to DOPA and also inhibiting the oxidation of DOPA to dopaquinone by tyrosinase (70). Jones *et al.* observed a dose-dependent decrease in tyrosinase activity following treatment normal human melanocytes with aloesin. Moreover, aloesin is used as a competitive inhibitor of tyrosinase as an alternative to hydroquinone because of no cytotoxicity effect (71).
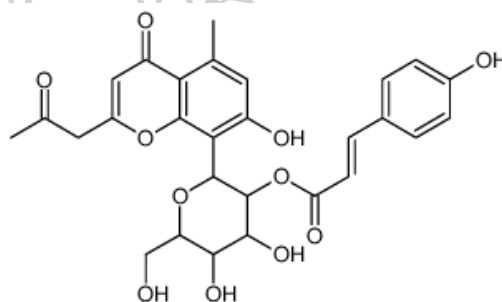
Figure 8. Aloesin structure (11)

2.1.3.8 Glabridin (Licorice extract)

      Glabridin (Figure 9) was obtained from the root of *Glycyrrhiza Glabra Linn Vu*, which is the hydrophobic fraction of Licorice. It has been used as a natural remedy for anti-inflammatory and anti-irritant properties. The depigmentation activity of glabridin has been shown to inhibit tyrosinase activity in melanogenesis (4). It was also shown that topical application of 0.5% glabridin could inhibit the induction of pigmentation by UVB and erythema formation in guinea pigs (72). In B16F10 melanoma cells cultured, it has the inhibitory activity of tyrosinase and melanin synthesis without affecting DNA synthesis rates. Moreover, it also has an anti-inflammatory effect by inhibition of superoxide anion production and cyclooxygenase activities (73, 74). Licorice extract has been studied for effective treatment of melasma with very mild irritation (75, 76).
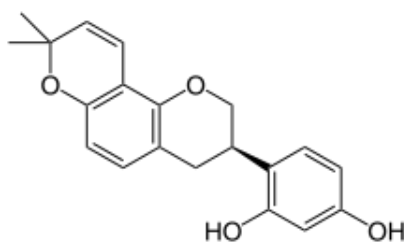
Figure 9. Glabridin structure (56)

2.1.3.9 Linoleic acid

Linoleic acid (Figure 10) is a topical unsaturated fatty acid that showed a depigmentation effect on guinea pig skin after exposed with UV radiation. The bleaching effect of linoleic acid may be due to the reduction in tyrosinase enzyme activity without changing mRNA levels and stimulating epidermal turnover of melanin pigment from the epidermis (4, 75).

Figure 10. Linoleic acid structure (77)

2.1.3.10 Niacinamide

Niacinamide (Figure 11) is the amide form of vitamin B_3 found in many vegetables such as beans, cereal grains, and yeast. It can induce skin lightening by downregulating melanosomes transfer from the melanocytes to the keratinocytes (78). Niacinamide has several benefits on the skin, including anti-inflammatory in moderate acne, antioxidant, increases intercellular liquid synthesis, prevents photoimmunosuppression and photocarcinogenesis (79). Hakozaki *et al*. found that using 5% niacinamide for 4 weeks effectively inhibited the transfer of melanosome approximately 35-68%, significantly reduced hyperpigmentation, and induced skin lightening in clinical trials. Moreover, the authors found that niacinamide has no effect on melanin synthesis and tyrosinase activity in cultured melanocytes (78).
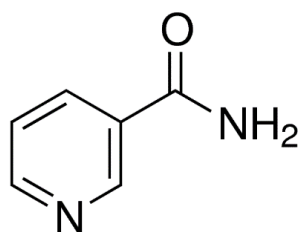
Figure 11. Niacinamide structure (80)

2.1.3.11 Ascorbic acid

Ascorbic acid (vitamin C) (Figure 12) is a water-soluble vitamin obtained from citrus fruits and green vegetables. Ascorbic acid has potent antioxidant activity in human skin because it acts as a reactive oxygen species (ROS) scavenger by donating electrons to neutralize free radicals in the aqueous compartment of the cells. The vitamin also affects different steps of melanin synthesis by reducing dopaquinone, interacting with copper ions at the active site of tyrosinase, and interrupting oxidation of 5,6-dihydroxyindole-2-carboxylic acid (DHICA), an intermediate in the biosynthesis of melanin (81).
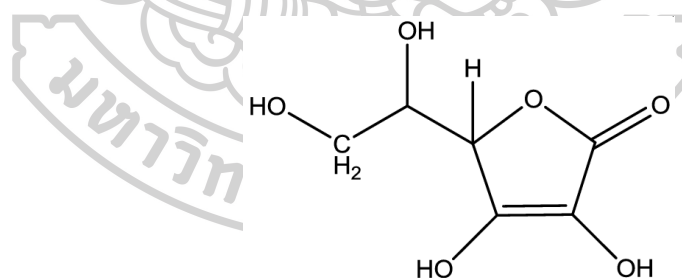
Figure 12. Ascorbic acid structure (82)

2.1.3.12 Alpha-tocopherol

Alpha-tocopherol (vitamin E) (Figure 13) is a fat-soluble antioxidant found in cereal, vegetables, vegetable oil, and nuts. It can terminate free radicals by donating hydrogen from the hydroxyl group on its chromane ring and interfere with the lipid peroxidation of the melanocyte membranes. The

depigmentation effect of alpha-tocopherol and its derivative is attributed to inhibit tyrosinase activity and increase intracellular glutathione (4, 6, 60).
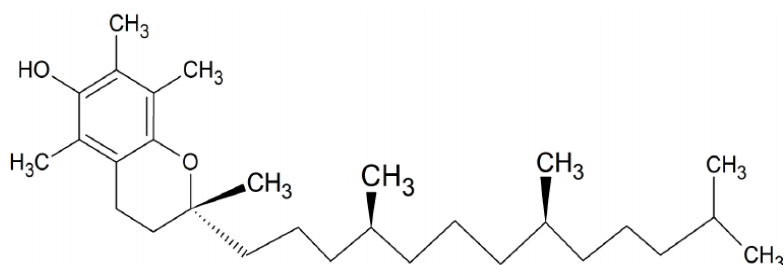
Figure 13. Alpha-tocopherol structure (83)

2.2 Alpha-arbutin

Arbutin is a hydroquinone derivative that consists of a phenol glycoside in the para position. It has been found in various plants such as bearberry, cranberry, blueberry, strawberry, pear trees, and the amount of arbutin in the plant is varied considerably according to the species (11, 84). In the plant, arbutin exists in a free ether or esterified form. According to the anomeric carbon conformation, it has two forms: alpha-arbutin (4-hydroxyphenyl-α-d-glucopyranoside) and beta-arbutin (4-hydroxyphenyl-β-d-glucopyranoside), as shown in Figure 14. Beta-arbutin is traditionally used in cystitis, urinary tract infections, and skin lightening (85).

Alpha-arbutin (AA) is one of the isoforms of arbutin and has a greater affinity at the active site than beta arbutin for inhibiting tyrosinase (12). Therefore, AA has been shown ten times stronger inhibitory effects of tyrosinase in mouse melanoma than beta arbutin (86). Moreover, AA does not affect cell viability and significantly reduced the melanin synthesis in human melanoma cell culture and a three-dimensional cultured human skin model, indicating that AA is effective for skin depigmentation with safe (87). The scientific Committee on Consumer Safety (SCCS) recommended that the use of AA in cosmetics products safe for consumers in a concentration of not more than 2% in facial cream and 0.5% in body lotions (14).
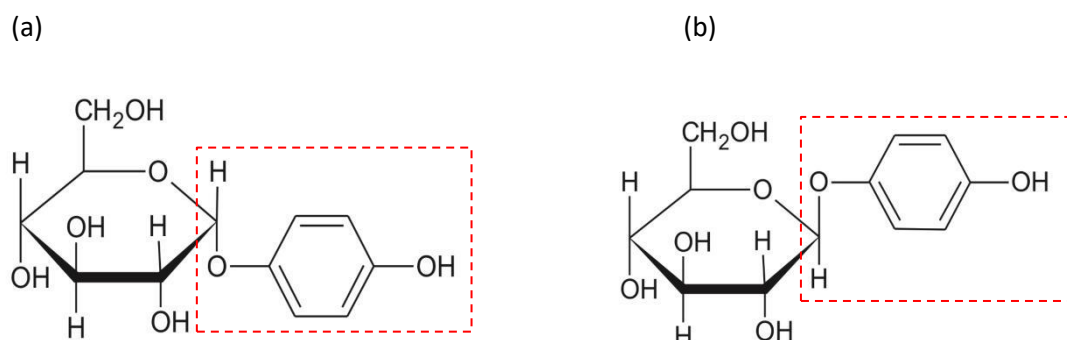
Figure 14. (a) Alpha-arbutin and (b) Beta-arbutin structures (88)

2.2.1 Physicochemical properties

The appearance of AA is a white crystalline powder and has a molecular weight of 272.25 g/mol. AA can be synthesized from hydroquinone enzymatically or chemically. It is stable in the range of pH 3.5-6.5 (89, 90). AA is a hydrophilic compound, which resistant to light. The stability of AA in cosmetic products is within pH ranging between 4 and 8. It is also relatively stable in ethanol extracts. However, it may undergo partial hydrolysis to hydroquinone and oxidize to benzoquinone in aqueous extracts (12).

2.2.2 Mechanism of action

Many studies reported that AA possesses various biological activities that can be applied in many cosmetic and pharmaceutical fields. AA is widely used as an effective treatment of hyperpigmentation disorder and shows less melanocyte cytotoxicity compared with hydroquinone. AA itself affected skin pigmentation by inhibiting tyrosinase activity due to structural similarities to the substrate tyrosinase, resulting in decreasing melanin synthesis and the conversion of tyrosine to L-DOPA. There is no effect on mRNA expression and synthesis. Maeda *et al*. reported that the depigmenting action of arbutin in human melanocyte cell culture was observed in inhibition of melanosomal tyrosinase activity, rather than suppressing the expression and synthesis of tyrosinase (91). Moreover, anti-inflammatory properties are also found in AA. Lee *et al*. found that arbutin reduced the nitric oxide (NO) production and NO synthase expressional of COX-2 in the BV2 microglial cell line stimulated by lipopolysaccharide resulting in inhibit pro-inflammatory cytokines, IL-1β, TNF-α, and

other inflammation-related genes such as MCP-1 and IL-6 (10). Moreover, AA promoted wound healing by decreasing ROS species by activating the oxidative pathway in human dermal fibroblast cells and upregulating insulin-like growth factor 1 receptor (IFG1R) (92). Li *et al*. investigated that AA inhibited TCCSUP (human urinary bladder cancer cell) proliferation through extracellular regulated kinase (ERK) inactivation and increased expression of P21 protein for antitumor activity (93).

2.2.3 Drug delivery techniques for alpha-arbutin

AA has been found in skin whitening, cosmetic products as a topical cream and emulsion. However, the application of AA via transdermal delivery has a limitation, such as its poor percutaneous absorption due to its high hydrophilic property. This result is restricted to penetrate the skin SC layer where melanocytes occupy (15). Therefore, several researchers have attempted to improve transdermal delivery of AA by developing the formulation processes or delivery techniques. In 2014, Won *et al*. attempted to enhance the penetration of AA using microporation based on radiofrequency (RF). RF microporator composed of 150 μm length of 64 stainless steel arrays with the sharpened edge was applied five times on guinea pig skin before applying arbutin. The results indicated that RF microporation significantly enhanced *in vitro* topical delivery of arbutin in guinea pig skin and improved *in vivo* depigmentation effects in the guinea pig (15). Moreover, Liao *et al*. showed that the combined treatment of ultrasound and albumin shelled microbubbles can improve AA delivery to inhibit melanin production without damaging the mice skin (94). In addition, Liang *et al*. developed 5% w/w arbutin encapsulated micelles using Urah[®] proprietary micellar technology and evaluated its cellular melanin suppression activity and *ex-vivo* skin penetration efficiency. The data provided that micellar arbutin cream could be significantly improved arbutin delivery and enhanced the suppression of melanin synthesis than non-micellar arbutin cream (95). Recently, Ayumi *et al*. formulated chitosan nanoparticles (CS-TPP-NPs), which are a suitable carrier for alpha- and beta-arbutin. Alpha- and beta-arbutin CSNPs successfully prepared using CS-TPP ionic gelation method, and their release studies were evaluated. Both alpha- and beta- CSNPs showed significant release in alpha- and beta- arbutin higher than that of their free form (96).

2.3 Resveratrol

Resveratrol (3,5,4′-trihydroxy-trans-stilbene) is a naturally occurring polyphenolic and stilbene compound with two isoforms, namely trans-resveratrol and cis-resveratrol (Figure 15). These compounds are found in various plant species, including berries, grapes, red wines, groundnut, mulberries, pines, and peanuts (23, 97). Trans-resveratrol is more stable and biologically active than cis-resveratrol. The isomerization of trans-isoform to cis-isoform is mainly influenced by visible light, high temperature, and low pH (23, 98). Resveratrol (Res) showed many health benefits such as antioxidant, anti-aging, anti-diabetic, anti-inflammatory, anti-obesity, cardioprotective, neuroprotective activities, antiproliferative, and anticarcinogenic agents (16-18, 25, 26, 99, 100). Moreover, Res can directly or indirectly inhibit melanin synthesis in human melanocytes (101). Hence, Res has been widely used in cosmetic and pharmaceutical formulations.

(a)   (b)
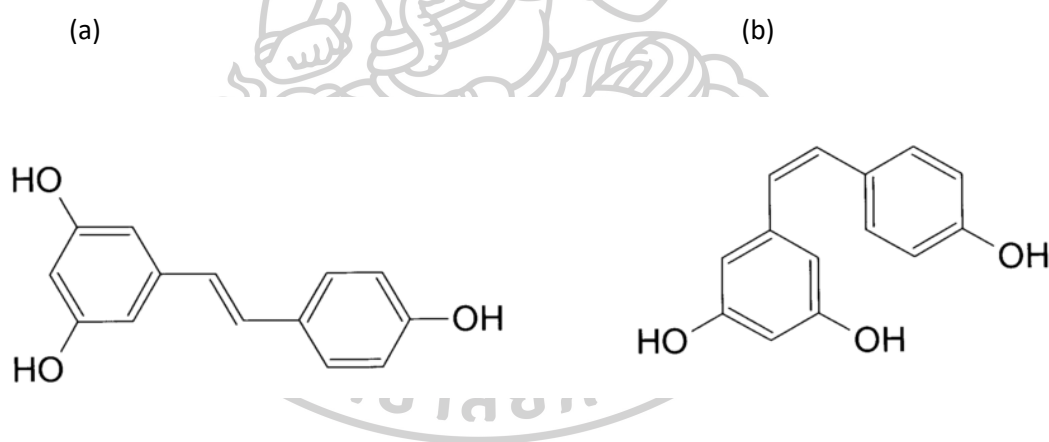
Figure 15. (a) Trans-resveratrol and (b) Cis-resveratrol structures (23)

2.3.1 Physicochemical properties

The appearance of Res is a fine white powder and has a molecular weight of 228.24 g/mol. The chemical structure of Res consists of two phenols joined together as a double styrene bond and known as a weak acid. Res has poor water solubility (0.05 mg/mL) with a partition coefficient of 3.1 and very low bioavailability. To increase the solubility of Res, ethanol (50 mg/mL) or other organic solvents are used

(25, 102). Res is relatively stable at pH 6-9. The stability and solubility of Res are mainly influenced by pH, light, and temperature (23).

2.3.2 Mechanism of action

The mechanism of action of Res depends on its chemical structure, which allows interacting with Res receptors, kinase, and other enzymes leading to the prevention of many disease conditions (103). Res has a strong scavenger ability of hydroxyl, superoxide, and metal-induced radicals and showed antioxidant activity in cells producing ROS (104). Res can be interfered in the aging process by enhancing the genetic expression of the silent information regulator 2 (Sir2), a gene associated with longevity known as sirtuin 1 (SIRT 1) in mammals, being responsible for codification of the sirtuin enzymes (histone deacetylase enzymes) (98, 103). Res is also known as an inhibition of α-MSH induced melanogenesis in melanoma cells by reducing TRP 1 and TRP 2 and MITF (105). Additionally, treatment with 29 µg/mL Res into normal human melanocytes (NHM) for 24 h resulting in significantly decreased the tyrosinase activity of melanocytes by direct inhibition and indirect downregulation of enzyme activity (101). Anti-inflammatory properties of Res are occurred by inhibiting the production of various inflammatory factors such as cyclooxygenase (COX), prostaglandin D_2 (PGD_2), prostaglandin E_2 (PGE_2), and hydroperoxidase (106). Res has also been reported as a significant anticancer property in various human tumor cells, including lymphoid and myeloid cancer cells, skin, stomach, breast, cervix, colon, liver, prostate, and thyroid carcinoma cells. In the various stages of carcinogenesis, Res affects initiation and promotion by affecting the diverse signal-transduction pathways that control cell growth and division, apoptosis, inflammation, metastasis, and angiogenesis (107).

2.3.3 Drug delivery techniques for resveratrol

The pharmacokinetic studies of Res via oral administration indicated that Res had poor bioavailability, was rapidly metabolized and excreted. Therefore, topical application of Res has become the effective alternative administration route for its pharmacological effects (108). To overcome the Res solubility and stability issues, micro- and nano-formulations, including polymeric nanoparticles, solid lipid nanoparticles, liposomes, liposphere, polymeric microsphere, and dendrimer, have

been developed to encapsulate Res (109). Caddeo *et al*. have been developed liposomal-loaded Res using oligolamellar vesicles to improve the efficacy of Res. The results showed that Res incorporated into liposomes improved the effectiveness of Res on viability and proliferation of the human embryonic kidney cells (HEK 293) caused by UV-B irradiation compared to free Res for the treatment of human skin disorders (28). Shao *et al*. have been reported Res-loaded nanoparticles prepared with methoxy-polyethylene glycol/polycaprolactone (MPEG/PCL) as a drug carrier which has a better efficacy against the growth of glioma cells by inducing intracellular ROS levels compared to the equivalent dose of free Res (29). Nan *et al*. investigated that the antioxidant activity of the immobilized Res was preserved in over 93% for 5 weeks compared to the raw Res (110). Recently, PAMAM dendrimer nanotechnology was used to solve the solubility and stability issue of Res. It showed that the dendrimer increased Res loading and skin penetration of Res, leading to innovative anti-aging cream and solutions for the commercial market (23).

2.4 Evaluation methods for depigmentation agents

2.4.1 *In vitro*

2.4.1.1 MTT assay

The MTT (3-(4,5-Dimethylthiazol-2-yl)-2,5-diphenyltetrazolium bromide) is commonly used to examine the cytotoxic effects of the drug by evaluating the cell viability. MTT is a well-known *in vitro* colorimetric assay based on assessing the mitochondrial activity of the living cell. The biochemical mechanism involves converting MTT into formazan crystals (E,Z)-5-(4,5-dimethylthiazol-2-yl)-1,3-diphenylformazan by living cells. This process allows occurring enzymatic reduction of the lightly colored, dissolved with dimethyl sulfoxide (DMSO). The purple color solution resulted gives an absorption at 540 nm, which can be quantified by spectrophotometer. The obtained absorbance value is directly proportional to the healthy and rapidly growing living cells (111, 112). Therefore, an MTT assay method has become popular among other methods to measure depigmentation agents' *in vitro* (melanin cell lines) cytotoxic effects at different concentrations.

2.4.1.2 Melanin content assay

Measuring the *in vitro* melanin content of cultured melanoma cells using spectrophotometry is an essential method to evaluate the efficacy of depigmentation agents. The amount of melanin content in cultured cells can be expressed as either melanin content per culture area or melanin content per cell. Moreover, it can be calculated from the melanin content at the beginning and the end of culture using various formulas. Melanin content assay provides reliable comparison results before and after the treatment cells with a specific reagent (113).

2.4.2 *In vivo*

2.4.2.1 Determination of skin depigmentation activity

Evaluation of skin depigmentation activity of the drug in mice or human skin is also necessary. For *in vivo* measurement, various machines such as mexameter or chromameter CR-200 photometer are widely used by dermatologists to indicate skin color. The melanin index, individual typology angle (ITA°) value, and luminance (L*) value are measured using the machine's skin color probe. The individual typology angel (ITA°) value base on spectrophotometric measurement and classify the skin types into six physiologically relevant groups: very light, light, intermediate, tan, brown, and dark. The higher ITA° value indicates the brighter skin color (114). The L^* value is designated from black ($L^* = 0$) to white ($L^* = 100$), giving the relative brightness of the tested skin. The skin depigmentation activity of the drug can be observed in tests animals or human volunteers by skin whitening index L^* value changes. Therefore, the increased L^* value of drug-treated volunteers indicates brighter skin color (38, 115).

2.5 Microneedles (MNs)

MNs is an alternative and minimally invasive useful transdermal delivery device composed of micron-sized needles in height 25 µm up to 2000 µm (33, 116). MNs are designed to pierce the SC by creating microholes in the skin without causing pain and bleeding. Moreover, MNs facilitated the transdermal drug delivery by increasing skin permeability for compounds that normally do not penetrate the SC.

Microneedles-based systems have been applied for drug delivery (39), cosmetics delivery (117), vaccination (118), bio-sensing (119), and diagnostic purposes (120). MNs can be manufactured from various materials such as metals, silicone, steel, polymer, ceramics, glass, and carbohydrates based on types of MNs (121).

2.5.1 Types of MNs

MNs can be widely classified based on the design, drug-loading technique, and materials used for fabrication, such as solid, hollow, coated, dissolving, and hydrogel-forming MNs (122). Solid and hollow MNs have been registered as the first patent in the MNs field by Gastrel and Place in 1971, and shortly after, coated MNs emerged as the second one by Paul in 1975. In 2000, the emergence of dissolving MNs became the current main application of MNs because it facilitates a wide range of applications to enhance transdermal drug delivery (123). Moreover, the recent development in MNs technology was reported in 2012, hydrogel-forming MNs made from swelling polymer (124).

2.5.1.1 Solid MNs (SMNs)

SMNs are designed as a two-step process called, "poke and patch" principle; the first step is to pierce solid MNs into the skin to create microholes and then apply a conventional drug formulation as a transdermal patch. The drug formulation passes through these created microholes via diffusion, enhancing drug permeability (Figure 16) (121). SMNs showed the most robust mechanical strength and were used for skin pretreatment before the topical application of cream, gel, ointment, and solution. However, an accurate dose penetration into the skin is difficult to control in solid MNs. SMNs can be made using lithographic, etching, laser metal cutting processes and assembling hypodermic needles or wires (125). Stainless steel MNs were utilized to investigate the enhancement of amantadine hydrochloride and pramipexole dihydrochloride across the *in vitro* porcine ear skin (126). SMNs device, dermaroller, with different lengths (150, 500, and 1000 μm) was applied to perforate the human full-thickness skin and invasome (phospholipid vesicles), which improved invasome penetration compared with an aqueous solution (127).
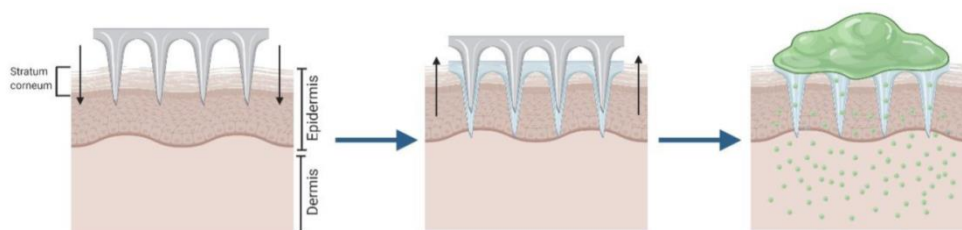
Figure 16. Schematic diagram for the "poke and patch" approach of solid MNs (123)

2.5.1.2 Hollow MNs (HMNs)

MNs with hollow cores are developed to inject the liquid formulation into the body in a painless way compared to a traditional hypodermic needle. Therefore, the principle of drug delivery through HMNs is termed as a "poke and flow" approach (Figure 17) (121). The advantage of HMNs over solid, coated, and dissolving MNs is delivering a larger amount of the drug. However, the clogging of HMNs has become a limitation for an extended period of application. HMNs are generally made with metals (titanium, tantalum, nickel) and glass using various fabrication methods, including electrochemical etching, laser machining, and electrode discharge machining (127). *In vivo* immunization of plasmid DNA encoding ovalbumin (pOVA) using HMNs combined with nanocarriers induced stronger IgG immune responses than conventional subcutaneous injection (128).
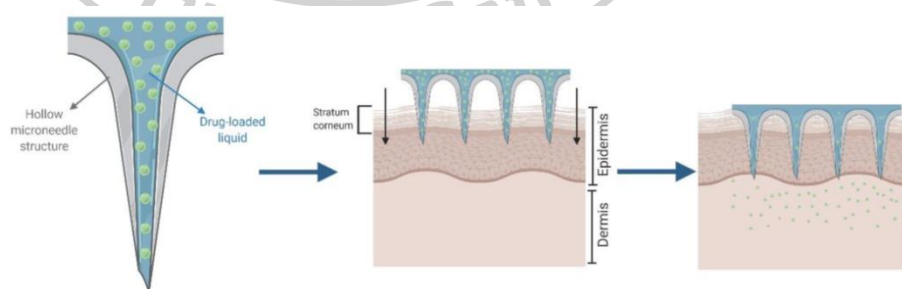
Figure 17. Schematic diagram for the "poke and flow" approach of hollow MNs (123)

2.5.1.3 Coated MNs (CMNs)

CMNs work on the "coat and poke" principle. This MNs type is based on SMNs in which the needles are coated with drug molecules to be delivered. The mechanism of CMNs allows a simple one-step application process, where MNs are allowed to penetrate the skin, and the drug coating is quickly dissolved when contact with skin interstitial fluid. The drug can be delivered into the tissue before removing CMNs (Figure 18) (121). The fabrication methods for CMNs, including the dip-coating process, micromilling, inject printing, drawing lithography, automized spraying, and droplet-born air blowing (129). Gold-coated silicon MNs were also fabricated using an optimized tetramethylammonium hydrochloride etching for biocompatibility improvement (130). Chen *et al*. have been developed polylactic acid (PLA) coated MNs using a dip-coating process, which is shown safe and effective coated MNs for transdermal drug delivery in mice (130).
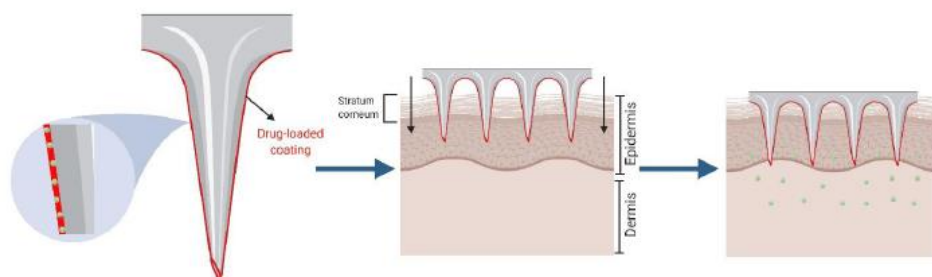
Figure 18. Schematic diagram for the "coat and poke" approach of coated MNs (123)

2.5.1.4 Dissolving MNs (DMNs)

Recently, DMNs have been more attention than other MNs types due to their ease of fabrication, biocompatibility, one-step application, the ability to adjust the drug loading, and control the drug release profile (122, 131). DMNs are prepared using biodegradable polymers or sugar, which is loaded with drug molecules. DMNs operate by a "poke and release" principle. Once applied, DMNs completely dissolve when contact with interstitial fluid in the skin and leaving the drug without any biohazardous sharps waste after

removing the patch (Figure 19) (122). González *et al*. found that the development of gentamicin-loaded hyaluronate/polyvinyl pyrrolidone DMNs was successfully penetrated the skin and provided gentamicin transdermal at therapeutic levels *in vivo* (132). Park *et al.* have been developed hyaluronate DMNs in which cosmetic ingredients were loaded using a laser-writing process. DMNs showed the significant enhancement of the skin permeability of niacinamide and the antioxidant activity of ascorbic acid after permeating the skin (133).
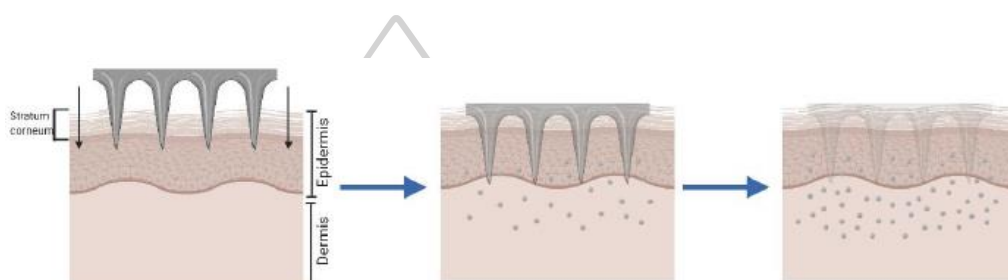
Figure 19. Schematic diagram for the "poke and release" approach of dissolving MNs (123)

2.5.1.4.1 Application of DMNs

DMNs are currently used for different purposes, such as disease treatment, vaccination, cosmetics, and diagnostic. It can deliver from the small to the large molecular weight of drugs and proteins (134). These DMNs has proven to be useful for the delivery of hydrophilic and hydrophobic drugs, including gentamicin (135), lidocaine (116), sinomenine hydrochloride (136), capsaicin (137), levonogestrol (40), acyclovir (138), doxorubicin (39), vitamin K (43), sumatriptan succinate (139), and artemether (140). DMNs has become a potent modern tool for intradermal vaccination, such as influenza (141), hepatitis B (142), tetanus (143), diphtheria (143), polio in rhesus macaques (144), measles (145), and HIV in mice (146) to create a self-administration platform. DMNs have been developed to incorporate the therapeutic peptides (30), insulin (47, 147), and human growth hormone (rhGH) (148). DMNs have been applied as an alternative method for glucose and vancomycin monitoring through dermal interstitial fluid in a non-invasive way (149, 150). Moreover, cosmetic compounds (skin depigmentation, whitening, and anti-aging) are the

best active ingredients for loading into DMNs, which are encapsulated in a polymer matrix and effectively delivered to melanocytes (115, 117, 151-153).

2.5.1.4.2 Fabrication methods of DMNs

Micromolding, photolithography, drawing lithography, and droplet-born air blowing techniques have been used to fabricate DMNs. DMNs have been produced mainly by micromolding method because they can be designed to deliver various drugs, easy to use, and inexpensive (134). It is the most common technique for the fabrication of polymeric DMNs. The biodegradable polymers prepared by micromolding technique are PVA, Gantrez® S-97, collagen, chitosan, polysaccharides such as CMC, HA, chondroitin, and cellulose (126). Micromolding method is done via silicone molding, injection molding, and hot embossing, depending on the type of materials used for DMNs fabrication (Figure 20). In this process, drug-loaded polymer solutions are filled into the mold cavities and peeled the fabricated DMNs from the mold (154). Centrifugation and vacuum are used to improve this process (134). Moreover, fabrication photolithography is a simple mold-free process using a photomask in which micro-lenses are embedded and used for DMNs fabrication. The formed DMNs provided robustly and sharpness, which is mainly influenced by embedded micro-lenses (155). A recently patented technology called drawing lithography was suggested to fabricate DMNs, creating three-dimensional microstructures from two-dimensional thermosetting materials (Figure 21). Although this method developed without using a mold, high temperature is required to draw and harden the thermosetting materials. Therefore, the major limitation of this technique is not suitable for heat-sensitive biological drugs (156). The DMNs can also be fabricated within 10 min using droplet-born air blowing in which the polymer droplet is solidified to MNs via air blowing to form a DMNs shape (Figure 22). This process is done at low temperatures, thus allowing the loading of heat-sensitive biological drugs such as vaccines or genetic materials. This technique has been used to fabricate DMNs using CMC, PVP, HA, and other

polymers (127, 156). However, the fabrication methods for DMNs are still facing some challenges, such as loss of drug activity during fabrication, time consumption, and difficulty adjusting the loading amount of the drug.
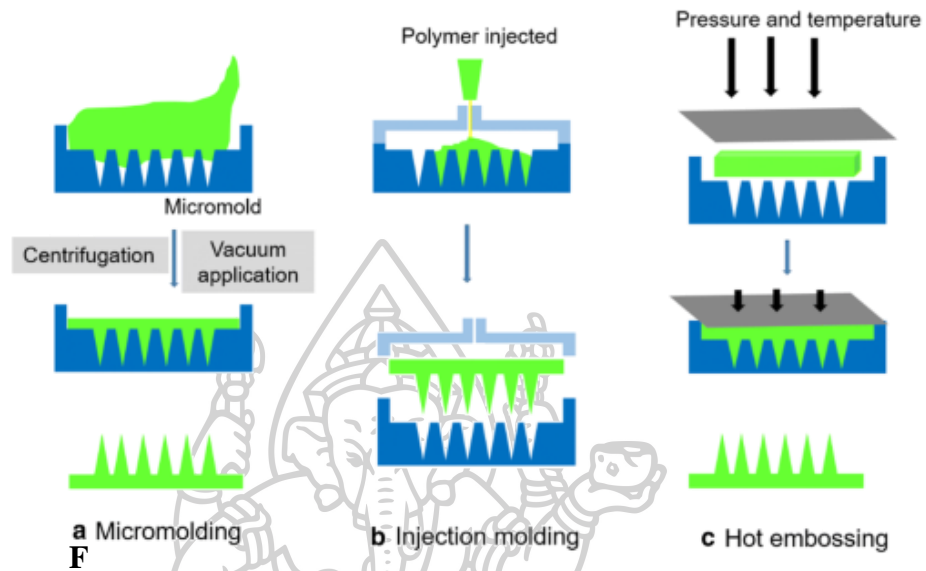
Figure 20. Schematic representation of various micromolding techniques used for the fabrication of DMNs (125)
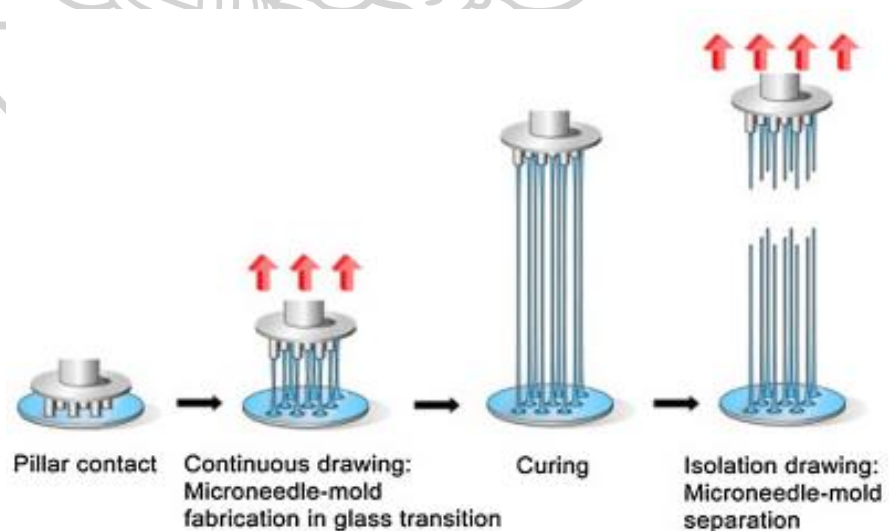
Figure 21. Schematic representation of drawing lithography process used for fabrication of DMNs (157)
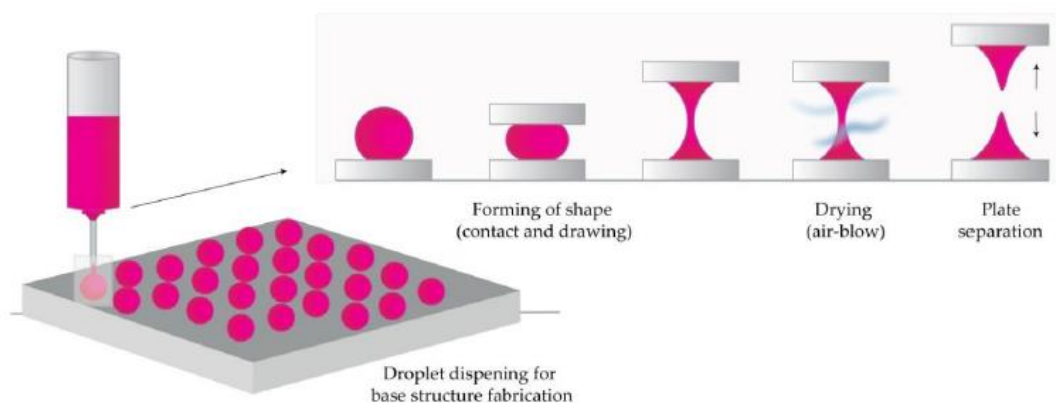
Figure 22. Schematic representation of droplet-born air blowing process used for fabrication of DMNs (158)

2.5.1.4.3 Materials used for fabrication of DMNs

Several materials such as polymers and carbohydrates are widely used for the fabrication of DMNs. Most polymers used for transdermal drug delivery are safe, inert, biodegradable, and biocompatible. Natural and synthetic polymers are used in the fabrication of DMNs. The types of polymers such as hydrophilic or hydrophobic are selected depending on the desirability DMNs, including (i) release kinetic of incorporating drug, (ii) dissolution time of DMNs, (iii) solubility of model drug, (iv) controlled drug delivery, (v) choice of the fabrication process, and (vi) cost of the polymer (159). DMNs are usually prepared with carbohydrates, the major ones being maltose, chitosan, sugar, dextran, sucrose, mannitol, galactose, xylitol, and polysaccharide (160).

2.5.1.5 Hydrogel-forming MNs (HGMNs)

The "poke and gel" approaches in HGMNs are composed of swelling materials or polymers. After applying HGMNs to the skin surface, they are swelled after absorbed the interstitial fluid and then easily released the encapsulated drug into the skin (Figure 23) (161). HGMNs have been successfully fabricated from PVA, CMC, polysaccharide mixture, or gelatin using crosslinking method (126). HGMNs provide the advantages of the higher drug-loading amount in comparison with DMNs and CMNs. For

example, metformin-loaded HGMNs, esterification of HGMNs between poly(methyl vinyl ether-co-maleic acid) (PMVE/MA) and poly(ethylene glycol) (PEG), provided promising technology improved the delivery of high-dose metformin transdermally in a sustained manner (162).
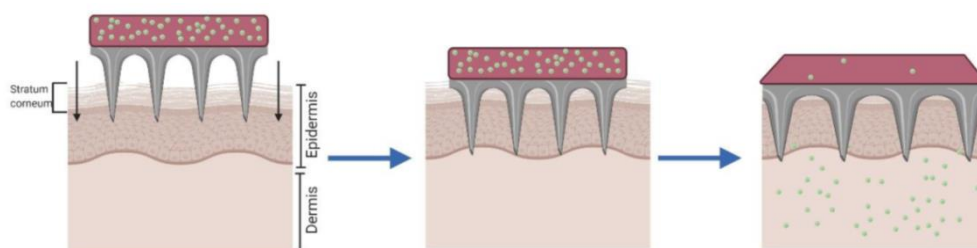
Figure 23. The schematic diagram for the "poke and gel" approach of hydrogel-forming MNs (123)

2.5.2 Materials used for fabrication of MNs

MNs are fabricated using a wide range of materials, such as metals, silicones, ceramics, glass, carbohydrates, and polymers depend on their properties. Materials constructed for MN fabrication of MNs should be inert, biocompatible, good mechanical strength, absence of immunogenicity, low corrosion rate, and stability (123, 126).

2.5.2.1 Metals

The biocompatibility metals have been used for MNs manufacture, including stainless steel, titanium, tantalum, and nickel. They are used to fabricate solid and hollow MNs for biomedical applications because they possess good malleability and robusticity. In addition, these materials can be designed in different lengths and geometries needle' shape, such as sharp, conical, tapered, and arrow-head for effective transdermal drug delivery (126, 159, 163).

2.5.2.2 Silicon

Silicon has hard and brittle properties. Although silicon MNs provide good tip sharpness, they are easy to break due to their fragile nature. Moreover, the disadvantages of silicon MNs are high material cost for

manufacturing, require a long time for fabrication, and clean room setup. Solid, coated, and hollow MNs had been made with silicon using etching and lithography methods (123, 126).

2.5.2.3 Ceramics

Ceramics are solid materials composed of metallic and nonmetallic elements by interatomic bonding of either ionic or covalent. The biologically compatible ceramics possess higher mechanical strength and better stability at high temperatures and humidity than most polymers. Examples of ceramics, such as alumina (Al_2O_3), zirconia (ZrO_2), calcium phosphate ($CaHPO_4$), calcium sulfate ($CaSO_4$), and hydroxyapatite, are commonly used for the fabrication of solid, hollow, and dissolving MNs (123, 126, 164).

2.5.2.4 Glass

Hollow MNs are generally prepared by micropipette pulling using glass (borosilicate) for drug delivery and diagnostic purposes. The advantages of glass are resisted high temperature and easy to sterilize using dry or moist heat sterilization. However, the limitations are easy to broken, time-consuming for the fabrication process, and suitable only for experimentation, not in practical use (123, 126).

2.5.2.5 Carbohydrates

Carbohydrate materials, including maltose, galactose, trehalose, fructose, sucrose, mannitol, xylitol, and sorbitol, are suitable alternatives for the fabrication of MNs as they are cheap and safe for human. However, they have poor mechanical properties and need to be combined with other materials for enough strength to pierce the skin and deliver the drug effectively. The temperature and relative humidity (RH) can be effected their types of MNs during storage conditions. As literature reviews, solid and dissolving MNs had been fabricated with carbohydrates by mixing with polymers (33, 126).

2.5.2.6 Polymers

Natural and synthetic polymers are widely used in drug delivery due to the biocompatibility, biodegradability, low cost, and safe as an alternative to metal and glass. Natural polymers, such as silk fibroin protein, HA, and chitosan, were utilized to create drug-loaded MNs to vaccinate in mice. Some typical examples of synthetic polymers used in the fabrication of polymeric MNs (DMNs and HGMNs) are PVP, PVA, CMC, Gantrez® S-97, PLA, polyglycolic acid (PGA), polycarbonate (PC), polymethylmethacrylate (PMMA), polystyrene (PS), PAMA and PCL (33, 126, 163). Hydroxypropyl methylcellulose is a non-ionic water soluble polymer, which is extensively used in oral, ophthalmic, and topical pharmaceutical formulation. The appearance of HPMC is white powder with a tasteless. The properties of HPMC such as its swelling and gelling can be affect drug dissolution and release kinetic. It also exhibits pH dependent drug release profile. The viscosity of HPMC depends on its molecular properties (molecular weight, degree of substitution, and substitution patterns) which affect on permeability, mechanical properties, and water solubility. HPMC is one of the cellulosic polymer which contains units linked together to help the retaining of water. Therefore, HPMC possess high water absorption capacity to give hydrophilic gel forming polymer (48, 165, 166). Polyvinyl alcohol is a water-soluble, non-toxic, biocompatible and biodegradable synthetic polymer has been applied in many pharmaceutical applications. PVA is highly stable and chemically inert due to its crystallization. Moreover, PVA exhibits good mechanical strength, film forming, and swelling properties in water due to its water retaining ability. PVA can be combined with other polymers to improve properties. The properties of PVA like viscosity, adhesive strength, tensile strength, and film-forming depend on its molecular weight and degree of hydrolysis (49, 167). Poly(acrylic acid-co-maleic acid) is an anionic copolymer of maleic acid and acrylic acid which are prepared by polymerization in water. The carboxylic acid group of PAMA has the hydrogen bonding ability with some polymer for crosslinking. (50). Polyvinylpyrrolidone-K90 is odorless, off-white and physiologically inert. It is non-ionic amorphous polymer which possess many

properties including non-toxicity, chemical stability, good solubility in water and many organic solvent, temperature resistance and pH stable and affinity to complex both hydrophilic and hydrophobic substances. The pharmaceutical industry has been interested PVP due to its excellent biocompatibility and capability to form stable complexes with many active substance (168). Eudragit polymers are chemically polymethacrylates special polymers which can be found as synthetic cationic, anionic, and non-ionic polymers of dimethylamioethyl methacrylates, methacrylic acid, and methacrylic acid esters in varying ratios. Among them, Eudragit RS100 and Eudragit RL100 are cationic polymers and commercially available for pharmaceutical excipients. They have versatile properties such as taste masking, and improve skin permeation, dissolution enhancement, enteric coating, sustained release, and pH dependent release. Eudragit E100 has the complex property with carboxylic acid group of drugs. It is used in oral and topical formulations as a carrier because it is non-toxic and non-irritant. Eudragit RS100 and Eudragit RL100 are copolymer of ethyl acrylate, methyl methacrylate, and methacrylic acid ester with quaternary ammonium groups which present as salt and make the polymer permeable. Eudragit RL100 possess more quaternary ammonium groups and more permeable than Eudragit RS100, the one containing less quaternary ammonium group. Eudragit polymers are use as ideal carriers for formulation of nanoparticles and to achieve the desired drug release profiles (169, 170).

2.5.3 Advantages and disadvantages of MNs

A summary of the advantages and disadvantages for each MNs type is described in Table 2.

Table 2. Advantages and disadvantages of each type of MNs (131), (159)

Types of MNs	Advantages	Disadvantages
Solid MNs	- Good mechanical strength - Physical stability - Reasonable drug loading	- Poor dose accuracy - Required rapid healing - Poor biocompatibility - Risk of infection - No precise dosing - Two-step application
Coated MNs	- Good mechanical strength - Precise dosing	- Poor biocompatibility - Dose limitation - Peeling during insertion - Formulation migration during manufacturing and storage - Reduction of MNs sharpness
Dissolving MNs	- Easy of manufacturing - One-step application - Low-cost manufacturing - Possible in controlled drug release profile	- Poor mechanical strength - Poor physical stability - Poor biocompatibility - Dose limitation
Hollow MNs	- Dose accuracy - Reasonable drug loading - Constant flow rate	- Risk of clogging - Requirement of a prefilled syringe - Risk of infection - Poor biocompatibility
Hydrogel-forming MNs	- Easy to manufacture - Reasonable drug loading - Possible in controlled drug release profile	- Poor mechanical strength - Poor physical stability - Ingressing body fluids

2.6 Characterization of DMNs

2.6.1 Morphology

The morphological analysis is one of the formulation screening methods to analyze the DMNs that appeared to be fully formed upon visual examination under a Dino-light microscope. Dino-Lite microscope, a digital microscope, is a magnifying device connected to a digital camera. Moreover, a scanning electron microscope (SEM) is also used to detect and confirm the well-structured of the DMN's arrays. SEM is a powerful magnification tool that utilizes focus beams of the electron to obtain information (30). In addition, it provides a rapid, simple method to compare different DMNs formulations (171).

2.6.2 Loading efficiency and loading capacity

The drug-loading efficiency is one of the evaluation methods for DMNs to measure the amount of recovering drug from DMNs by comparison with the initial loaded. The loading capacity refers to the maximum amount of drug that can be loaded to delivery carriers, polymers. The drug loading efficiency and loading capacity can be evaluated by extracting the drug from the polymer using suitable solvents, followed by a quantification test using a suitable machine (117).

2.6.3 Mechanical properties study

The mechanical properties study is one of the essential studies to confirm the needle strength and allow the penetration of skin SC. For the transdermal delivery of the drugs from the DMNs into the skin, the DMNs had sufficient rigidity to enable skin penetration. Moreover, the polymeric MNs arrays should be suitably robust to withstand handling by the patient prior to insertion (172). The compression force (0.089 N/array) is the maximum force humans typically reach when manually applying MNs (171). So, MNs should have the ability to resist this compression force for practical use. The height changes between and after compression load of the Texture analyzer can be assessed with a light microscope and measured using the ruler function of the microscope software (171).

2.6.4 *In vitro* **skin insertion and visualization studies**

In vitro skin insertion study plays an essential role in the selection of optimized formulations of DMNs. This experiment is generally performed using ParafilmM® and neonatal porcine skin to confirm DMNs insertion before *in vitro* skin permeation study (171, 173). The polymeric film (ParafilmM®, a blend of hydrocarbon wax and polyolefin) is used as a model membrane for MNs insertion study. A sheet of ParafilmM® is folded to obtain an eight-layer film before the experiment to approximate the thickness of the excited neonatal porcine skin closely. The neonatal porcine skin is considered an excellent alternative to human skin regarding their lipid composition and thickness compared with adult porcine skin. MNs can be inserted using a Texture analyzer and manual insertion by thumb pressure. The number of holes created in each ParafilmM® sheet and the neonatal porcine skin is evaluated using a lighting microscope following the microholes are stained with dye (methylene blue). Therefore, skin insertion and visualization studies have become a reliable insertion method for comparative formulation studies (171).

2.7 Evaluation method for DMNs

2.7.1 Dissolution study

Dissolution is one of the factors for DMNs to predict the dissolution time of a biodegradable polymer. Ideally, DMNs should dissolve when it makes contact with interstitial fluid to penetrate the skin and release the drug (40). Analysis of the dissolved DMNs tips after the application of minutes to hours shows the dissolution rate of DMNs. This dissolution rate mainly depends on the DMNs composition, such as polymer types, the polymer's viscosity, and the solubility of drugs (174). The remaining height of dissolved DMNs tips at designated time points was evaluated and imaged under a digital light microscope (117).

2.7.2 Skin permeation and accumulation studies

2.7.2.1 *In vitro* **study**

Franz diffusion cells are widely used to evaluate *in vitro* permeation for researching transdermal drug technology (175). Dr. Thomoas J. Franz developed this method in 1970 to determine the relationship between skin, drugs, and formulations (176). The neonatal porcine skin or synthetic

membrane (cellulose) is used as barriers for drug permeation. Diffusion cells can be divided into two types, static and flow-through cells. The popular Franz diffusion cell is static cells in which the donor, the membrane, and the receptor are placed either vertically or horizontally. Franz diffusion cells have many advantages, such as (i) low amount of sample required for analysis, (ii) few handling of tissues, and (iii) no continuous sample collecting (177). At present, *in vitro* permeation study using Franz diffusion cells has become a highly reproducible methodology in any laboratory. After completing the skin permeation study, a skin accumulation study can be carried out to determine the accumulated amount of drug inside the neonatal porcine skin. The drug sample is extracted from the skin using the suitable solvent and then measured by an appropriate qualitative method.

2.7.2.2 *In vivo* study

Study skin permeation *in vivo* experiments on humans is expensive and has ethical implications; therefore, a variety of animal models, including mouse, rat, pig, guinea pig, shed snake skin, and cultured human skin model, was used as an alternative to human skin to assess transdermal formulations (178). Among them, rodent skin (mice, rats, and guinea pigs) is the most commonly used animal model *in vivo* permeation study due to its low cost, availability, ease of handling, and small size. *In vivo* skin permeation study is a key to the successful development of new DMNs formulation intendant for human use.

2.7.3 Skin resealing study

The skin resealing study is essential to determine the kinetics of skin resealing time following MNs application and subsequent removal of the DMNs. The principle of DMNs is to release the drug when contact skin interstitial fluid and should be naturally resealed in a timely manner to minimize the risk of potential infections (179). The resealing time of skin's barrier properties after insertion of DMNs has been influenced by MNs design and geometries such as MNs length, number, thickness, width, and shape (180). The resealing of the SC regulated by the formation of a water gradient when the skin has been breached. Thus, the skin

eliminates this gradient leads to over-hydrating the SC and slowing the sealing process. The speed of skin resealing was significantly faster in non-occlusive conditions compared with occlusive conditions (179).

CHAPTER 3
MATERIALS AND METHODS

3.1 Materials

3.1.1 Materials for preparing drug-loaded DMNs

- Alpha-arbutin (MW = 272.25, Xi'an Ganoyuan, Biochem Co., Ltd., China)
- Resveratrol ((MW 228.24) Xi'an Gaoyuan Bio-Chem Co., Ltd., China)
- Hydroxypropyl methylcellulose (HPMC; MW= 1261.4 Da, Sigma-Aldrich® St. Louis, MO, USA)
- Polyvinyl pyrrolidone K-90 (PVP-K90; MW= 360 kDa, Sigma-Aldrich® St. Louis, MO, USA)
- Poly(acrylic acid-co-maleic acid) (PAMA; MW = 3000 Da, Sigma-Aldrich® St. Louis, MO, USA)
- Poly(vinyl alcohol) (PVA; MW = 85,000–124,000 Da, Sigma-Aldrich® St. Louis, MO, USA)
- Eudragit E100 (Evonik R¨ohm GmbH, Germany)
- Eudragit RS100 (Evonik R¨ohm GmbH, Germany)
- Eudragit RL100 (Evonik R¨ohm GmbH, Germany)
- Ethanol HPLC grade (Honeywell, QRёC)

3.1.2 Reagents for HPLC analysis

- Methanol HPLC grade (Honeywell, QRёC)
- Ultrapure water

3.1.3. Melanin cell and cell culture reagents

- B16F10 cell line (Mouse skin melanoma cell, American Type Culture Collection, ATCC)
- Dulbecco's modified Eagle's medium (DMEM; Gibco BRL, Rockville, MD, USA)
- Roswell Park Memorial Institute-1640 medium (RPMI-1640; Gibco BRL, Rockville, MD, USA)
- Fetal bovine serum (FBS; AMRESCO, OH, USA)

- Penicillin/Streptomycin (AMRESCO, OH, USA)

- Triton X-100 (AMRESCO, OH, USA)

- α-melanocyte-stimulating hormone (α-MSH; Sigma-Aldrich, MO, USA)

- Melanin and methyl thiazolydiphenyl-tetrazoline bromide (MTT; Sigma-Aldrich, MO, USA)

- Dimethyl sulfoxide (DMSO; EuroClone S.p.A., Milan, Italy)

3.1.4 All other chemicals

- Alpha-arbutin commercial cream (ENCOS Corporation, Korea)

- Disodium hydrogen phosphate (Na_2HPO_4; Ajazx Finechem, Australia)

- Kojic acid (Sigma-Aldrich, MO, USA)

- Potassium chloride (KCL; Ajazx Finechem, Australia)

- Potassium dihydrogen orthophosphate (KH_2PO_4; Ajax Finechem, Australia)

- Sodium chloride (NaCl; Ajazx Finechem, Australia)

- Methylene blue (Sigma-Aldrich, MO, USA)

3.2 Equipment

- 1.5 mL microcentrifuge tube (Eppendorf®, Corning Incorporated, NY, USA)

- 2 mL microcentrifuge tube (Eppendorf®, Corning Incorporated, NY, USA)

- 15, 50 mL centrifuge tubes-sterile (Biologix Research Company, KS, USA)

- Adhesive tape

- Aluminum foil

- Amicon® Ultra filter (Merck KGaA, Darmstadt, Germany)

- Analytical balance (Sartorius CP224S; Scientific Promotion Co., Ltd., Bangkok, Thailand)

- Autoclave (Model:LS-2D; Scientific romotion Co., Ltd)

- Automated cell counter (TC20TM)
- Beaker (Pyrex, USA)
- Centrifuge (Sorvall® Biofuge Stratos)
- Centrifuge tube (Biologix Research Company, KS, USA)
- CO_2 incubator (Heraeus HERA Cell 240, Heraeus Holding GmbH., Germany)
- Desiccator
- DermaLab® series (SkinLab Combo, Cortex Technology, Hadsund, Denmark)
- Dino-Lite microscope (AM 7915 series, Hsinchu, Taiwan)
- Dry bath incubator (Hangzhou Allsheng instruments Co., Ltd., China)
- Dual-chamber counting slides
- Franz diffusion cell; a volume of receiver 6 mL
- Gloves
- Homoginizer (IKA® T25 ULTRA-TURRAX®,Sigma-Aldrich, MO, USA)
- Hot air oven (XUO 32, Meritech Co., Ltd, Thailand)
- HPLC (Agilent 1269 series, Waldbronn, Germany)
- HPLC vial
- Incubator Model 3111 Thermo Scientific (Forma Series II water jacket CO_2 Incubator, USA)
- Inverted microscope
- Laminar airflow (BIO-II-A, Telstar Life Science Solutions, Spain)
- Magnetic stirrer (Framo, German) and magnetic bar
- Medical scissor
- Microcentrifuge (Microfuge 16®, Model :A46473, Beckman Coulter Inc., IN, USA)
- Microfoam® tape
- Micropipette 0.1-2.5 µL, 2-20 µL, 20-200 µL, 100-1000 µL, 1-5 mL, and micropipettetip

- Microplate reader (VICTOR Nivo^{TM} Multimode Plate Reader, PerkinElmer, Germany)
- Nylon membrane filter (diameter 47 mm, pore size 0.45 μm)
- Parafilm (PM-996, USA)
- pH meter (Mettler Toledo, Switzerland)
- Water bath with circulator (WCR-P6, Daihan Scientific Co., Ltd, Korea)
- Refrigerator (4-8°C)
- Scanning electron microscope (SEM; Mixa TC, Czech Republic)
- Security guard column (KJO-4282)
- Silicone engineering micromold
- Syringe (1 mL, 3 mL, 5 mL)
- Tegaderm™ occlusive film
- Texture Analyzer (TA-XT plus, Stable Micro System, Haslemere, UK)
- VertiSep® GES C18 column (250 × 4.6 mm, 5 μm, Thermo-Fisher Waltham, Massachusetts, USA)
- Vortex mixer (VX100, Model :Labnet, NJ, USA)
- Water bath (WiseBath with digital Fuzzy Control System, Korea)
- 96 well-plate (Corning Incorporated, NY, USA)
- 24 well-plate (Corning Incorporated, NY, USA)

3.3 Methods

3.3.1 Depigmentation activity in B16F10 melanoma cells

3.3.1.1 Cell culture

B16F10 melanoma cells were cultured in RPMI 1640 medium supplemented with 10% FBS and 1% penicillin/streptomycin. The cells were incubated at 37ºC with 5% CO_2 in a humidified environment. After three days, the culture medium was changed; the cells were then cultured using a DMEM medium consisting of α-MSH for the experiments.

3.3.1.2 Cell viability assay

Cell viability of B16F10 cells was determined by MTT assay. The cells were seeded in 96-well plates at density of 0.3×10^4 cells/well and then incubated at 37ºC with 5% CO_2. After 24 h, the cultured cells induced with α-MSH were treated with various AA concentrations (10-4000 µg/mL) and Res (5-50 µg/mL). The treated cells were incubated at 37ºC with 5% CO_2 for 48 h. The old medium was then gently removed and washed with fresh PBS. Then, 25 µL of MTT solution (0.5 mg/mL in PBS) and 100 µL of fresh medium (DMEM) were added to each well and incubated for 3 h. Afterward, the MTT solution was then replaced by DMSO (100 µL) to dissolve formazan crystals. The absorbance was measured at 550 nm using a microplate reader. The percentage of cell viability was calculated regarding untreated control using equation 1 (181).

$$\% \ \textbf{\textit{Cell viability}} = \frac{\text{Absorbance of sample}}{\text{Absorbance of control}} \times 100 \qquad (1)$$

3.3.1.3 Melanin content assay

B16F10 melanoma cells were used to investigate the effect of AA and Res treated on melanogenesis. The cells were cultured in 24-well plates at a density of 1×10^5 cells/well and stimulated with α-MSH (100 µM). After 24 h, the cells were treated with various AA concentrations (100-2000 µg/mL) and Res concentrations (5-25 µg/mL) and then incubated at 37ºC with 5% CO_2 for 48 h. Kojic acid (60 µg/mL) was used as a positive control. After 48 h of incubation period, cells were dissociated by trypsin and transferred from each well into a 1.5 mL eppendorf tube. To collect cell pellets, cells were centrifuged at 3000 xg for 10 min. The supernatant was removed, and cell pellets were solubilized with 250 µL of 1 N NaOH containing 10% DMSO and incubated at 80ºC for 1 h. Afterward, the melanin contents were measured at an absorbance of 405 nm using a microplate reader. Finally, the melanin content was calculated based on the standard curve (182).

3.3.1.4 Drug synergism analysis of alpha-arbutin and resveratrol

Drug synergism analysis was determined based on the combination index (CI) theorem of Chou Talay 1985 (183). The synergistic effect of AA and Res was measured by melanin content assay using a non-constant ratio experiment. The analysis of the combination study on melanin contents was determined according to the protocol mentioned above. Briefly, exponentially growing B16F10 melanoma cells induced with α-MSH were exposed to a combination of different AA concentrations (500-3000 μg/mL) with a fixed Res concentration (20 μg/mL) or different Res concentrations (5-30 μg/mL) with a fixed AA concentration (2000 μg/mL) for 48 h. The percentage of melanin contents inhibition was obtained and calculated synergistic effect using CompuSyn software (Version 1.0). The percentage of melanin contents inhibitions was translated to a fraction of effect (Fa) and calculated using following equation 2. Next, the actual data point, including treatment concentration (μg/mL) and Fa was inputted into software to calculate synergism activity (CI value). CI value indicated the interactions between two drugs, where CI=1, CI<1, CI>1 expressed an additive, synergism, or antagonism effect, respectively. Based on drug synergism activity, the formulation showing the best synergism effect with the lowest cell toxicity was selected for loading into the DMNs formulation (184).

$$Fraction\ of\ effect\ (Fa) = \frac{1 - \%\ melanin\ contents\ inhibition}{100} \qquad (2)$$

3.3.2 Fabrication method

3.3.2.1 Preparation of polymers blending solutions

In this study, four different water-soluble polymers (HPMC, PVP-K90, PAMA, and PVA) and three different water-insoluble polymers of the Eudragit series (E100, RS 100, RL 100) were used to fabricate DMNs. In a pre-formulation study, different concentrations of each polymer solution were prepared by dissolving the polymers into distilled water and 97% ethanol

depending on their solubility. The polymer blended solutions were then prepared by combining two polymer solutions at the suitable weight ratios and stirred until a homogenous mixture was obtained. To remove air bubbles, the blended polymer mixtures were centrifuged at 3000 rpm for 20 min.

3.3.2.2 Pre-formulation of optimal blank DMNs

There are seven different kinds of polymers, including 8%w/w HPMC, 100%w/w PAMA, 20%w/w PVA, 40%w/w PVP-K90, 14%w/w Eudragit E100, 14%w/w Eudragit RS100, and 14%w/w Eudragit RL100 polymer solutions were prepared and mixed to find the optimal formulations of blank DMNs. Each blended polymer mixture, including HPMC/PVP-K90, PAMA/PVA, Eudragit E/PVP-K90, Eudragit RS/PVP-K90 and Eudragit RL/PVP-K90 were fabricated with the different weight ratios (1:1, 1:2, 1:3, 1:4, 2:1, 3:1, and 4:1), respectively. All blended polymer mixtures were stirred until homogenous solutions were obtained. Among different combination weight ratios, the optimal ratios of each suitable blended polymer formulation were selected for fabricating blank DMNs.

3.3.2.3 Fabrication of blank DMNs

The fabrication process was carried out under the controlled room at $25\pm1°C$ with $75\pm2\%$ RH. Laser-engineered silicone micromold template composed with 121 (11x11) conical-shaped arrays (height 600 μm, base width 300 μm, and interspacing diameter 300 μm) were used to fabricate DMNs. Each polymer blended solution listed in Table 1 was cast (0.67 g per mold) onto a silicone micromold. The blank DMNs molds were then centrifuged at 3500 rpm for 20 min to remove any air bubbles and fill the polymer solution into the mold cavities. The blank DMNs were gently removed from the micromolds after 48 h and carefully cut the sidewalls using a heated scalp. All blank DMNs were stored in a desiccator until used.

3.3.2.4 Fabrication of AA-loaded DMNs

The 8%w/w HPMC/40%w/w PVP-K90 (1:1) and 100%w/w PAMA/20%w/w PVA (1:4) were selected as the best formulation to fabricate

AA-loaded DMNs. These two polymers mixture were mixed with AA to obtain a polymer:AA at the weight ratio of 92:8. The fabrication process was similar to the method for fabricating blank DMNs as previously described. AA-loaded DMNs were kept in a desiccator until further testing.

3.3.2.5 Fabrication of Res-loaded DMNs

Res-loaded DMNs were prepared by mixing the polymer blends containing 14%w/w Eudragit E/40%w/w PVP-K90 (1:2) and 14%w/w Eudragit RS/40%w/w PVP-K90 (1:2) with Res to obtain a mixture of polymer solution:Res (95:5%w/w). To enhance the resveratrol dissolution, the formulations were homogenized at 6000 rpm. The fabrication process was similar to the method for fabricating blank DMNs as previously described. All Res-loaded DMNs were kept in a desiccator by wrapping with aluminium foil to avoid degradation of Res.

3.3.2.6 Fabrication of the combination of AA and Res-loaded DMNs

According to the CI value, the best synergism effect of AA and Res with the lowest cell toxicity was selected to fabricate AA and Res-loaded DMNs, as mentioned above in section 3.3.1.4. The best synergism concentration of AA and Res was obtained at the weight ratio of 5:1. Briefly, the amount of AA (10%w/w) was allowed to dissolve in 40%w/w of PVP-K90 solution. On the other hand, 14%w/w of Eudragit RL solution was mixed with 2%w/w of Res and stirred to enhance the solubility of Res. Next, the prepared drug-loaded polymer solutions were combined to obtain the weight ratio of Eudragit RL/PVP-K90 at 1:2. Then, the combination of 10% AA and 2% Res-loaded DMNs was stored in a desiccator wrapped with aluminium foil until used.

3.3.3 Characterization of DMNs

3.3.3.1 Morphology of DMNs

To evaluate the formulation screening, the morphology of all DMNs formulations, including blank DMNs, AA-loaded DMNs, Res-loaded DMNs, the combination of AA and Res-loaded DMNs, was observed using a Dino-Lite

microscope. According to formulation screening, DMNs were imaged and measured for their dimensions (height, width, and interspace) of each array using Dinocapture 2.0 software. Moreover, they were photographed under a scanning electron microscope (SEM) to assure the complete fabrication of the DMNs. The SEM was performed at a beam voltage of 5.0 kV; the images were captured at magnifications of 50x, 120x and 400x.

3.3.3.2 Mechanical properties study

The mechanical strength of DMNs plays an important factor in the practical use of DMNs. A compression mode of TA-XT plus Texture analyzer was used to investigate the effects of compression tests on individual needles' heights of the DMNs patch. To evaluate the mechanical properties of DMNs, DMN arrays were imaged before and after application of compression loaded using a Dino-Lite microscope. Briefly, DMNs were carefully attached to the movable flat probe using double-sided tape. The known axil vertical compression force of 3.388 N to 13.31 N per 121 needles (0.028 N to 0.11 N per needle) at a speed of 0.5 mm/s and the trigger force of 0.049 N was applied on the DMNs. Next, DMNs was then pressed against a flat aluminium block. The reduction height of DMNs was measured before compression force (H1) and after compression force (H2) using a Dino-Lite microscope. Finally, the mean percentage reduction height of needles was calculated using equation 3 (154).

$$\% \textbf{ Reduction of needles height} = \frac{[H1-H2]}{H2} \; x \; 100 \qquad (3)$$

3.3.3.3 Loading Efficiency and loading capacity

To evaluate the amount of drug-loaded into DMNs, accurate weight of DMNs was added into 10 mL of PBS (pH 7.4) solution and stirred until DMNs were completely dissolved. After that, each sample solution (500 µL) was centrifuged at 14,000 ×g for 20 min using Amicon® filter (MW cut-offs < 3000 Da) to filtrate the polymer. The content of drugs (AA and/or Res) was

measured using HPLC. The percentages of loading efficiency and loading capacity were calculated according to the following equations 4 and 5.

$$\% \; \boldsymbol{Loading \; efficiency} = \frac{Amount \; of \; drug \; (mg)}{Initial \; amount \; of \; drug \; (mg)} \times 100 \qquad (4)$$

$$\% \; \boldsymbol{Loading \; capacity} = \frac{Amount \; of \; drug \; (mg)}{Amount \; of \; polymer \; (mg)} \times 100 \qquad (5)$$

3.3.4 Quantitative analysis of AA and Res using HPLC

Quantification of AA and Res are carried out using high-performance liquid chromatography (HPLC) (Agilent 1269 series, Waldbronn, Germany) with UV visible detector. Twenty microliters of the sample were injected into an HPLC. The separations are performed in C18 (VertiSep® GES 250 × 4.6 mm, 5 μm, Thermo-Fisher Waltham, MA, USA). HPLC conditions to quantify the concentrations of AA and Res were described in Table 3.

Table 3. HPLC conditions for alpha-arbutin and resveratrol quantification

Active ingredients	Mobile Phases		Flow rate (mL/min)	UV detection (nm)	Retention time (min)
	Water	Methanol			
Alpha-arbutin (AA)	92	8	0.6	280	11
Resveratrol (Res)	60	40	1	308	12

3.3.5 *In vitro* studies

3.3.5.1 Skin insertion and visualization studies

In this experiment, a full thickness neonatal porcine abdominal skin (0.9 ± 0.15 mm) was used as an alternative model instead of a human skin model (173). The neonatal porcine skin was wrapped with aluminium foil and stored at -20ºC until used. The subcutaneous layer was carefully removed; and the skin was cleaned with PBS (pH 7.4) before used. Then, the neonatal porcine skin was placed on a flat wax sheet with the epidermis upward and

allowed to be equilibrated with PBS (pH 7.4) for 1 h. AA- and/or Res-loaded DMNs were inserted into the neonatal porcine skin using a thumb pressure for 30 s. Following removal of DMNs from the skin, 1% methylene blue solution was dropped on the applied area and left for 5-10 min. Any surplus methylene blue was removed and then washed out using PBS. Afterward, the blue holes which appeared on the damaged skin were imaged under a Dino-Lite microscope. The percentages of stained blue microholes were calculated using equation 6 (154).

$$\textbf{\% Penetration efficiency} = \left[\frac{\text{Number of stained holes}}{\text{Number of needles}}\right] \times 100 \qquad (6)$$

3.3.5.2 Dissolution study

To determine the dissolution rate of AA- and/or Res-loaded DMNs, the neonatal porcine skin was shaved, and the skin's subcutaneous layer was removed. The skin was placed on tissue paper, which was equilibrated with PBS (pH 7.4) for 1 h (154, 185). AA- and/or Res-loaded DMNs were manually pierced using thumb press into the porcine skin for 30 s. The experiment was carried out in the incubator cabinet at 37ºC. To prevent the DMNs from slipping off the porcine skin, a steel weight (10 g) was placed during testing. To determine the dissolution rates, DMNs were removed from the skin at designated time points (5, 10, 15, 30, 45 min, and 1 h). The remaining height of the needle was investigated using a Dino-Lite microscope (186).

3.3.5.3 Skin permeation and accumulation studies

In vitro skin permeation of AA and Res from DMNs, gel, and cream formulations was investigated using vertical Franz diffusion cells described previously (43, 132). The neonatal porcine skin used in this experiment was prepared as described above in section 3.3.5.1. A neonatal porcine skin was placed on the receptor compartment, which was filled with PBS (pH 7.4) and thermostatically maintained the chamber at 32±1ºC. AA- and/or Res-loaded DMNs inserted into the center of the neonatal porcine skin by thumb pressure

for 30 s. For AA- and/or Res- loaded gel and cream formulations, an equal amount of drugs was applied on the neonatal porcine skin. In this study, 5% AA commercial cream and a self-prepared combination of AA and Res cream formulations were used to compare with AA- and/or Res-loaded DMNs. The receptor chamber was maintained at 32±1℃ and agitation using a magnetic stirrer at 600 rpm. During the experiment, 500 µL of the sample was collected from the receptor compartment at appropriate time intervals of 0.25, 0.5, 1, 2, 4, 6, 8, 12, and 24 h, the same amount of fresh PBS (pH 7.4) was added into the receptor. Finally, the amount of AA and Res was determined using the HPLC as mentioned above. The flux values were obtained by plotting the cumulative amount of drug obtained in each formulation against the time point (n=3) (39). At the end of the experiment, the accumulated amount of AA and Res in neonatal porcine skin was evaluated. The neonatal porcine skin was chopped into small pieces using scissor. AA and Res were extracted from the skin with acetonitrile:water (0.1:1). Next, the sample solution was centrifuged at 14,000 rpm for 20 min to precipitate the skin residue. Finally, the supernatant was filtered and quantified using HPLC.

3.3.6 *In vivo* study in mice

3.3.6.1 *In vivo* dissolution study

In vivo dissolution of AA and/or Res-loaded DMNs into mice was conducted to determine the DMNs application time *in vivo* study. *In vivo* dissolution study was investigated using ICR mice (female, 8 weeks old, 20-25 g) which were purchased from the National Laboratory Animal canter, Mahidol University, Thailand. Animal study in this research was approved by the Committee of the Faculty of Pharmacy, Silpakorn University (U1-08575-2563). The mice were acclimatized under laboratory conditions for one week, with free access to food and water. At the time of study, the mice were anesthetized with Zoletil 100 (tiletamine-zolazepam) (50-80 mg/kg) mixed with xylazine (8-16 mg/kg) by intraperitoneal injection. The hairs on the abdominal skin were shaved by a razor. AA and/or Res-loaded DMNs were applied on the abdominal skin using thumb pressure for 30 s. To avoid

removing the DMNs from the mice, Tegaderm[TM] occlusive film was attached to cover the DMNs patch area. Inserted DMNs were withdrawn at specific time intervals, including 5 min, 10 min, 15 min, 30 min, 45 min, and 1 h. The remaining height of DMN arrays was immediately observed using a Dino-Lite microscope (186).

3.3.6.2 *In vivo* skin permeation and accumulation studies

The *in vivo* study was performed to evaluate the efficacy of AA and/or Res-loaded DMNs. The female ICR mice, 8 weeks old (22~25 g), were used for *in vivo* experiment and divided into five groups as described in Table 4. The animal was acclimatized before the time of the experiment, as described above. After mice were anesthetized, AA-loaded HPMC/PVP-K90 DMNs, AA-loaded PAMA/PVA DMNs, and the combination of AA and Res-loaded Eudragit RL/PVP-K90 DMNs were manually pierced on the back skin (1 DMNs patch per mice) using thumb pressure for 30 s. Tegaderm[TM] occlusive film was attached to the treated skin and left for 24 h. On the other hand, 5% AA commercial cream and the combination of 10% AA and 2% Res cream were applied in the 3 mm circular hole of the Microfoam[®] tape, covered with Tegaderm[TM] occlusive film, and left in place for 24 h. After 24 h, each formulation was removed from mice. The blood sample was collected via cardiac puncture following euthanized with diethyl ether.

To investigate the amount of AA and Res accumulated in mice skin, the surface of the skin was cleaned using PBS to remove excess formulation attached. The skin sample (~ 1 cm^2) where the DMNs or cream formulations applied were cut using scissors and chopped into small pieces. The drug extraction was performed the same to *in vitro* accumulation study as described above. Finally, the amount of AA and Res from blood and skin samples of each group was evaluated by HPLC.

Table 4. *In vivo* permeation study of AA and Res in each group

Mice Groups (n=6)	Formulations
1	AA-loaded HPMC/PVP K-90 DMNs
2	AA-loaded PAMA/PVA DMNs
3	5% AA commercial cream
4	10% AA and 2% Res-loaded Eudragit RL/PVP-K90 DMNs
5	Self-prepared 10% AA and 2% Res combination cream

3.3.6.3 *In vivo* **skin resealing study**

In vivo skin resealing ability was examined after removing AA- and/or Res-loaded DMNs from mice skin. This study was done to evaluate the safety and resealing time of DMNs in mice. The process for manipulating animals before the testing was similar to the *in vivo* dissolution and skin permeation studies. Briefly, AA- and/or Res-loaded DMNs were applied on the back of anesthetized mice using thumb pressure for 30 s and kept in place for 2.5 h. The DMNs were removed from all mice; the treated skin was stained with 1% methylene blue solution for 10 min at a designated time point, including 0, 1, 2, 4, 6, 8, 12, and 24 h. Afterward, the excess methylene blue was cleaned with PBS solution. The skin was examined under a Dino-Lite microscope to determine the characteristic of the skin and the number of stained microholes. During the study, the mice were monitored for any skin abnormality sign within 24 h (135).

3.3.7 Human study

3.3.7.1 Study approval and study subjects

The human study was conducted following the International Council on Harmonisation of Technical Requirements for Registration of Pharmaceuticals for Human Use (ICH) and good clinical practice guidelines (GCP). Fifteen healthy volunteers (three men and twelve women) who met the

inclusion criteria of aged between 25-40 years old were randomized included in the study. The study exclusion criteria were pregnancy, child, a medical history of any active skin diverse, the immunosuppressive therapies within 3 months, and the presence on damaged skin or around the test sites. The number of subjects was calculated using G*Power 3.1. (187). All participants have received the information protocol containing the terms and conditions for clinical testing and signed a research compliance agreement. Moreover, they were not allowed to apply cosmetic products around the study's skin site before the experiment for at least 12 h. All participants stayed under the controlled room (20-25ºC and 40-60% RH) for 10 min before the assessment. DMNs patch used in the human study were sterilized under a UV lamp for 15 min (23).

3.3.7.2 Analysis of skin melanin, skin erythema, transepidermal water loss (TEWL), skin hydration, and skin elasticity

The forearm of each participant was used as the test site. Before the experiment, the skin melanin, skin erythema, TEWL, skin hydration, and skin elasticity of the application skin site was measured by the DermaLab® series (Cortex). Afterward, the skin was cleaned using 70% ethanol with a cotton patch and dried. The test site was marked, then the sterilized combination of AA and Res-loaded DMNs were applied on the forearm of each participant using thumb pressure for 30 s. The DMNs patch was left at the application site for 24 h by covering with waterproof adhesive film. At 24 h, DMNs were carefully removed from the skin of each volunteer. The skin melanin, skin erythema, TEWL, skin hydration, and skin elasticity of the volunteer's skin was immediately measured by DermaLab® series. The observed data were compared before and after the application of DMNs patch (188).

3.3.7.3 Safety assessment

The sign of any skin abnormalities such as swelling, redness, erythema, and itching was observed throughout the application period of DMNs. Moreover, the applied area of the forearm was physically examined and imaged using a Dino-Lite microscope.

3.3.8 Stability study

The physical and chemical stability of AA- and/or Res-loaded DMNs were analyzed at various periods (0, 1, 2, 3, and 6 months). All formulations were separated into two groups: 1) sealed in PE packaging to prevent humidity and 2) unsealed in ambient air. According to ICH guidelines, both groups were kept at $25\pm2°C$, $60\pm5\%$ RH in the incubator. To compare the stability of resveratrol by light effect and temperature, another group of the combination of AA and Res-loaded DMNs were stored at $5\pm3°C$ by wrapping with a sealed aluminum bag. At the determined time point, the physical stability of DMNs (color, shape and mechanical strength) was evaluated. In the case of chemical stability, DMNs were completely dissolved in 10 mL PBS, and the sample solutions were collected. Then, the sample solution was transferred into an Ultrafilter (Amicon®, MW cut-offs < 3 kDa) and centrifuged at 14,000 ×g for 20 min. Finally, the contents of AA and Res were measured by HPLC.
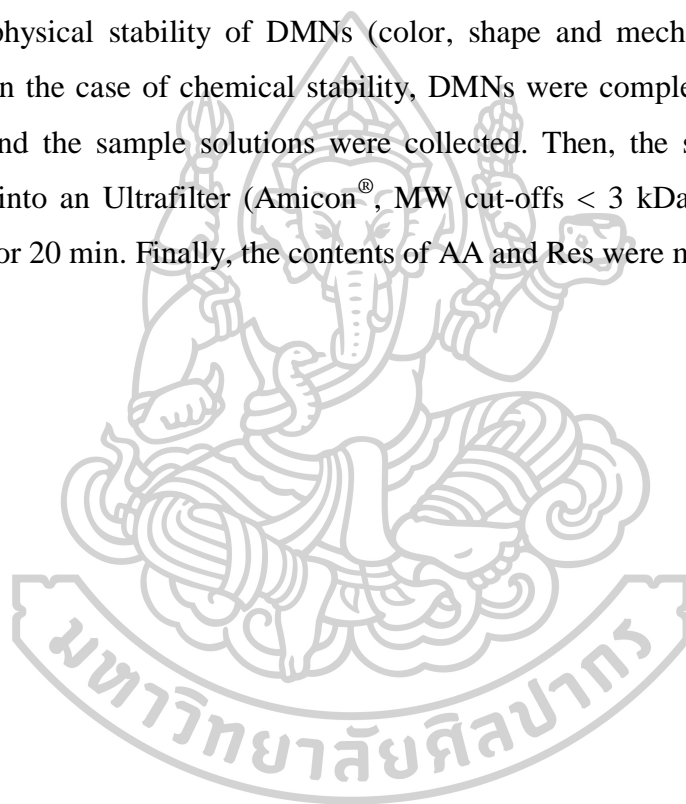
CHAPTER 4

RESULTS AND DISCUSSION

4.1 Cell viability

4.1.1 Effect of alpha-arbutin (AA)

The cell viability of B16F10 melanoma cells after AA treatment was investigated using an MTT assay. The result of the AA effect on B16F10 melanoma cells at 48 h is presented in Figure 24. The numbers of viable cells were more than 80% at 10-2000 μg/mL of AA, which confirmed no cytotoxicity on B16F10 melanoma cells at these concentrations. However, the viable cells were slightly decreased when increasing AA concentration from 2000 to 4000 μg/mL. The percentage of cell viability decreased to 67.84% at 4000 μg/mL AA.
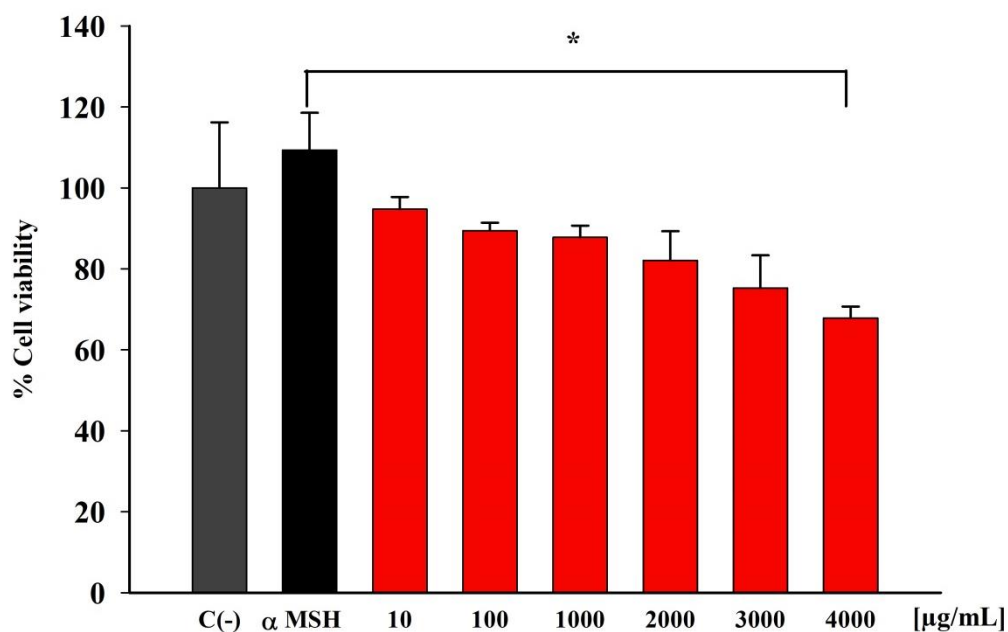
Figure 24. Effects of alpha-arbutin (AA) on cell viability in B16F10 melanoma cells induced with α-MSH (100 nM) for 48 h (*$p<0.05$, n=3)

4.1.2 Effect of resveratrol (Res)

The percentage cell viability of Res on B16F10 melanoma cells is shown in Figure 25. After 48 h cells incubation, the viable cells were slightly decreased when increasing Res concentration. However, the amounts of viable cells were more than 80% at 5-20 µg/mL Res. Hence, there were no significant cytotoxic on B16F10 cells at Res concentration of 5-20 µg/mL. However, Res significantly decreased the number of viable cells in a concentration-dependent manner at 25 µg/mL (67.90%) and 50 µg/mL (46.59%).
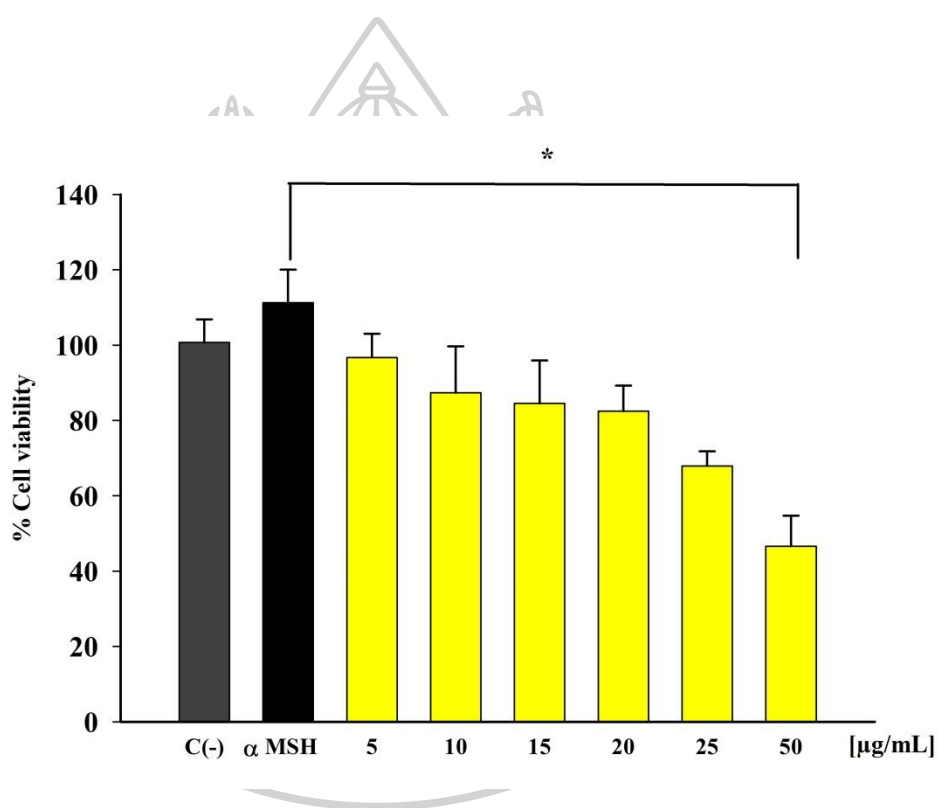
Figure 25. Effects of resveratrol (Res) on cell viability in B16F10 melanoma cells induced with α-MSH (100 nM) for 48 h (*$p<0.05$, n=3)

4.2 Melanin content

4.2.1 Effect of alpha-arbutin (AA)

The inhibitory effect of AA on melanogenesis in B16F10 melanoma cells induced by α-MSH compared with negative control and positive control (kojic acid-treated) is shown in Figure 26. The melanogenesis was assessed by the determination of melanin content in which increased approximately 20% in α-MSH (100 nM) treated control cells when compared with untreated control cells ($p<0.05$). According to the results, dose-dependent inhibition of α-MSH stimulated melanogenesis by AA was observed and significantly decreased compared to the α-MSH treated control group ($p<0.01$). The percentage of melanin contents following treated by AA was 80% at 100 µg/mL, 70% at 500 µg/mL, 65% at 1000 µg/mL, 56% at 1500 µg/mL and 42% at 2000 µg/mL, respectively. Additionally, AA at the 2000 µg/mL concentration can inhibit α-MSH induced melanin synthesis similar to kojic acid (60 µg/mL). According to the percentage cell viability and percentage melanin content results, 2000 µg/mL AA was selected as a fixed concentration for combination treatment with Res against melanogenesis.
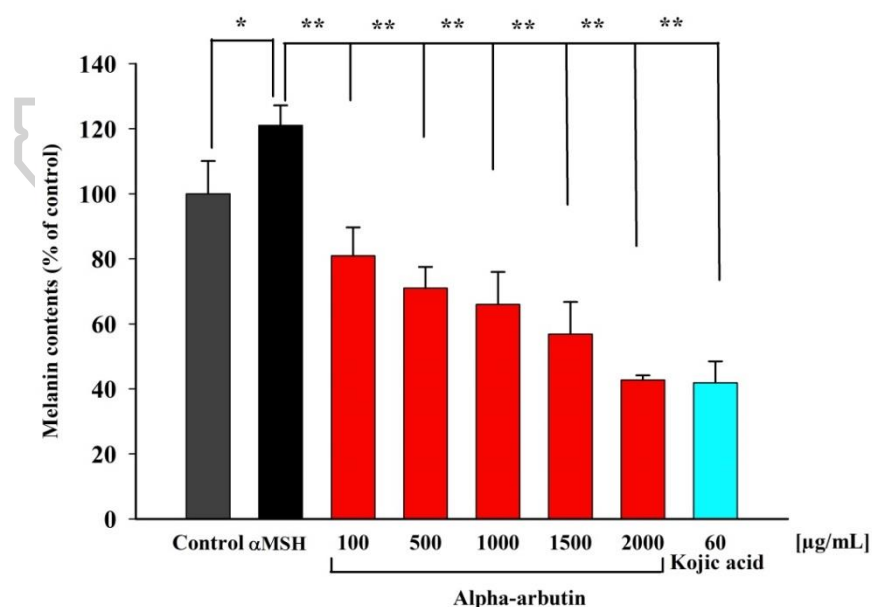
Figure 26. Effects of alpha-arbutin (AA) on melanin content in B16F10 melanoma cells. All cells except the control group were stimulated melanogenesis by α-MSH (100 nM) for 48 h. (*$p<0.05$ vs. control, ** $p<0.01$ vs. α-MSH treated group, n=3)

4.2.2 Effect of resveratrol (Res)

In Figure 27, the percentage of melanin contents increased in α-MSH (100 nM) stimulated B16F10 melanoma cells compared to the non-stimulated B16F10 melanoma cells. Moreover, Res reduced the melanin contents depending on the concentration manner by approximately 97% at 5 µg/mL, 94% at 10 µg/mL, 68% at 15 µg/mL, and 45% at 20 µg/mL. Although the results of all Res concentrations were significantly different when compared with the α-MSH induced control group ($p<0.01$), there was no significant difference between Res (20 µg/mL) and kojic acid (60 µg/mL). Therefore, Res (20 µg/mL) was chosen for next combination experiment of melanin content assay.
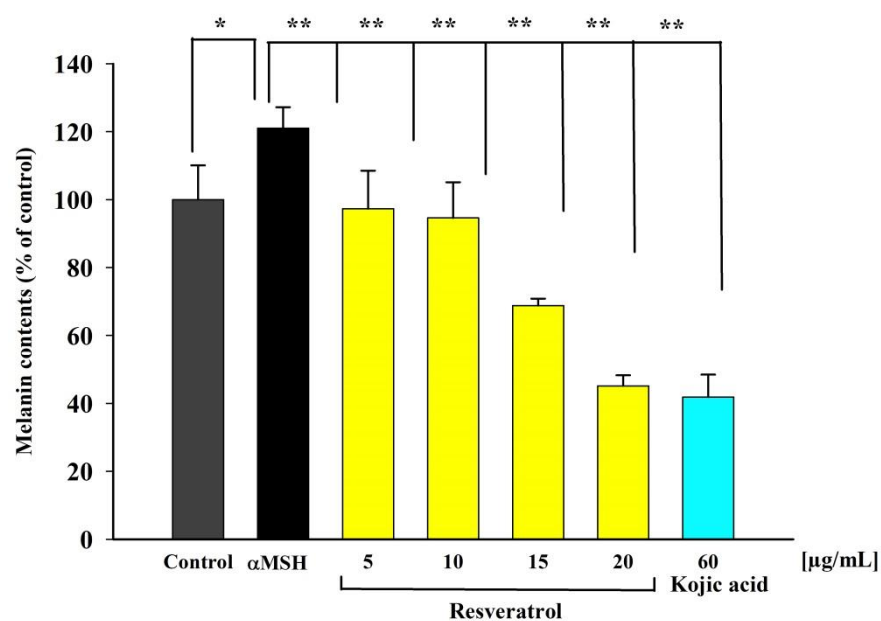

Figure 27. Effects of resveratrol (Res) on melanin content in B16F10 melanoma cells . All cells except control group were stimulated melanogenesis by α-MSH (100 nM) for 48 h. (*$p<0.05$ vs. control, ** $p<0.01$ vs. α-MSH treated group, n=3)

4.2.3 Combination treatment of alpha-arbutin (AA) and resveratrol (Res) on melanin cell inhibition

The cell growth inhibition effects of AA alone (500-3000 µg/mL) or Res alone (5-30 µg/mL) and combination of AA and Res against B16F10 melanoma cells for 48 h are illustrated in Figure 28 (a) and (b). According to the results, the percentage of melanin cell growth inhibition was dependent on the concentration treatment. It can be seen that both combination treatment of AA with Res had a potent inhibitory effect when compared to a single treatment of AA or Res alone.

The combination index (CI) value for each drug mixture was calculated using computer CompuSyn where a drug combination had a synergistic or an antagonistic effect. Tables 5 and 6 summarized the CI values of AA and Res from melanin content assay. Most of the combination mixtures showed an antagonistic effect (CI>1). Antagonistic effects can be found when the AA concentration ranged from 1000 to 3000 µg/mL, which was combined with the fixed concentration of Res at 20 µg/mL. Furthermore, combination treatment of increasing the concentration of Res (10-30 µg/mL) with a fixed amount of AA (2000 µg/mL) was also induced the antagonistic effects on melanin cells. Of note, the cytotoxic effects were observed when the cells were treated with the concentration higher than their fixed concentration amount as discussed in section 4.1. The CI values lower than 1 were found in the combination of AA (100 µg/mL and 500 µg/mL) and 20 µg/mL of Res mixtures which represented the synergistic effects (Table 5). Moreover, the synergistic effect (CI<1) was found in a combination mixture of AA (2000 µg/mL) with Res (5 µg/mL) (Table 6). Therefore, it can be suggested that a synergistic effect can be produced a potent inhibition of melanogenesis in B16F10 melanoma cells, which is a benefit for skin whitening. Among them, the lowest CI value (0.58) was found in the group of 20 µg/mL Res mixed with 100 µg/mL AA (ratio of 1:5), which was selected for a combination formulation of 10 % AA and 2 % Res-loaded DMNs fabrication.
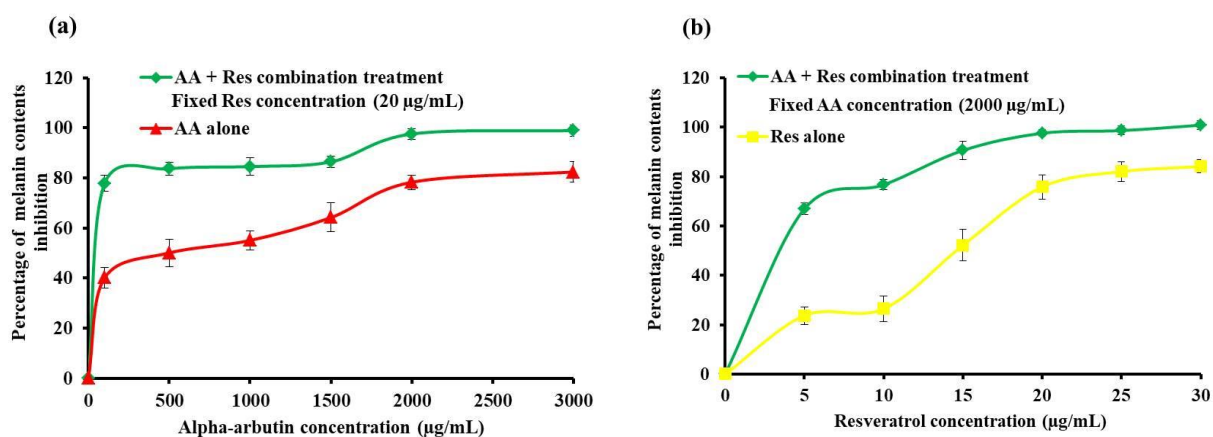
Figure 28. The percentage of cell growth inhibition in B16F10 melanoma cells after treatment with (a) AA alone (500-3000 µg/mL) compared to a combination of AA (500-3000 µg/mL) with Res at fixed concentration of 20 µg/mL and (b) Res alone (5-30 µg/mL) compared to a combination of Res (5-30 µg/mL) with AA (Fixed concentration at 2000 µg/mL) for 48 h (mean ± SD, n=3)

Table 5. CI analyses of combination treatment at different concentrations of AA (100-3000 µg/mL) with a fixed concentration of Res in B16F10 melanoma cells for 48 h

AA (µg/mL)	Res (µg/mL)	AA:Res ratio	CI values*
100	20	5:1	0.58 ± 0.01
500	20	25:1	0.76 ± 0.02
1000	20	50:1	1.10 ± 0.01
1500	20	75:1	1.04 ± 0.02
2000	20	100:1	0.98 ± 0.05
3000	20	150:1	2.13 ± 0.03

* CI<1 means synergism, while CI>1 means antagonism

Table 6. CI analyses of combination treatment at different concentration of Res (5-30 µg/mL) with a fixed concentration of AA in B16F10 melanoma cells for 48 h
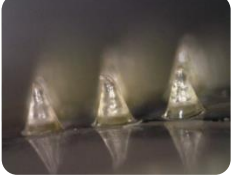
AA (µg/mL)	Res (µg/mL)	AA:Res ratio	CI values*
2000	5	400:1	0.66 ± 0.01
2000	10	200:1	1.25 ± 0.01
2000	15	133:1	1.24 ± 0.03
2000	20	100:1	0.98 ± 0.01
2000	25	80:1	1.26 ± 0.05
2000	30	67:1	1.63 ± 0.04

* CI<1 means synergism, while CI>1 means antagonism

4.3 Optimal formulation for blank DMNs

The polymer mixture of some weight ratio was separated into two layers, and they are not suitable for the fabrication of DMNs such as 14%w/w Eudragit E/40%w/w PVP-K90 (1:1) and 14%w/w Eudragit RS/ 40%w/w PVP-K90 (1:1). Although most of the polymer mixture was homogenous, DMNs fabricated from these combination weight ratios were brittle and easily broken when DMNs were removed from the micromold, including 14%w/w Eudragit E/40%w/w PVP-K90 (4:1), and 14%w/w Eudragit RS/ 20%w/w PVA (2:1). Moreover, some formulations including 14%w/w Eudragit RS/ 40%w/w PVP-K90 (2:1), 100%w/w PAMA/ 20%w/w PVA (1:1), and 14%w/w Eudragit RS/ 20%w/w PVA (1:1) did not completely form DMNs arrays. The pre-formulation data of blank DMNs are listed in Table 7. The suitable weight ratios of polymers mixtures used to fabricate the optimal blank DMNs are listed in Table 8.

Table 7. Pre-formulation results of blank DMNs

Blank DMNs formulations	Images	Description
14%w/w Eudragit E : 40%w/w PVP-K90 (1:1)	-	Not homogenous
14%w/w Eudragit RS : 40%w/w PVP-K90 (1:1)	-	Not homogenous
14%w/w Eudragit E : 40%w/w PVP-K90 (4:1)		DMNs were brittle and easily broken
14%w/w Eudragit RS : 40%w/w PVP-K90 (2:1)		All needles did not completely formed
8%w/w HPMC : 40%w/w PVP-K90 (2:1)		DMNs were bend and not strong
8%w/w HPMC : 40%w/w PVP-K90 (1:2)		DMNs were brittle and easily broken
100% w/w PAMA : 20%w/w PVA (1:1)		DMNs were soft and not strong

100% w/w PAMA : 20%w/w PVA (1:2), (1:3)		DMNs were not strong

Table 8. The selected combination weight ratios of blended polymer solutions for the optimal blank DMNs

No.	Combination weight ratios of polymers mixture						
	HPMC (8%w/w)	PAMA (100%w/w)	PVA (20%w/w)	Eudragit E100 (14%w/w)	Eudragit RS100 (14%w/w)	Eudragit RL100 (14%w/w)	PVP-K90 (40%w/w)
1	1	-	-	-	-	-	1
2	-	1	4	-	-	-	-
3	-	-	-	1	-	-	2
4	-	-	-	-	1	-	2
5	-	-	-	-	-	1	2
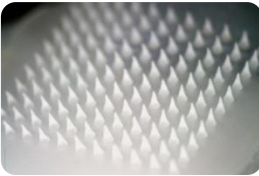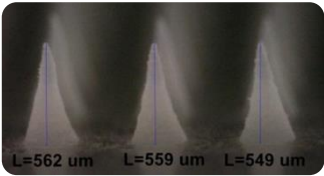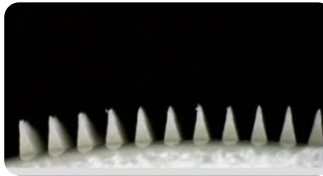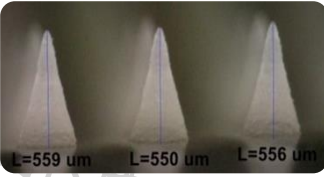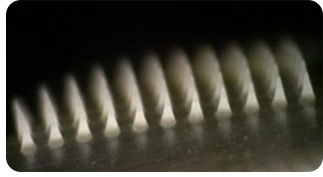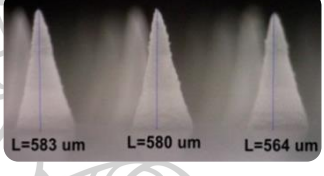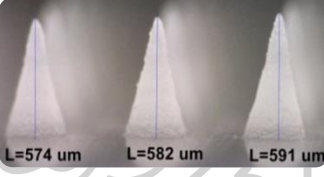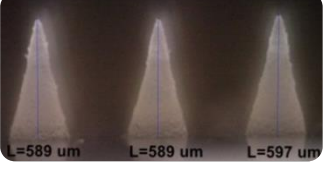
4.4 Characterization of DMNs

4.4.1 Morphology of DMNs

4.4.1.1 Blank DMNs

Table 9 shows the morphology of all optimal blank DMNs formulations characterized using a Dino-Lite digital microscope. It can be seen that all blank DMNs were completely formed cone-shaped needles with elegant appearance and sharp arrays on a strong baseplate. Table 10 illustrates the height of needles from each blank DMNs formulation measured by a Dino-Lite microscope. All needle heights were found between 555-591 μm depending on the types of polymer used for fabrication. Furthermore, the details of the physical appearance of all blank DMNs, including shape and sharpness, were investigated by SEM using the magnification of 30x, 120x, and 400x, respectively (Table 11).

Table 9. Morphology of blank DMNs imaged by Dino-Lite microscope
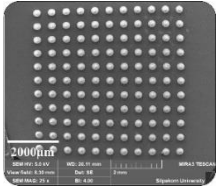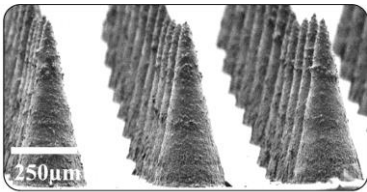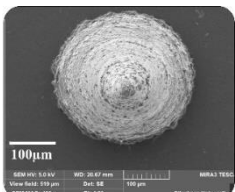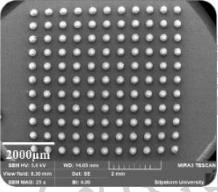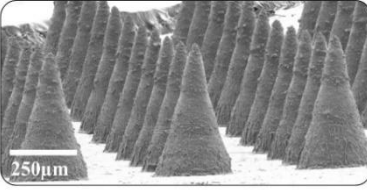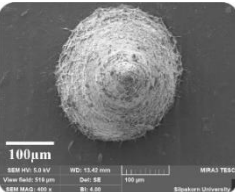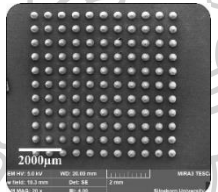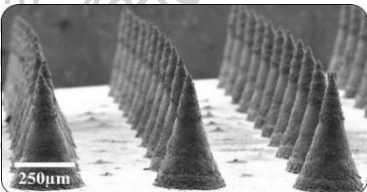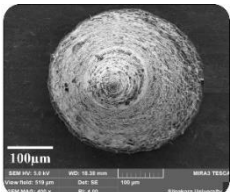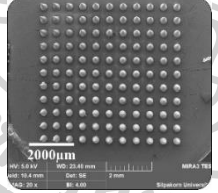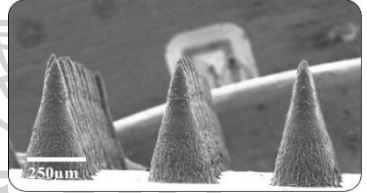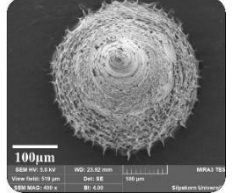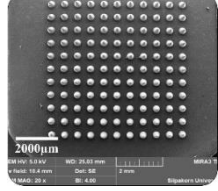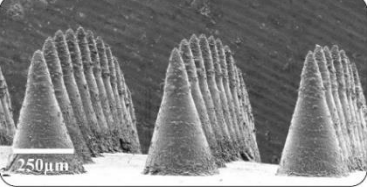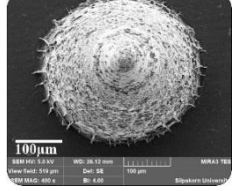
Types of blank DMNs	Images of blank DMNs by Dino-Lite microscope		
	Top view (31x)	Side view (200x)	Tilt view (45x)
HPMC/PVP-K90 DMNs		L=562 um L=559 um L=549 um	
PAMA/PVA DMNs		L=559 um L=550 um L=556 um	
Eudragit E/PVP-K90 DMNs		L=583 um L=580 um L=564 um	
Eudragit RS/PVP-K90 DMNs		L=574 um L=582 um L=591 um	
Eudragit RL/PVP-K90 DMNs		L=589 um L=589 um L=597 um	

Table 10. Averages needles height of blank DMNs (mean ± SD, n=3)

Types of blank DMNs	Averages needles height (µm)
HPMC/PVP-K90	556.67 ± 6.81
PAMA/PVA	555.00 ± 4.10
Eudragit E/PVP-K90	575.67 ± 9.14
Eudragit RS/PVP-K90	582.33 ± 7.61
Eudragit RL/PVP-K90	591.67 ± 4.13
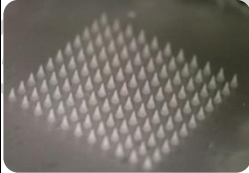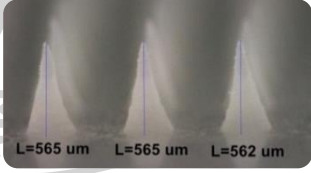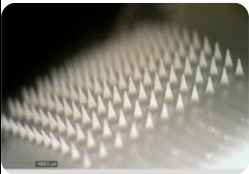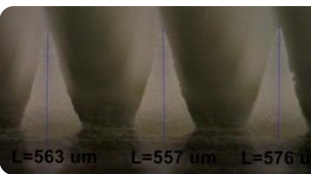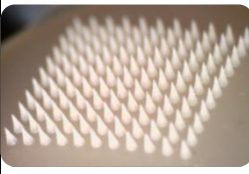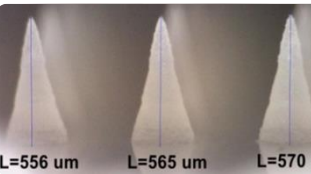
Table 11. Morphology of blank DMNs imaged by SEM

Types of blank DMNs	Images of blank DMNs by SEM		
	Top view (30x)	Side view (120x)	Tilt view (400x)
HPMC/PVP-K90 DMNs			
PAMA/PVA DMNs			
Eudragit E/PVP-K90 DMNs			
Eudragit RS/PVP-K90 DMNs			
Eudragit RL/PVP-K90 DMNs			

4.4.1.2 AA- and/or Res-loaded DMNs

The morphology of AA-loaded DMNs, Res-loaded DMNs, and the combination of AA and Res-loaded DMNs were imaged by Dino-Lite microscope, as shown in Table 12. All formulations of DMNs contained 121 needles with cone-shape; the baseplates appeared solid and smooth without any defects. Moreover, all arrays were sharp, strong, and had an elegant appearance. The height of cone-shaped needles was measured by Dino-Lite software and presented in Table 13. According to the results, all needles showed a minor deviation from the micromold dimensions. Their heights were enough to penetrate through the SC and upper dermis of the skin. Chang *et al.* proved that approximately 300 μM of MN's height was sufficient to penetrate the dermis layer in a histology study. Moreover, in this study, SEM measurement was done to confirm the morphology of DMNs (Table 14).

Table 12. Morphology of AA- and/or Res- loaded DMNs imaged by Dino-Lite microscope
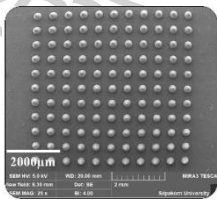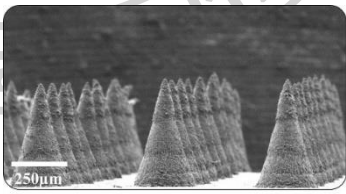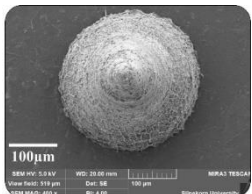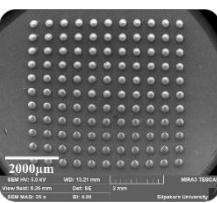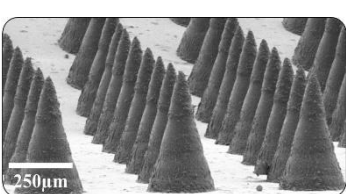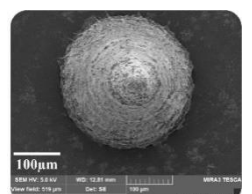
Types of DMNs	Images of DMNs by Dino-Lite microscope		
	Top view (31x)	Side view (200x)	Tilt view (45x)
8 % AA-loaded HPMC/PVP-K90 DMNs		L=565 um L=565 um L=562 um	
8 % AA-loaded PAMA/PVA DMNs		L=563 um L=557 um L=576 um	
5% Res-loaded Eudragit E/PVP-K90 DMNs		L=556 um L=565 um L=570 um	

5% Res-loaded Eudragit RS/PVP-K90 DMNs		L=568 um L=566 um L=574 um	
10% AA- and 2% Res-loaded Eudragit RL/PVP-K90 DMNs		L=594 um L=594 um L=591 um	

Table 13. Averages needles height of AA- and/or Res-loaded DMNs (mean±SD, n=3)

Types of drugs-loaded DMNs	Averages needles height (µm)
8 % AA-loaded HPMC/PVP-K90	563.67 ± 1.37
8 % AA-loaded PAMA/PVA	565.33 ± 8.69
5% Res-loaded Eudragit E/PVP-K90	563.67 ± 6.35
5% Res-loaded Eudragit RS/PVP-K90	569.33 ± 3.72
10% AA and 2% Res-loaded Eudragit RL/PVP-K90	593.00 ± 1.55

Table 14. Morphology of AA- and/or Res-loaded DMNs imaged by SEM

Types of DMNs	Images of DMNs by SEM		
	Top view (30x)	Side view (120x)	Tilt view (400x)
8 % AA-loaded HPMC/PVP-K90 DMNs			
8 % AA-loaded PAMA/PVA DMNs			

5% Res-loaded Eudragit E/PVP-K90 DMNs			
5% Res-loaded Eudragit RS/PVP-K90 DMNs			
10% AA- and 2% Res-loaded Eudragit RL/PVP-K90 DMNs			
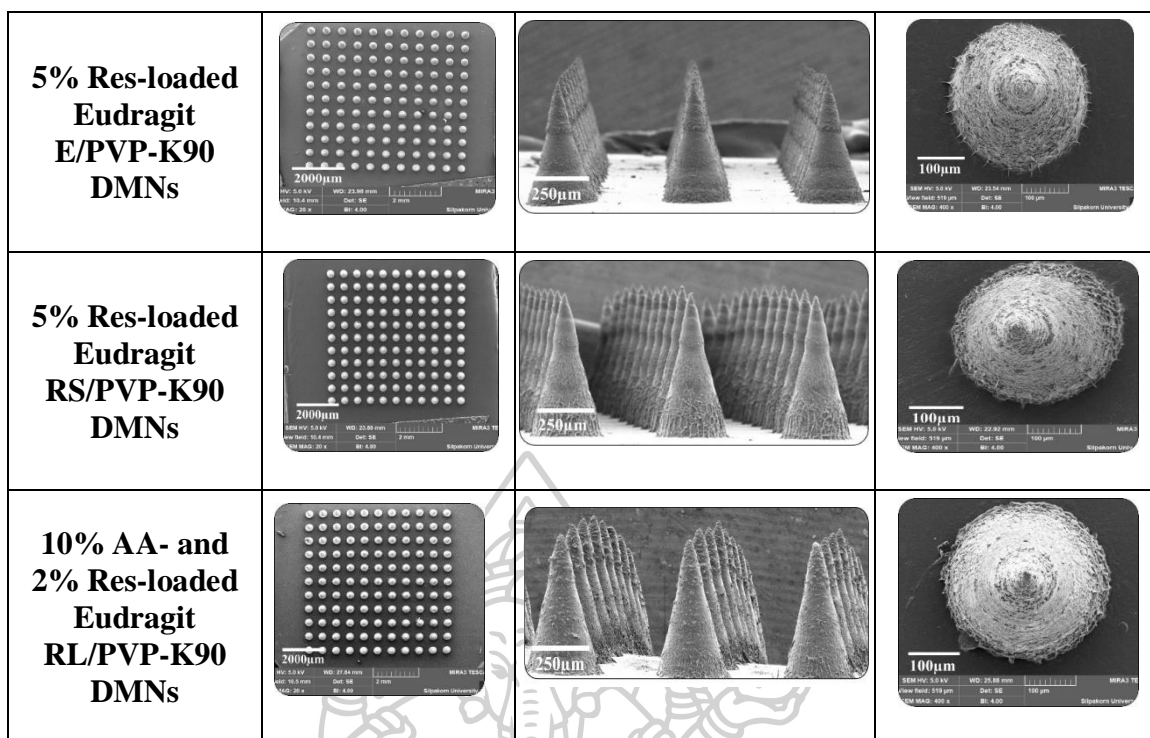
4.4.2 Mechanical properties study

4.4.2.1 Blank DMNs

The mechanical properties study was performed to evaluate the ability of needles to resist the force applied. A Texture analyzer was used to analyze the effect of compression on the heights of individual needles for all blank DMNs (Figure 29). The results described that all blank DMNs' height reduction was gradually increased when increasing the compression force from 0.028 N to 0.11 N, respectively. According to the compression results of percentage of reduction of DMNs height, Eudragit RL/PVP-K90 DMNs exhibited higher mechanical resistance than other blank DMNs; the reduction ranged between 1.5% and 3.8% of the initial height. On the other hand, the percent reduction in the original DMNs height was significantly increased in Eudragit E/PVP-K90 DMNs, approximately 8.8% among other blank DMNs. In PAMA/PVA DMNs, Eudragit RS/PVP-K90 DMNs, and HPMC/PVP-K90; the reduced height following the application force of 0.089 N per needle (10.769 N per patch) was 1.9 - 3.9%, 1.5 - 6%, and 3.9 - 5.7% of the initial

height, respectively. Furthermore, there was no found cracking of the baseplates from all blank DMNs formulations. These compression results revealed that all blank DMNs had a percentage reduction height less than 10%, indicating that the fabricated DMNs were strong enough to be inserted into the skin. The application force of 0.089 N per needle was the maximum human typically insertion force on MNs; therefore, the DMNs formulation should have the ability to resist the human application force (171).
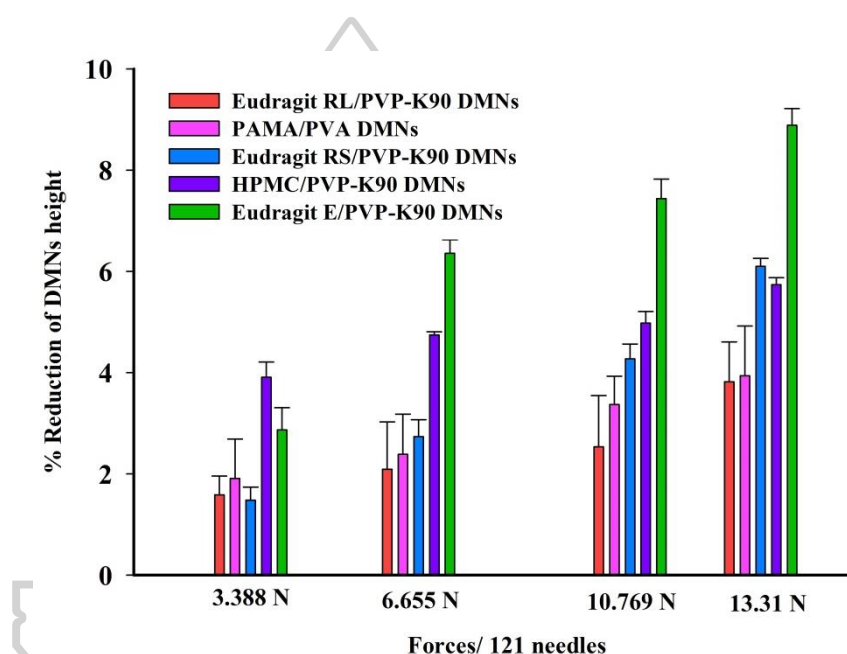
Figure 29. The percentage reduction of DMNs height of ■ blank Eudragit RL/PVP-K90 DMNs, ■ blank PAMA/PVA DMNs, ■ blank Eudragit RS/PVP-K90 DMNs, ■ blank HPMC/PVP-K90 DMNs, ■ blank Eudragit E/PVP-K90 DMNs following the different compression forces (3.388 N, 6.655 N, 10.769 N, and 13.31 N per patch), (mean ± SD, n=3)

4.4.2.2 AA-loaded DMNs

The percentage reduction heights of 8% AA-loaded HPMC/PVP-K90 DMNs and 8% AA-loaded PAMA/PVA DMNs are illustrated in Figure 30. The reduction height of 8% AA-loaded PAMA/PVA DMNs ranged between 0.78-3.22% of the original height, whereas 8% AA-loaded HPMC/PVP-K90 DMNs ranged between 1.2-4.47%. Moreover, both 8% AA-loaded DMNs showed good physical features without cracking at the baseplate in the mechanical test. The results showed that 8% AA-loaded PAMA/PVA DMNs exhibited the ability to resist the compression force slightly higher than that of 8% AA-loaded HPMC/PVP-K90 DMNs.
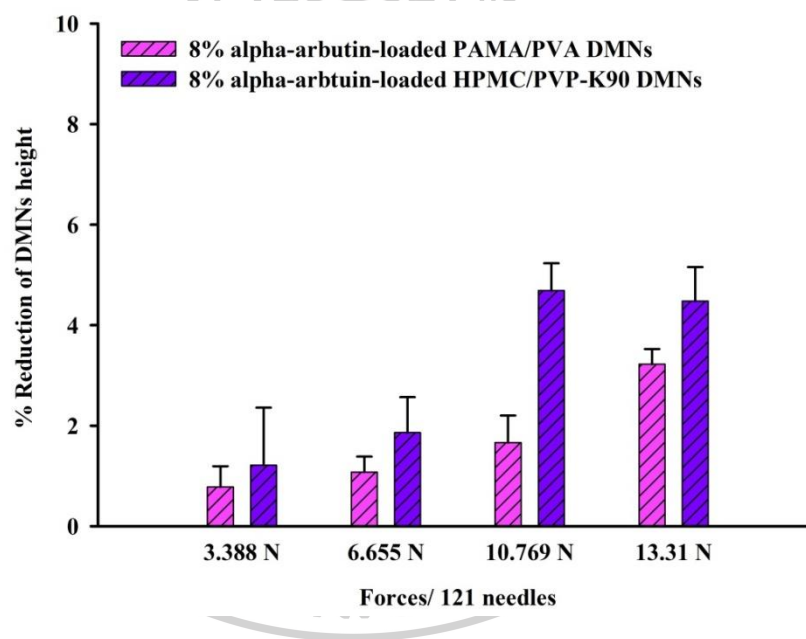
Figure 30. The percentage reduction needles height of 8% AA-loaded HPMC/PVP-K90 DMNs and 8% AA-loaded PAMA/PVA DMNs following the various compression forces (3.388 N, 6.655 N, 10.769 N, and 13.31 N per 121 needles)

4.4.2.3 Res-loaded DMNs

The mechanical properties of 5% Res-loaded Eudragit E/PVP-K90 DMNs and 5% Res-loaded Eudragit RS/PVP-K90 DMNs are shown in Figure 31. The results suggested no significant difference between the mechanical resistance of 5% Res-loaded Eudragit E/PVP-K90 DMNs and 5% Res-loaded Eudragit RS/PVP-K90 DMNs. The percentage reduction height of 5% Res-loaded Eudragit E/PVP-K90 DMNs ranged between 1.92% and 10.11%. In the case of 5% Res-loaded Eudragit RS/PVP-K90 DMNs, the reduction height was between 0.84% and 9.55% of the initial height. In addition, the baseplates of both DMNs were smooth and flat without any fracture after applying the compression forces.
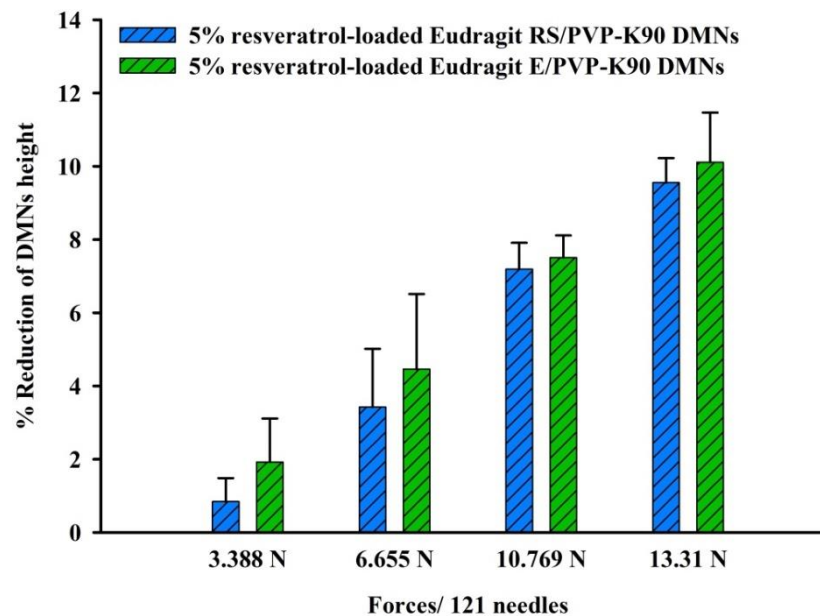
Figure 31. The percentage reduction needles height of 5% Res-loaded Eudragit E/PVP-K90 DMNs and 5% Res-loaded Eudragit RS/PVP-K90 DMNs following the various compression forces (3.388 N, 6.655 N, 10.769 N, and 13.31 N per 121 needles)

4.4.2.4 The combination of AA and Res-loaded DMNs

The mechanical strength of 10% AA and 2% Res-loaded Eudragit RL/PVP-K90 DMNs are examined in compression forces, including 3.388 N, 6.655 N, 10.769 N, and 13.31 N per patch as shown in Figure 32. The results presented that the reduction in DMNs height was exhibited between 1.49% and 8.97% of the initial height. Moreover, the physical appearance of DMNs did not show any cracking of the baseplate.
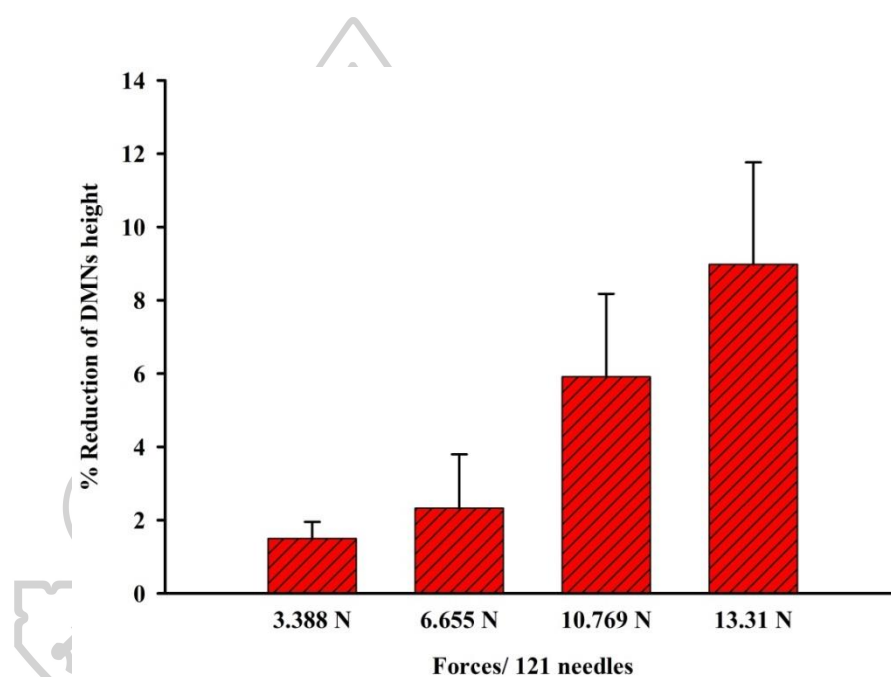
Figure 32. The percentage needles reduction height of the combination of 10% AA and 2% Res-loaded Eudragit RL/PVP-K90 DMNs following the various compression forces (3.388 N, 6.655 N, 10.769 N, and 13.31 N per 121 needles)
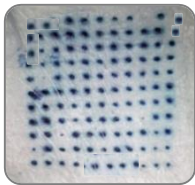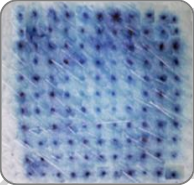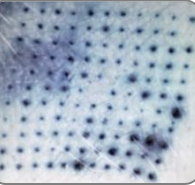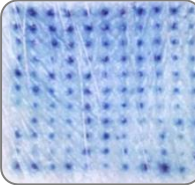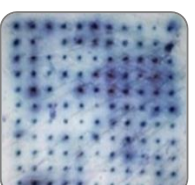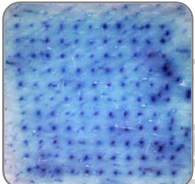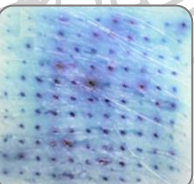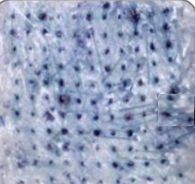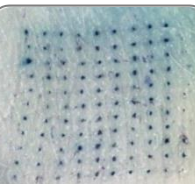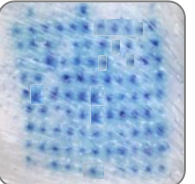
4.4.3 *In vitro* skin insertion and visualization studies

The characteristics of DMNs insertion study were performed with the full thickness neonatal porcine skin. For this experiment, a manual insertion method was used to apply all formulations of DMNs following the methylene blue staining after withdrawal of the DMNs. Table 15 shows that the image of stained microholes created in each neonatal porcine skin from different formulations of DMNs. These

results revealed that all DMNs were successfully inserted into the neonatal porcine skin and created the stained microholes almost 100%. Therefore, all formulations of blank DMNs and drugs-loaded DMNs were efficiently penetrated the SC of the skin.

Table 15. Images of stained microholes from neonatal porcine skin following the application of various DMNs formulations

	HPMC/PVP K90 DMNs	PAMA/PVA DMNs	Eudragit E/PVP K-90 DMNs	Eudragit RS/PVP K-90 DMNs	Eudragit RL/PVP K-90 DMNs
Blank					
Drug	8 % AA	8% AA	5% Res	5% Res	10%AA+2%Res

4.4.4 Loading efficiency and loading capacity

4.4.4.1 AA-loaded DMNs

The maximum amount of AA that could be loaded into the polymer blends of HPMC/PVP-K90 DMNs and PAMA/PVA DMNs is presented in Figure 33. The results suggested that the percentage of the loading efficiency and loading capacity of 8% AA-loaded HPMC/PVP-K90 DMNs higher than that of 8% AA-loaded PAMA/PVA DMNs ($p<0.05$). The percentage loading efficiency of 8% AA-loaded HPMC/PVP-K90 DMNs and 8% AA-loaded PAMA/PVA DMNs was $88.81 \pm 2.05\%$ and $79.72 \pm 7.50\%$, respectively. The percentage loading capacity of 8% AA-loaded HPMC/PVP-K90 DMNs and 8% AA-loaded PAMA/PVA DMNs was $35.82\pm1.55\%$ and $23.17\pm5.60\%$,

respectively. This finding in line with Zhang *et al*. who found that the drug loading capacity gradually increased when decreasing in molecular weight of the polymer (189, 190). Although the molecular weight of the HPMC/PVP-K90 polymer mixture was higher than PAMA/PVA polymer mixture, the weight ratio used for fabrication of PAMA/PVA DMNs (1:4) had a higher amount than HPMC/PVP-K90 DMNs (1:1). Thus, HPMC/PVP-K90 DMNs had been found to increase percentage loading efficiency and loading capacity than PAMA/PVA DMNs.
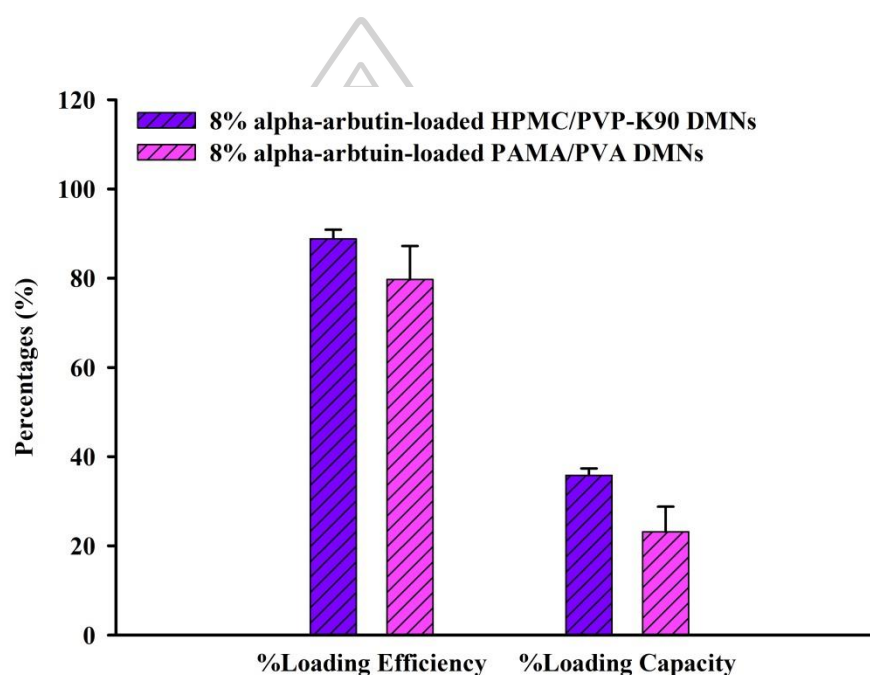
Figure 33. The percentage loading efficiency and loading capacity of 8% AA-loaded HPMC/PVP-K90 DMNs and 8% AA-loaded PAMA/PVA DMNs

4.4.4.2 Res-loaded DMNs

The percentage loading efficiency and loading capacity of 5% Res-loaded Eudragit E/PVP-K90 DMNs and 5% Res-loaded Eudragit RS/PVP-K90 DMNs are shown in Figure 34. According to the results, the percentage loading efficiency of 5% Res-loaded Eudragit RS/PVP-K90 DMNs (95.95±0.69) greater than 5% Res-loaded Eudragit E/PVP-K90 DMNs (92.48±1.87), respectively. In addition, the resveratrol capacity that could be loaded into the polymer mixture was 22.86±4.37% for Res-loaded Eudragit

RS/PVP-K90 DMNs and 21.49±1.69% for 5% Res-loaded Eudragit E/PVP-K90 DMNs. However, there were no significant difference between loading efficiency and loading capacity of both DMNs (p>0.05). The results corresponded to Calis *et al*. who described that the maximum capacity of the drug that can be loaded is around 20-30% because there is a limited capacity of the interaction between the hydrophobic polymer and hydrophobic drug (190). Typically hydrophobic drug has a greater affinity to hydrophobic polymer because of hydrophobic-hydrophobic interaction. For this reason, a lower amount of loading capacity was found in DMNs fabricated by Eudragit polymer (hydrophobic polymer) and Res (hydrophobic drug). Hence, the hydrophilic polymer (PVP-K90) was used to prepare a polymer mixture solution (191). According to the results, Res can be successfully loaded into each type of polymer mixture in this study.
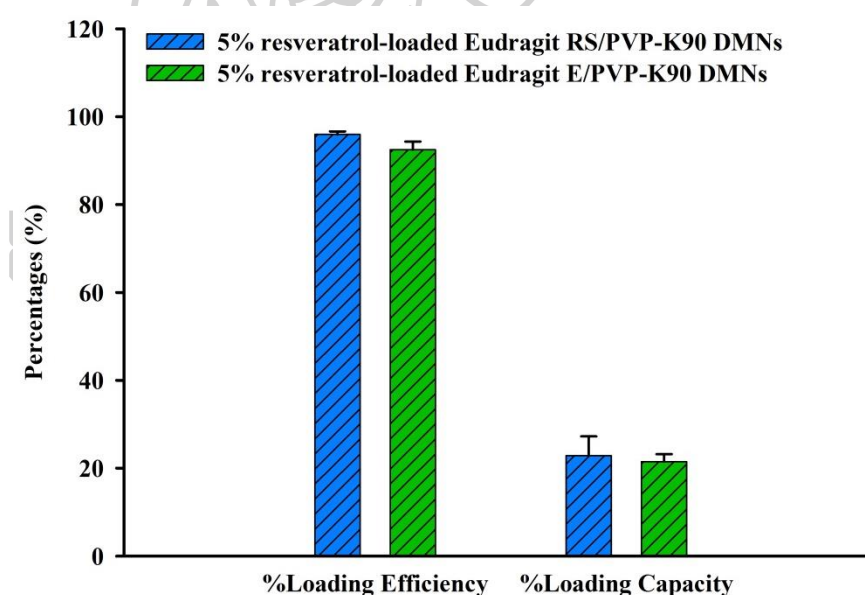
Figure 34. The percentage loading efficiency and loading capacity of 5% Res-loaded Eudragit E/PVP-K90 DMNs and 5% Res-loaded Eudragit RS/PVP-K90 DMNs

4.4.4.3 The combination of AA and Res-loaded DMNs

The percentage amount of AA and Res loaded into the Eudragit RL/PVP-K90 polymer mixture is shown in Figure 35. The results showed that the percentage loading efficiency of AA and Res from the DMNs was 95.19±0.94% and 96.17±2.80%, whereas the loading capacity was 36.76±2.53% and 13.84±2.09%, respectively. These results described that both kinds of drugs, including AA (hydrophilic drug) and Res (hydrophobic drug), were successfully loaded into Eudragit RL/PVP-K90 polymer mixture.
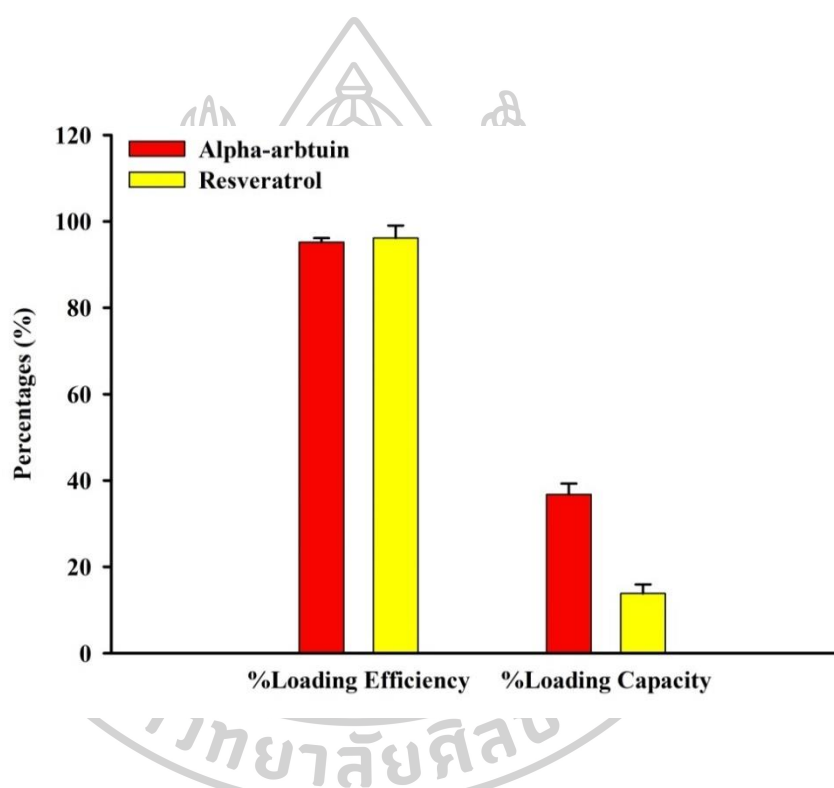
Figure 35. The percentage loading efficiency and loading capacity of the combination of 10% AA + 2% Res-loaded Eudragit RL/PVP-K90 DMNs

4.5 *In vitro* dissolution study

4.5.1 AA-loaded DMNs

The delivery of AA into the skin depends on the dissolution of the needles from DMNs when they contact the skin interstitial fluid. Therefore, dissolution study has become one of the crucial experiments for DMNs. Figure 36 displays the *in vitro* dissolution images of 8% AA-loaded HPMC/PVP-K90 DMNs and 8% AA-loaded PAMA/PVA DMNs at different time points (0, 5, 15, 30, 45 min, and 1 h) captured

by a Dino-Lite microscope. The dissolution of needles was observed within 5 min and completely dissolved within 45 min following the application of DMNs into the neonatal porcine skin.
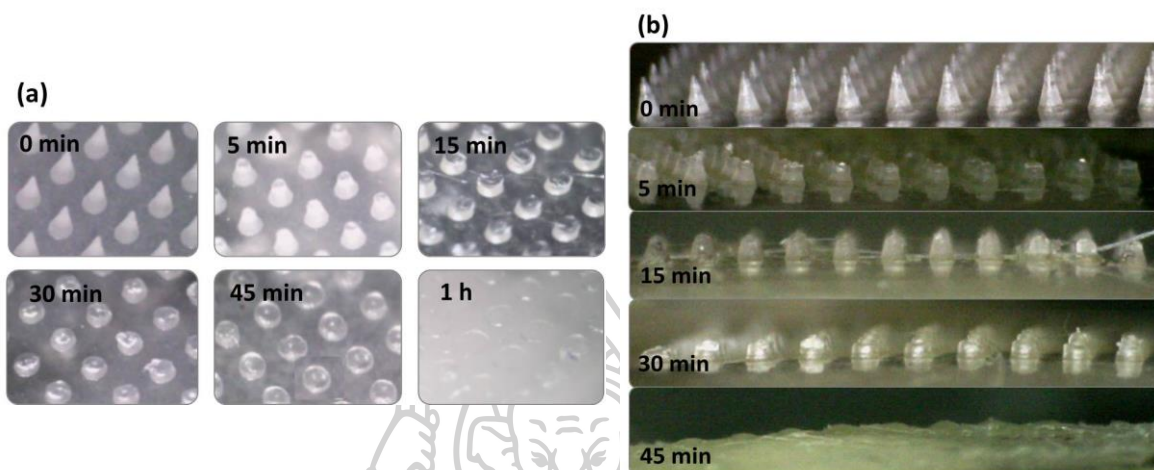
Figure 36. *In vitro* dissolution images following the application of (a) 8% AA-loaded HPMC/PVP-K90 DMNs and (b) 8% AA-loaded PAMA/PVA DMNs at different time points (0, 5, 15, 30, 45 min, and 1 h) into neonatal porcine skin

4.5.2 Res-loaded DMNs

In vitro dissolution study of Res-loaded DMNs was performed to predict the time required to release Res from 5% Res-loaded Eudragit E/PVP-K90 DMNs and 5% Res-loaded Eudragit RS/PVP-K90 DMNs. Figure 37 describes the *in vitro* dissolution behaviors of 5% Res-loaded Eudragit E/PVP-K90 DMNs and Eudragit RS/PVP-K90 DMNs at various time intervals. After applying both types of Res-loaded DMNs into the neonatal porcine for 5 min, the DMN tips were initially dissolved, and all needles wholly dissolved within 30 min. The results could be suggested that the incorporation of Res into a Eudragit/PVP-K90 polymer mixture decreased the dissolution time of DMNs which initiated to rapid release of the Res. Taking into consideration that the dissolution rate for the use of a polymer mixture (Eudragit/PVP-K90) was easy to dissolve when contacted with PBS (mimic the skin interstitial fluid) as their material composition and then quickly released the hydrophobic nature of Res.
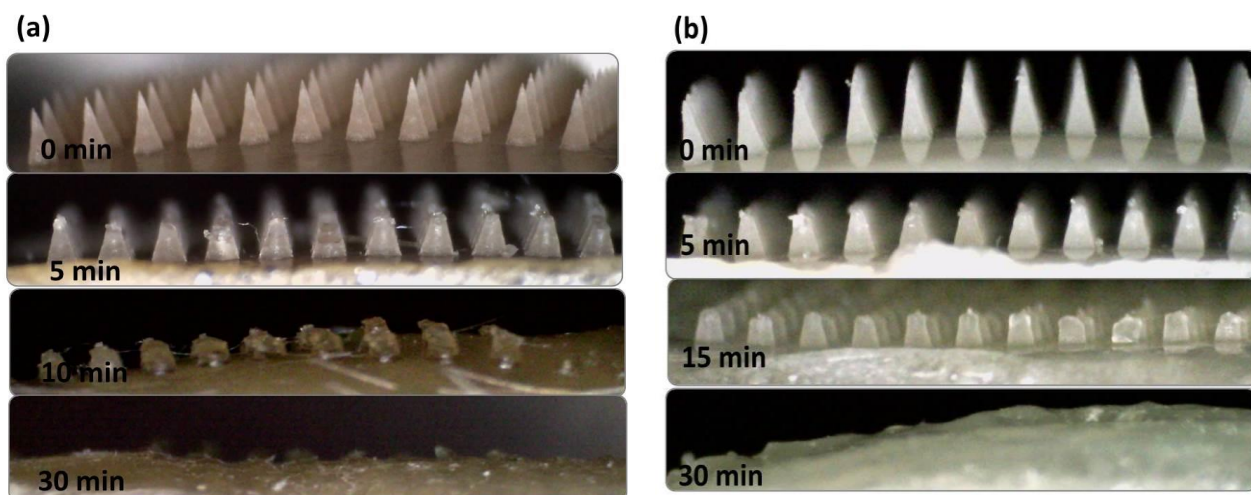
Figure 37. *In vitro* dissolution image following the application of (a) 5% Res-loaded Eudragit E/PVP-K90 DMNs and (b) 5% Res-loaded Eudragit RS/PVP-K90 DMNs at different time points (0, 5, 15, 30, and 30 min) into neonatal porcine skin

4.5.3 The combination of AA and Res-loaded DMNs

The dissolution rate of the combination of 10% AA and 2% Res-loaded DMNs was also observed in the neonatal porcine skin using a Dino-Lite microscope. The tip needles following removal of DMNs were imaged, as shown in Figure 38. The results founded that all needles of the DMNs were entirely dissolved within 15 min. This result revealed that the dissolution rate of Eudragit RL/PVP-K90 DMNs was more rapid time than previous Eudragit E/PVP-K90 DMNs and Eudragit RS/PVP-K90 DMNs. Therefore, the types of polymer blended and drugs used for DMNs fabrication affected the dissolution efficiency of DMNs.
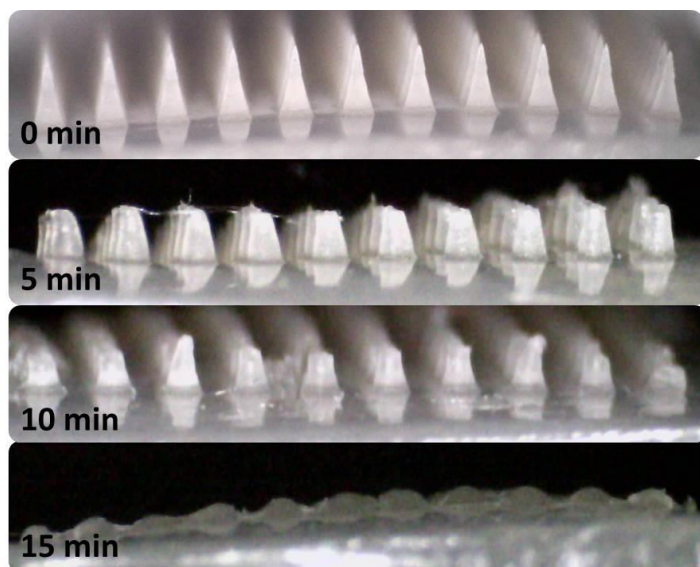
Figure 38. *In vitro* dissolution image following application of 10% AA and 2% Res-loaded Eudragit RL/PVP-K90 DMNs (0, 5, 10, and 15 min) into neonatal porcine skin

4.6 *In vitro* **skin permeation and accumulation studies**

4.6.1 AA-loaded DMNs

The cumulative amount of AA from 8% AA-loaded HPMC/PVP-K90 DMNs, 8% AA-loaded HPMC/PVP-K90 gel, 8% AA-loaded PAMA/PVA DMNs, 8% AA-loaded PAMA/PVA gel, and 5% AA commercial cream across the neonatal porcine skin is illustrated in Figure 39 (a) and (b). The permeation profiles of AA over 24 h following an application of both AA-loaded DMNs were significantly higher than that of their gel formulations and commercial cream ($p<0.05$). The deliver amount of AA from 8% AA-loaded HPMC/PVP-K90 DMNs was 2308.22 ± 280.12 $\mu g/cm^2$, while 8% AA-loaded HPMC/PVP-K90 gel only delivered 270.12 ± 100.28 $\mu g/cm^2$ (Figure 39 (a)). As shown in Figure 39 (b), the cumulative amount of AA for 24 h from 8% AA-loaded PAMA/PVA DMNs and gel was 1784.61 ± 90.32 $\mu g/cm^2$ and 396.26 ± 32.99 $\mu g/cm^2$, respectively. In the case of 5% AA commercial cream formulation, the drug permeated was only 626.13 ± 169.77 $\mu g/cm^2$. According to these results, AA delivered using HPMC/PVP-K90 DMNs was approximately 8.5- and 3.7-folds higher than that of the gel and AA commercial cream formulation, respectively. On the other hand, AA from PAMA/PVA DMNs permeated about 4.5 and 2.8 times higher than that of gel and AA commercial cream formulation, respectively. These

results proved that DMNs successfully penetrated the SC layer of porcine skin and enhanced the permeation of AA.

The flux values of AA-loaded DMNs and gel formulations prepared from HPMC/PVP-K90 were 74.24 ± 6.21 µg/cm^2/h and 24.87 ± 8.73 µg/cm^2/h, while PAMA/PVA was 74.16 ± 6.21 µg/cm^2/h and 35.74 ± 2.21 µg/cm^2/h for AA-loaded DMNs and gel formulation, respectively (Figure 39 (c)). The flux value from commercial cream was 51.26 ± 2.34 µg/cm^2/h.

At the end of the experiment, the amounts of AA accumulated in the neonatal porcine skin from both DMNs formulations were observed compared to gel and commercial cream formulations. As presented in Figure 39 (d), the skin accumulated profile of AA-loaded HPMC/PVP-K90 DMNs (156.11 ± 2.45 µg/cm^3) was significantly superior to that of gel formulation (60.05 ± 8.88 µg/cm^3). In the case of AA, skin accumulation observed from the AA-loaded PAMA/PVA DMNs were 276.68 ± 24.56 µg/cm^3, which was 8.6 times significantly higher than that of gel formulation (32.14 ± 8.70 µg/cm^3). In addition, the amount of AA in both types of AA-loaded HPMC/PVA DMNs and PAMA/PVA DMNs were 1.84- and 3.2- folds higher than AA commercial formulation (*p<0.05*). These differences indicated that DMNs patch was a useful technique to deliver AA into the skin.

(a)

(b)
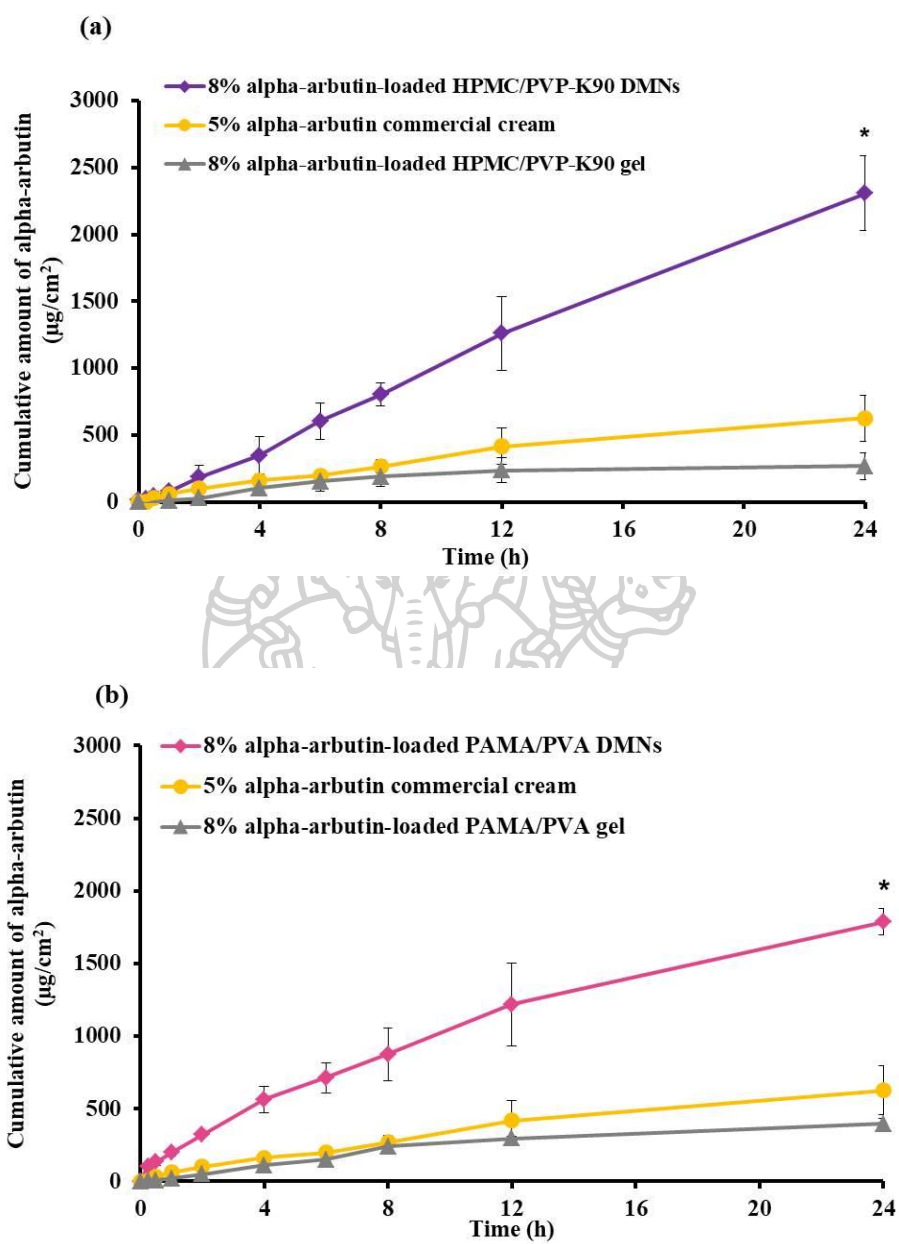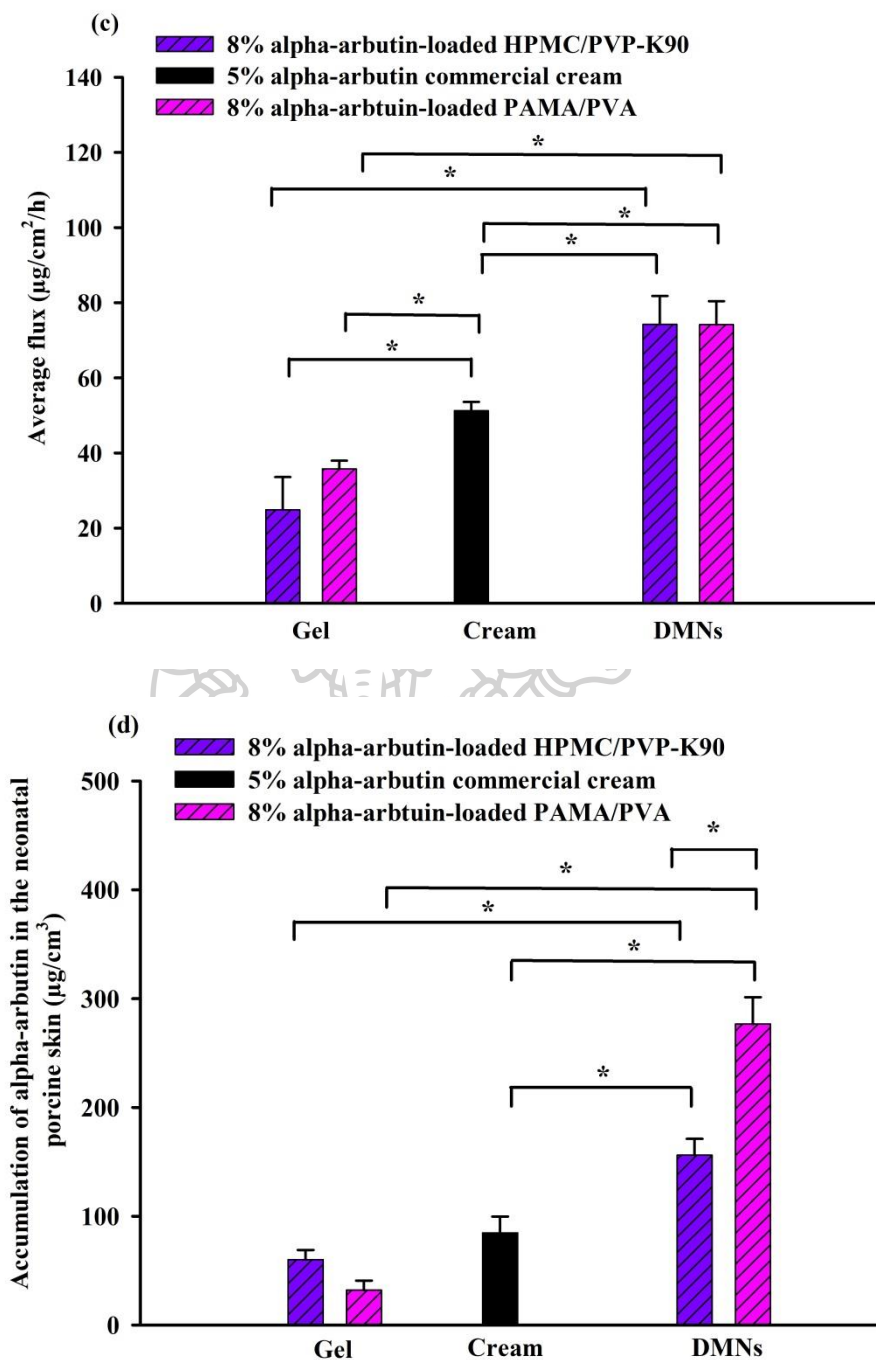
Figure 39. The cumulative amount of AA across the neonatal porcine skin from (a) 8% AA-loaded HPMC/PVP-K90 DMNs, AA gel, and commercial AA cream (b) 8% AA-loaded PAMA/PVA DMNs, AA gel, and commercial 5 % AA cream (c) average flux values and (d) AA accumulation in the neonatal porcine skin (mean±SD, n=3) *Statistically significant ($p<0.05$)

4.6.2 Res-loaded DMNs

Figure 40 shows the *in vitro* skin permeation profiles of Res delivered from 5% Res-loaded Eudragit E/PVP-K90 DMNs, 5% Res-loaded Eudragit RS/PVP-K90 DMNs, and their gel formulations. The Res-loaded DMNs delivered significantly more drugs through the neonatal porcine skin compared with gel formulations over 24 h ($p<0.05$). In the case of 5% Res-loaded Eudragit E/PVP-K90 DMNs, the delivery amount was 258.96 ± 37.12 µg/cm^2, while gel formulation was 69.14 ± 17.29 µg/cm^2. 5% Res-loaded Eudragti RS/PVP-K90 DMNs delivered the Res 438.38 ± 70.75 µg/cm^2 at 24 h, whereas delivered 127.89 ± 45.36 µg/cm^2 for the gel formulation. It was found that the delivery amount of Res-loaded Eudragit E/PVP-K90 DMNs and Eudragit RS/PVP-K90 DMNs were approximately 3.4 and 3.8 times greater than gel formulation, respectively. Although the loading efficiency and loading capacity between both DMNs were not significant, the amount of Res permeated into the neonatal porcine skin from 5% Res-loaded Eudragit RS/PVP-K90 DMNs increased approximately 1.7 folds compared to 5% Res-loaded Eudragit E/PVP-K90 DMNs. These results confirmed that the quaternary ammonium group present in the Eudragit RS polymer mixture enhances the release kinetic (192). Furthermore, Chantasart *et al*. reported that piroxicam release rated from Eudragit RL 100 transdermal film was increased compared to Eudragit RS 100, resulting from the number of quaternary ammonium groups present in Eudragit polymers, which serves as favorable salts to attract the water more easily into the drug-polymer matrix (193).

Average flux values of 5% Res-loaded Eudragit E/PVP-K90 DMNs and 5% Res-loaded Eudragit RS/PVP-K90 DMNs were 10.64 ± 1.53 µg/cm^2/h and 18.02 ± 3.05 µg/cm^2/h, while both gel formulations had a flux value of 2.24 ± 0.04 µg/cm^2/h (5% Res-loaded Eudragit E/PVP-K90) and 4.47 ± 0.45 µg/cm^2/h (5% Res-loaded Eudragit RS/PVP-K90 DMNs), respectively (Figure 40 (c)).

The accumulated amount of Res in the neonatal porcine skin following the application of DMNs and gel for 24 h is presented in Figure 40 (d). Hence, both DMNs demonstrated a high level of Res compared with gel formulations (*p<0.05*). The amount of Res accumulated in the skin after applied 5% Res-loaded Eudragit E/PVP-K90 DMNs and 5% Res-loaded Eudragit RS/PVP-K90 DMNs was 707.15 ± 145.68 µg/cm^3 and 1107.15 ± 131.54 µg/cm^3, respectively. In the case of gel

formulation, the skin accumulated amount of Res from 5% Res-loaded Eudragit E/PVP-K90 gel and 5% Res-loaded Eudragit RS/PVP-K90 gel was 56.16 ± 8.21 $\mu g/cm^3$ and 192.81 ± 8.43 $\mu g/cm^3$, respectively. According to the results, the accumulated level of Res from DMNs formulation was significantly higher than the gel formulations. The reason may be that DMNs successfully overcame the skin barrier and retained the Res in skin tissue. Moreover, the lipophilic drug can be accumulated mainly in the epidermic layer of the skin (108). As the results of the skin permeation profile and skin accumulation, both Eudragit/PVP-K90 DMNs presented that Res were successfully incorporated into the DMNs and effectively enhanced the release kinetic of Res into the skin.

(a)

(b)
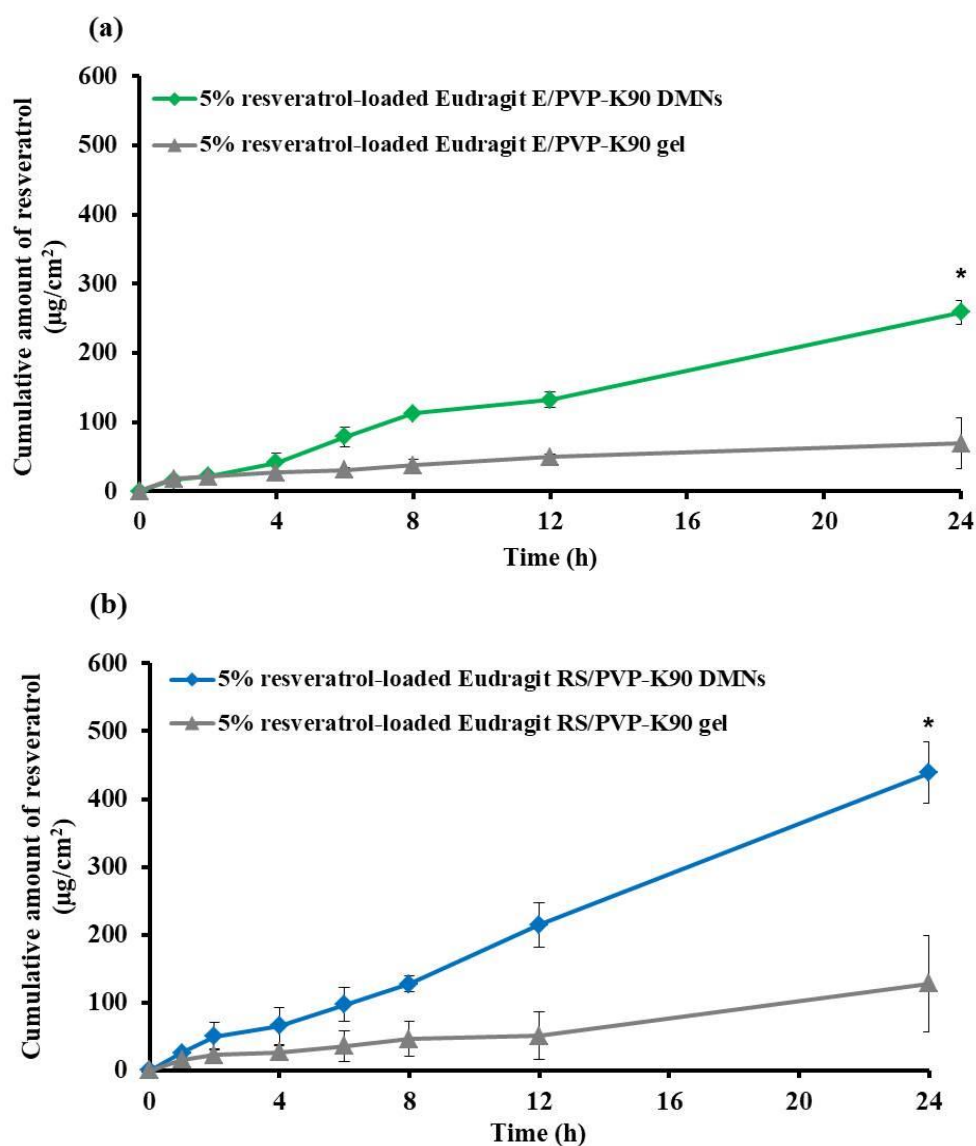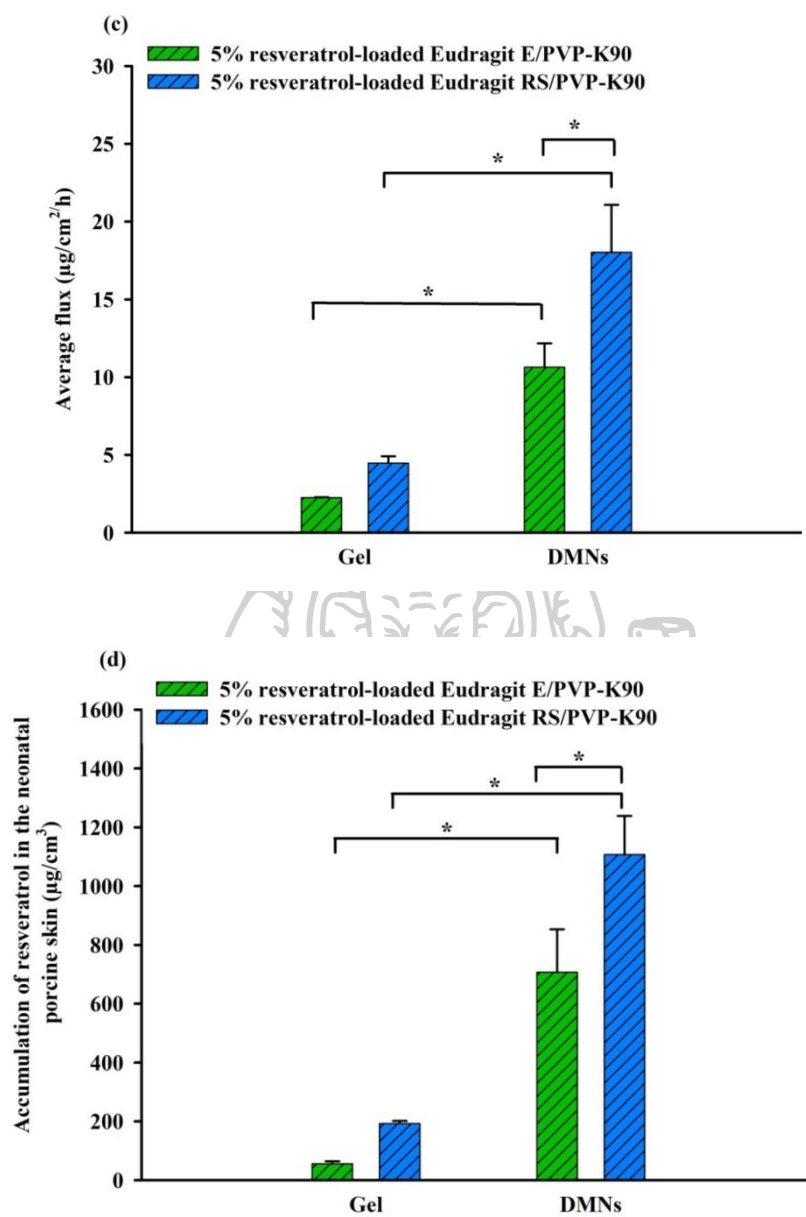
Figure 40. The cumulative amount of Res across the neonatal porcine skin from (a) 5% Res-loaded Eudragit E/PVP-K90 DMNs (b) 5% Res-loaded Eudragit RS/PVP-K90 DMNs (c) average flux values (d) Res accumulation in the neonatal porcine skin from 5% Res-loaded Eudragit E/PVP-K90 DMNs, 5% Res-loaded Eudragit RS/PVP-K90 DMNs, 5% Res-loaded Eudragit E/PVP-K90 gel and 5% Res-loaded Eudragit RS/PVP-K90 gel, (mean±SD, n=3) *Statistically significant ($p<0.05$)

4.6.3 The combination of AA and Res-loaded DMNs

The cumulative amount of AA and Res permeated across the neonatal porcine skin after application of 10% AA and 2% Res-loaded Eudragit RL/PVP-K90 DMNs, 10% AA and 2% Res-loaded Edragit RL/PVP-K90 gel, and 10% AA and 2% Res combination cream over 24 h is depicted in Figure 41 (a) and (b). The quantity of AA and Res delivered from Eudragit RL/PVP-K90 DMNs was significantly greater than gel and cream formulation. The delivery amount of AA from the combination of 10% AA and 2% Res-loaded Eudragit RL/PVP-K90 DMNs, gel, and cream formulation was 1263.93 ± 123.21 µg/cm^2, 42.43 ± 12.50 µg/cm^2, and 85.69 ± 29.75 µg/cm^2, respectively. In addition, the amount of Res delivered from DMNs, gel, and cream was 45.24 ± 4.23 µg/cm^2, 3.02 ± 1.45 µg/cm^2, and 3.98 ± 1.87 µg/cm^2, respectively.

The average flux values of AA permeated from 10% AA and 2% Res-loaded Eudragit RL/PVP-K90 DMNs, gel, and cream formulation were 36.95 ± 5.92 µg/cm^2/h, 1.33 ± 0.40 µg/cm^2/h, and 3.33 ± 1.16 µg/cm^2/h, respectively. On the other hand, the flux values of Res delivered from DMNs, gel, and cream were 2.54 ± 0.36 µg/cm^2/h, 0.17 ± 0.04 µg/cm^2/h, and 0.28 ± 0.15 µg/cm^2/h, respectively, as shown in Figure 41 (c). Thus, the flux values of AA and Res from DMNs were significantly superior to that of gel and cream formulation ($p<0.05$).

Figure 41 (d) demonstrates the amount of AA and Res accumulated in the skin at the end of the permeation study. The retained amount of AA in the neonatal porcine skin was 838.59 ± 99.03 µg/cm^3 from 10% AA and 2% Res-loaded DMNs, which is significantly higher approximately 30.5 and 8.5 times than that of gel (27.53 ± 4.35 µg/cm^3), and cream formulation (99.34 ± 6.54 µg/cm^3). In the case of Res, the accumulated amount was 108.52 ± 8.40 µg/cm^3 following the application of 10% AA and 2% Res-loaded DMNs, which was approximately 28 and 4.8 folds significantly greater than that of gel (3.87 ± 1.05 µg/cm^3) and cream formulation (22.71 ± 5.60 µg/cm^3). Thus, the results confirmed that Eudragit RL/PVP-K90 DMNs could bypass SC and released AA and Res directly into the skin for a synergistic depigmentation effect.

(a)

(b)
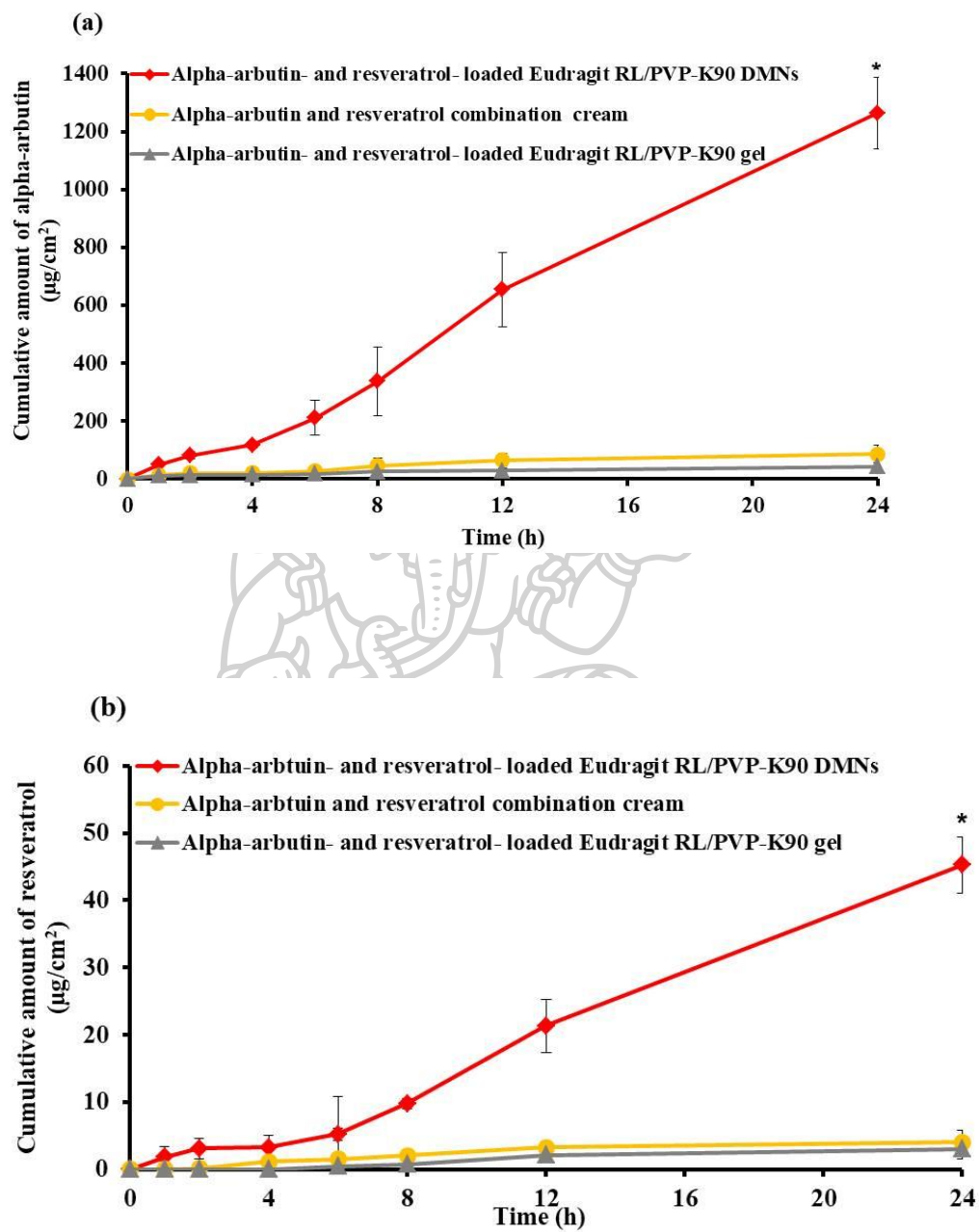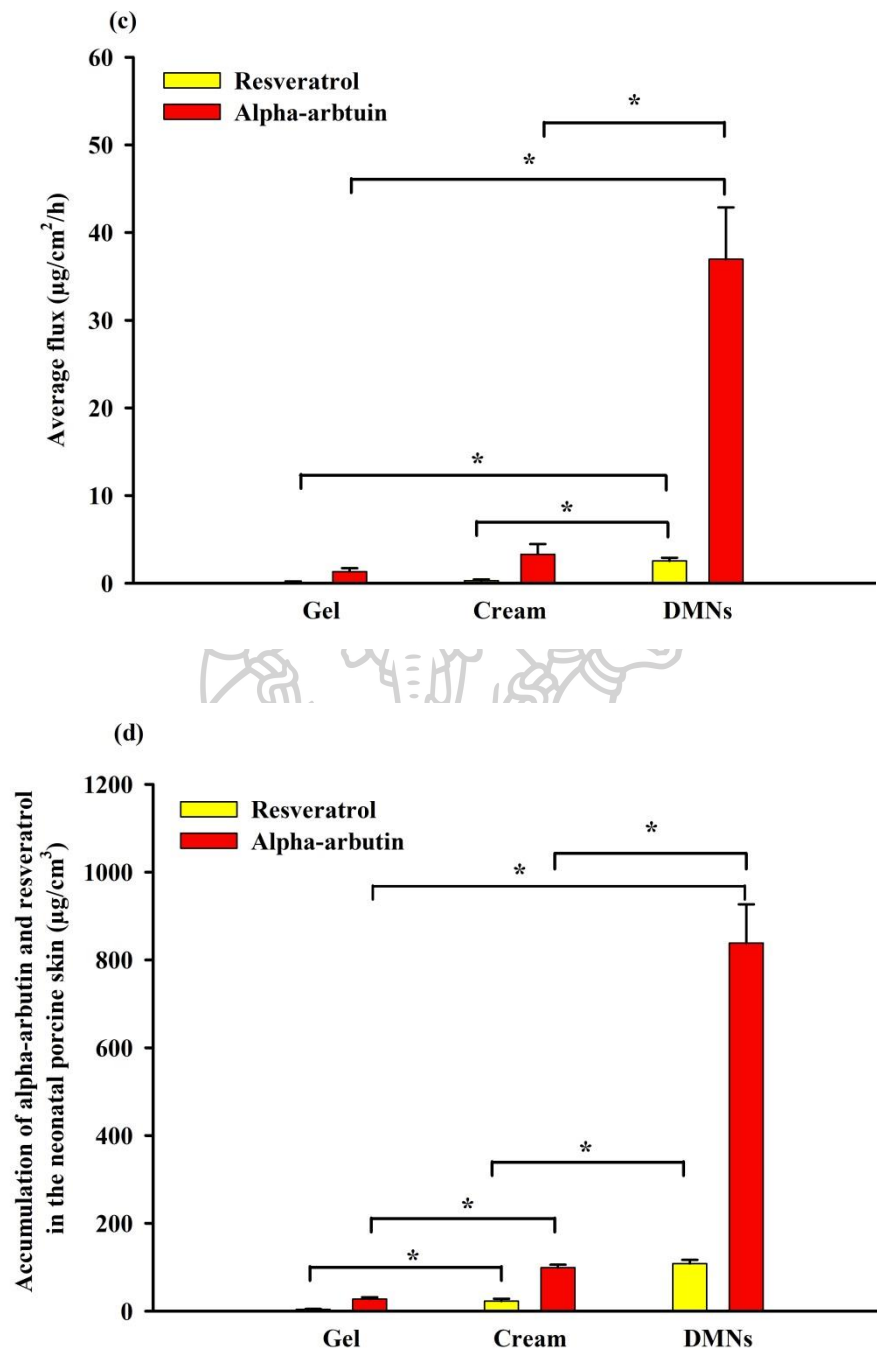
Figure 41. The cumulative amount of (a) AA (b) Res across the neonatal porcine skin (c) average flux values and (d) AA and Res accumulation in the neonatal porcine skin from 10% AA- and 2% Res-loaded Eudragit RL/PVP-K90 DMNs, 10% AA and 2% Res-loaded Eudragit RL/PVP-K90 gel, and 10% AA and 2% Res combination cream (mean ± SD, n=3) *Statistically significant ($p<0.05$)

4.7 *In vivo* skin permeation and accumulation studies

4.7.1 AA-loaded DMNs

According to the preliminary study of DMNs as previously described, the 8% AA-loaded HPMC/PVP-K90 DMNs and 8% AA-loaded PAMA/PVA DMNs formulations were selected for *in vivo* experiments compared with 5% AA commercial cream. *In vivo* plasma concentration of AA following application of 8% AA-loaded HPMC/PVP-K90 DMN, 8% AA-loaded PAMA/PVA DMNs, and 5% AA commercial cream on mice skin over 24 h is shown in Figure 42 (a). The concentration of AA in plasma following application of 8% AA-loaded PAMA/PVA DMNs and 5% AA commercial cream was 5.33±0.16 µg/mL and 0.15±0.09 µg/mL, respectively. On the other hand, AA could not be found in the blood of mice of blank HPMC/PVP-K90 DMNs, and blank PAMA/PVA DMNs (data not shown). However, no AA was detected in the blood sample of mice applied by 8% AA-loaded HPMC/PVP-K90 DMNs. These are probably the factors that influence drug delivery of DMNs reported by Donnelly *et al.* in 2010, including (i) types of materials for DMNs fabrication, (ii) dissolution of DMNs upon contact with the skin interstitial fluid, and (iii) release the drug molecules from the polymer matrix for local or systemic delivery (194).

As shown in Figure 42 (b), the amount of AA accumulated in mice skin after applied with 8% AA-loaded HPMC/PVP-K90 DMNs (28.8±0.08 µg/cm^2) and 8% AA-loaded PAMA/PVA DMNs (35.39±2.13 µg/cm^2) was approximately 4 and 4.9 times significantly higher than 5% AA commercial cream (7.2±0.03 µg/cm^2) ($p<0.05$). It has been suggested that AA, a hydrophilic drug, presented low permeation into the skin. However, DMNs may improve the delivery of the hydrophilic drug into and pass the skin compared to the traditional method, cream application, due to the mechanism of DMNs, poke and release the drug into the skin. The skin depigmentation effect against melanogenesis mainly occurs in the stratum basale in which melanocytes occupy (15). DMNs could penetrate the SC and enhanced the intradermal delivery of AA compared with 5% AA commercial cream formulation.
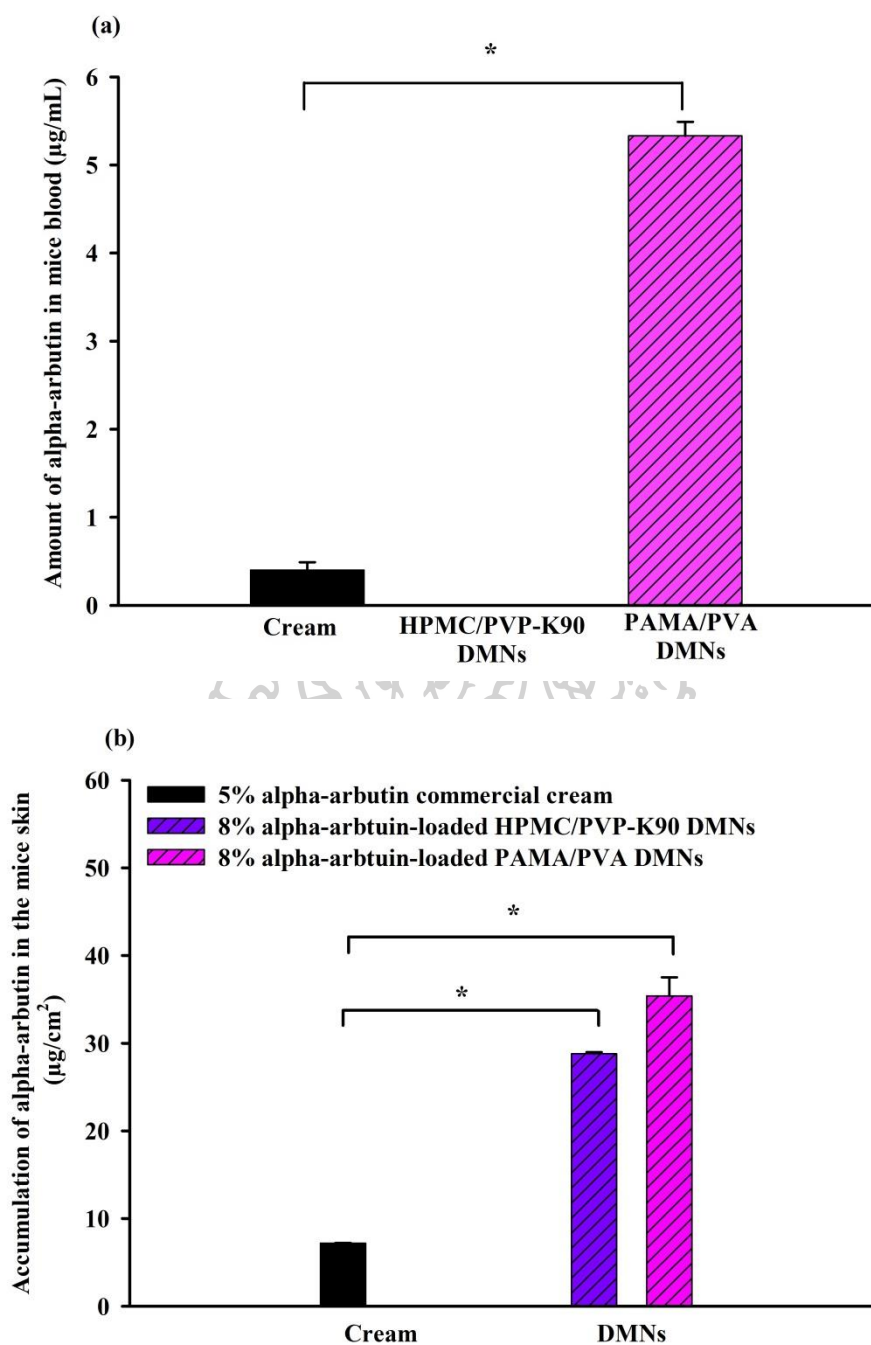
Figure 42. (a) AA concentration in mice blood following application of 8% AA-loaded HPMC/PVP-K90 DMNs, 8% AA-loaded PAMA/PVA DMNs, and 5% AA commercial cream (b) accumulations of AA in mice skin from 8% AA-loaded HPMC/PVP-K90 DMNs, 8% AA-loaded PAMA/PVA DMNs, and 5% AA commercial cream at 24 h (mean±SD, n=6) *Statistically significant (*P*<0.05)

4.7.2 The combination of AA and Res-loaded DMNs

A profile of the drugs delivered after applying 10% AA and 2% Res-loaded Eudragit RL/PVP-K90 DMNs and the combination of 10% AA and 2% Res cream application in mice is illustrated in Figure 43 (a and b). As shown in Figure 43 (a), the mean concentration of AA in plasma was 36.37 ± 5.50 µg/mL for 10% AA and 2% Res-loaded Eudragit RL/PVP-K90 DMNs and 17.66 ± 1.01 µg/mL for the cream formulation. It can be seen that DMNs enhanced the permeation amount of AA approximately about 2 times compared with cream formulation ($p < 0.05$). On the other hand, the plasma concentration of Res was not detected in the blood sample after the applied DMNs and cream formulation because Res build a depot in SC due to its lipophilic nature and could be the factors influencing on drug delivery of DMNs as previously discussed in section 4.7.1.

The amount of AA and Res accumulated in mice skin after 24 h of *in vivo* study is shown in Figure 43 (b). The AA and Res accumulated in the skin after application of 10% AA and 2% Res-loaded Eudragit RL/PVP-K90 DMNs were 36.01 ± 0.14 µg/cm^2 and 0.39 ± 0.06 µg/cm^2, respectively, which were significantly higher than that of cream formulation approximately 2.6 times for AA (13.69 ± 3.15 µg/cm^2 delivered from cream formulation) and 1.9 times for Res (0.21 ± 0.14 µg/cm^2 delivered from cream formulation). Therefore, *in vivo* study found that fabricated DMNs were able to penetrate the mice skin to deliver AA and Res and retained the drugs at their application site for skin depigmentation.
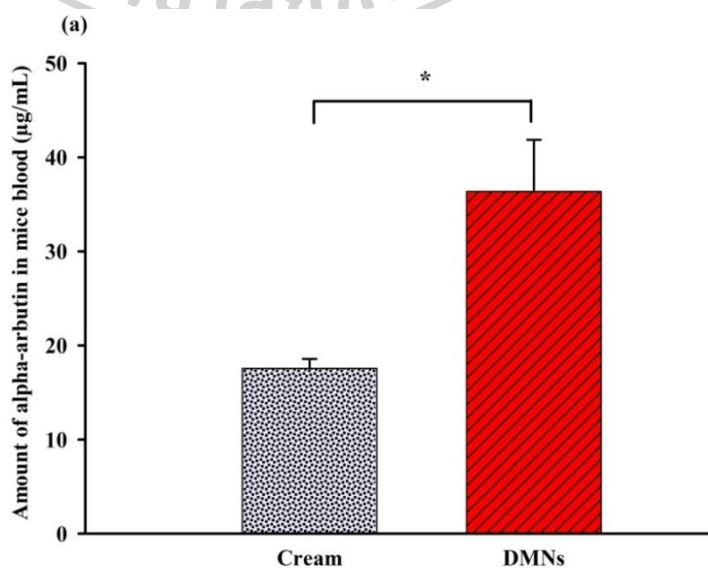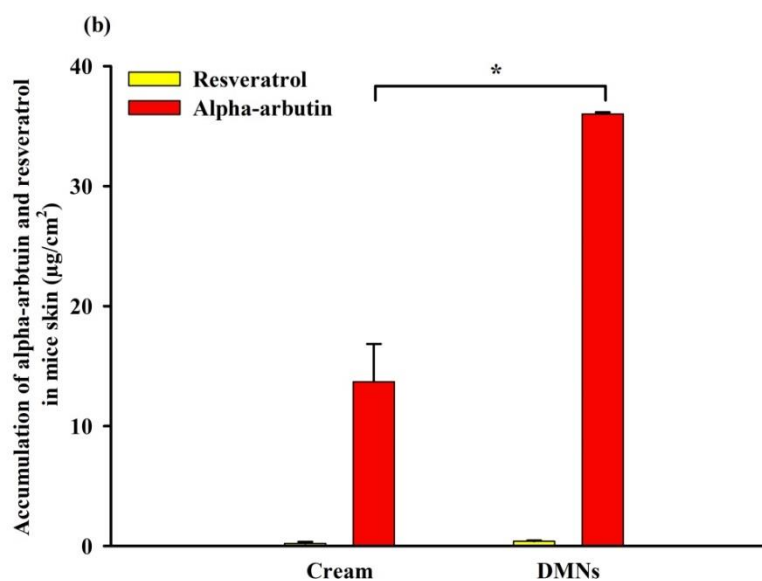
Figure 43. (a) AA blood concentration in mice blood and (b) accumulations of AA and Res in mice skin following application of 10% AA and 2% Res-loaded Eudragit RL/PVP-K90 MNs and cream formulation at 24 h (mean±SD, n=6) *Statistically significant (*P<0.05*)

4.8 *In vivo* dissolution study

4.8.1 AA-loaded DMNs

In vivo dissolution of DMNs tips from 8% AA-loaded PAMA/PVA DMNs was performed in mice to confirm the dissolution study mimic in real-used by a human. Figure 44 shows that the initial dissolution of the DMNs tips was observed within 5 min following DMNs application due to contact with interstitial fluid in mice. At 45 min, all needles were entirely dissolved. The result proved that DMNs were successfully dissolved *in vivo* mimic the actual dissolution in the body.
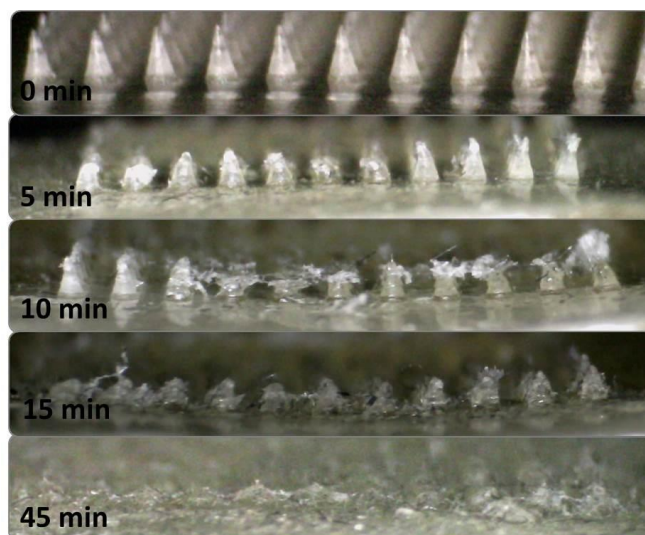
Figure 44. *In vivo* dissolution images following application of 8% AA-loaded PAMA/PVA DMNs in mice at different time points (0, 10, 15, and 45 min)

4.8.2 The combination of AA and Res-loaded DMNs

In vivo dissolution of DMNs tips from 10% AA and 2% Res-loaded Eudragit RL/PVP-K90 DMNs was performed in mice, as shown in Figure 45. The initial dissolution of all needles from the DMNs was investigated at approximately 5 min. Then, the needles were dissolved entirely at 15 min. The dissolution result in mice was found that corresponds to the dissolution profile of *in vitro* study.
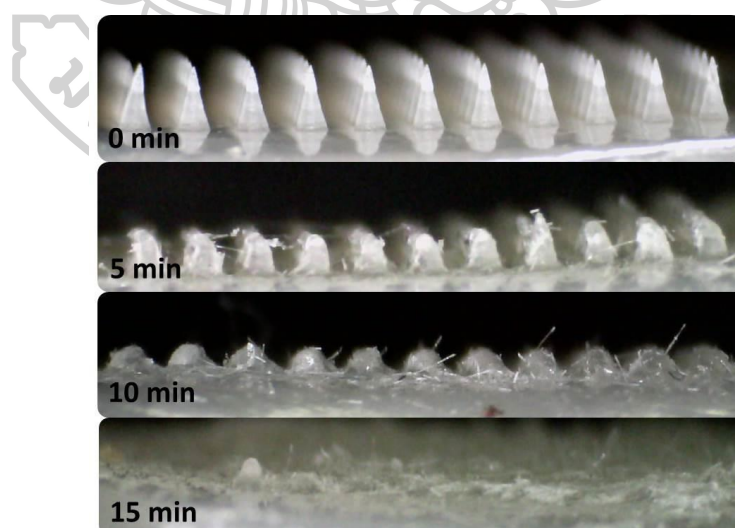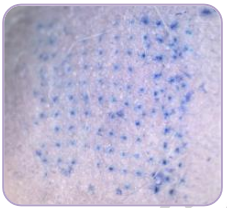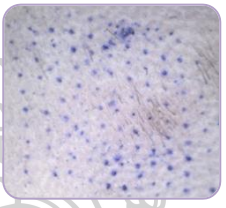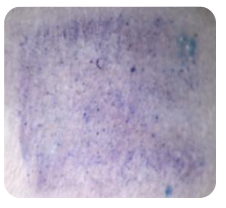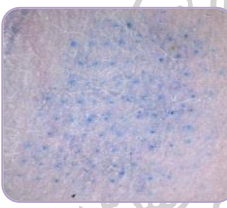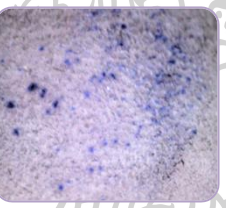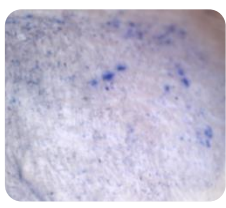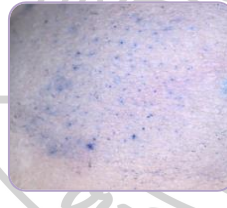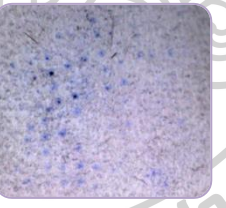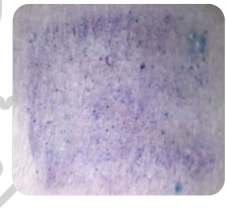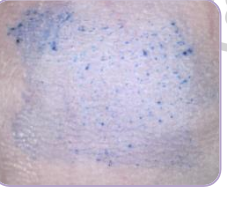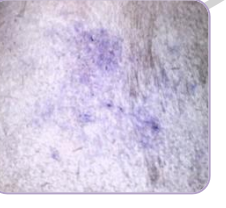
Figure 45. *In vivo* dissolution images of 10% AA- and 2% Res-loaded Eudragit RL/PVP-K90 DMNs after application in mice at different time points (0, 10, and 15 min)

4.9 *In vivo* skin resealing study

  In vivo skin resealing time following the removal of DMNs is one of the crucial factors to confirm safety and recovering ability after the application of DMNs. The image of the mice's skin resealing was observed at specific time points (0, 2, 4, 8, 12 and 24 h) following removal of 8% AA-loaded HPMC/PVP-K90 DMNs, 8% AA-loaded PAMA/PVA DMNs, and 10% AA and 2% Res-loaded Eudragit RL/PVP-K90 DMNs (Table 16). According to the result, at 0 h, all DMNs formulations were successfully created ~98% of microholes on each mice. An increasing in period of time following application of 8% AA-loaded HPMC/PVP-K90 DMNs, the number of visible microholes was decreased depending on the recovery time points, including ~62% at 2 h, ~43% at 4 h, ~29% at 8 h, ~11% at 12 h, and ~6% at 24 h, respectively. In the case of 8% AA-loaded PAMA/PVA DMNs, the number of visible microholes also decreased when increased in wear-off duration as follows: ~70% at 2 h, ~53% at 4 h, ~30% at 8 h, at ~10% 12 h, and ~2% at 24 h, respectively. The result noted that; almost all visible microholes had disappeared within 12 h after removing 10% AA and 2% Res-loaded Eudragit RL/PVP-K90 DMNs. The decreased in the number of visible microholes was also investigated in 10% AA and 2% Res-loaded Eudragit RL/PVP-K90 DMN, which showed that ~68% (2 h), ~45% (4 h), ~20% (8 h), respectively. The result showed that the mice's skin was able to repair and restore their SC naturally. The skin resealing is based on the formation of a water gradient of the SC and the secretion of lamella bodies followed by the lipid synthesis in the skin (195-197). Moreover, any signs of skin abnormality on the mice was not found overall in the experiments. For this reason, DMNs formulations were suitable for transdermal drug delivery systems due to the skin's resealing ability within a reasonable period of time.

Table 16. Reseals image of mice skin after applying 8% AA-loaded HPMC/PVP-K90 DMNs, 8% AA-loaded PAMA/PVA, and 10% AA and 2% Res-loaded Eudragit RL/PVP-K90 DMNs at various time points (0, 2, 4, 8, 12, and 24 h)

Times	8% AA-loaded HPMC/PVP-K90 DMNs	8% AA-loaded PAMA/PVA DMNs	10% AA and 2% Res-loaded Eudragit RL/PVP-K90 DMNs
0 h			
2 h			
4 h			
8 h			
12 h			

| 24 h | | | |

4.10 Human study of 10% AA and 2% Res-loaded DMNs

To confirm the safety of DMNs patch, human study was performed. The forearm of human volunteer's image following an application of 10% AA and 2% Res-loaded DMNs patch is shown in Figures 46 (a) and (b).
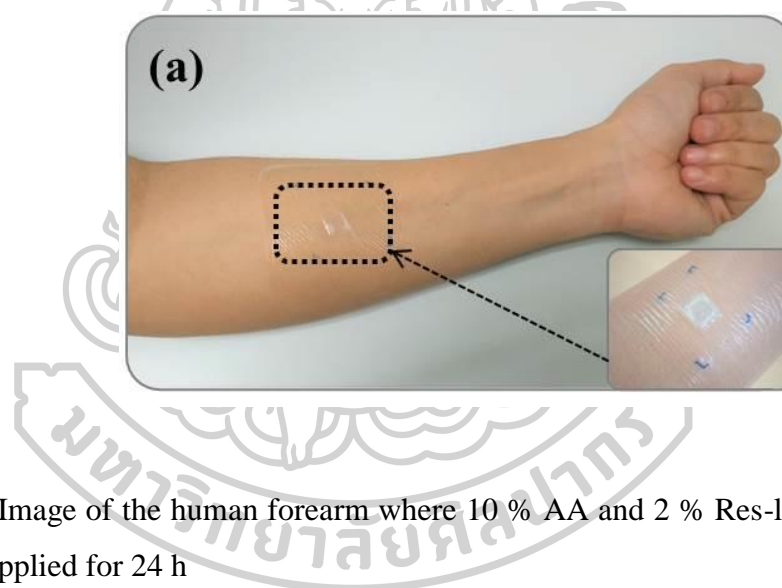
Figure 46. Image of the human forearm where 10 % AA and 2 % Res-loaded DMNs patch was applied for 24 h

4.10.1 Analysis of skin melanin, skin erythema, transepidermal water loss (TEWL), skin hydration, and skin elasticity

The skin melanin, skin erythema, TEWL, skin hydration, and skin elasticity were analyzed after applying the combination of 10 % AA and 2 % Res-loaded DMNs on the forearm of all volunteers using DermaLab® series, as shown in Figure 47. Skin melanin reveals the skin color and pigmentation level (198). After the applied DMNs patch at 24 h, a decrease in the amount of skin melanin content (32.56±3.71, 93.89 % melanin index) was observed

compared with before applied DMNs (34.68±4.25, 100 % melanin index) (p>0.05), as presented in Figure 47 (a). The result corresponds to the research of Park *et al*. which reported the hyaluronic acid (HA) DMNs patch contained melatonin, arbutin, niacinamide, and tranexamic acid showed a significantly decreased in the skin melanin index between before and after application of HA DMNs patch (151). The erythema index was performed to analyze the skin reaction, including irritants and allergies (188). Skin erythema is the superficial redness of the skin from external stimulus and hypersensitivity to an allergen (199). The result revealed that there was no significant difference in erythema index between before an application (10.77±2.63, 92.61 % erythema index) and after removal of DMNs patch (11.63±3.46, 100 % erythema index) (Figure 47 (b)). Moreover, a physical examination of the applied area could not observe severe redness and irritation of the skin. In the case of skin hydration, skin hydration represents the moisture contents of the skin in the cosmetic field and pathological skin diseases (200). The mean result of skin hydration before application and after removal of DMNs is presented in Figure 47 (c). The result showed that application of DMNs slightly reduced the hydration of SC within 24 h; however, there was no significant difference (210.13±44.94 arbitrary unit (AU) (100%) before application and 198.07±37.56 AU (94.26%) after removal of DMNs). The study of skin hydration implied that the epidermal SC layer tends to lose some water contents from skin perforation after DMNs puncture by evaporation effect because SC plays a barrier to water loss (201). Skin elasticity is one parameter to measure the skin deformation where typically the values were exhibited between 2 and 15 MPa. An increase in MPa corresponds to the higher vacuum strength requirements for skin lifting (202). Figure 47 (d) shows that skin elasticity was found to be 5.21±1.05 MPa before an application and 5.53±1.13 MPa after removal of DMNs patch. Kalra *et al.* (2016) reported that the skin elasticity increased due to stretching of bonds at the low hydration level, whereas the hydrogen bond becomes weak at the higher hydration level of the skin. Thus, the results representing skin elasticity and skin hydration in this study were correlated with Kalra *et al*. (203). In the

case of TEWL, TEWL level was dependent on many factors such as skin temperature, skin blood flow, the degree of corneocyte formation, and the SC lipid contents (204). Therefore, in this study, TEWL was measured at 24 h to observe the skin barrier disruption after removing DMNs (198). The results revealed that there was no significant difference between before an application (6.42 ± 1.85 g/m^2/h) and after removal of DMNs (6.78 ± 2.10 g/m^2/h), as shown in Figure 47 (e). According to the results, an application of DMNs may induce to minimize the SC of the skin associated with the formation of micropores in the SC after DMNs application. Moreover, it is possible to recovery following a period of time. Therefore, DMNs exhibited sufficient human skin puncturability because of the elevated TEWL.
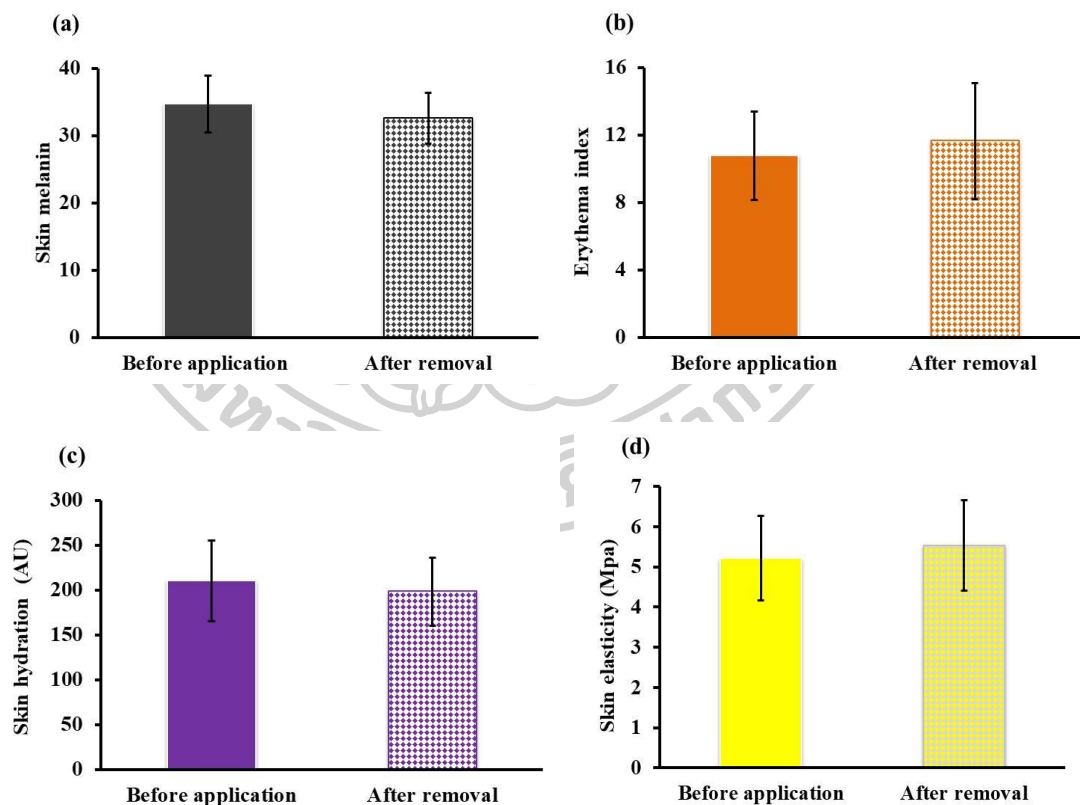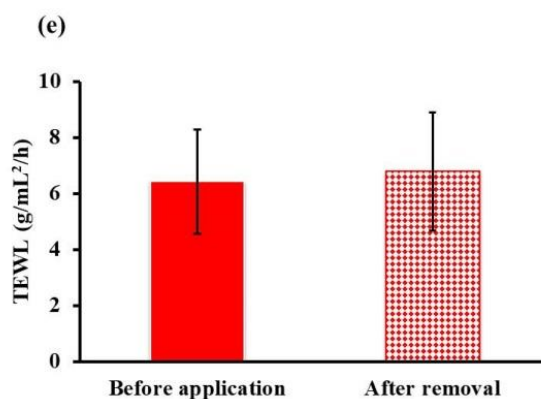
Figure 47. Mean values of (a) melanin index (b) erythema index (c) skin hydration (d) skin elasticity (e) TEWL analyzed by DermaLab® series. The data were compared before application and after removal of 10 % AA and 2 % Res-loaded DMNs patch (mean ± SD, n=15)

In this study, although melanin index slightly decreased after applied DMNs, a significant change in skin melanin assessment between before and after applied DMNs was not seen within 24 h of application period. This is due to the short period of patching, only 24 h. The study from Lim *et al*. (2009) found that treated the skin tissue models of brownish guinea and human skin tissues with 10 mM (2722.51 µg/mL) of AA for 72 h significantly decreased melanin content in both tissues compared to the control (205). Moreover, Park *et al*. reported that after applied 2% AA-loaded MNs patch on cheek of thirty-four volunteers twice a week for 8 weeks, a significant decreased in melanin index was seen at 4 and 8 weeks (151). Lee et al. also confirmed that Res regulates UVB-induced pigmentation and decreased skin hyperpigmentation by applying 1% Res solution (200 µL) on dorsal skins of guinea pigs (2 cm^2) every day for 2 weeks. In addition, melanin production in the skin epidermis was also decreased when compared with control group (4). *In vivo* skin depigmentation efficacy of Res in human volunteers was examined by Jo *et al*. in 2018. Twenty-two women were applied with 0.4% Res containing cream twice daily on UV irradiated forearms for up to 8 weeks. The visual assessment and instrumental measurement showed that the pigmentation degree and melanin index of the test group were significantly decreased in weeks 6 and 8 ($p<0.05$) (206). According to these supportive publications, skin was depigmented after using AA continuously for 4 weeks and Res continuously for 6 weeks. Moreover, based on data shown in *in vitro*

melanin content assay, treating cell lines with AA (2000 µL) and Res (20 µL) were significantly decreased the melanin content at 48 h. Although in this clinical study proved that DMNs patch has been accepted as a promising approach for transdermal drug delivery, the clinical study could be done at least 4 weeks to confirm the significant outcome of DMNs for skin depigmentation.

4.10.2 Safety assessment

For the safety assessment, the changes of the skin's human volunteers at the applied area throughout the clinical study were observed. The images of the applied area before and after 10 % AA and 2 % Res-loaded DMNs application were captured using a Dino-Lite microscope, as shown in Figure 48 (a-c). The pictures showed that needle holes appeared at the skin applied area immediately at the time of removal DMNs, which is confirmed the ability of the needles to penetrate the human skin (Figure 48 (b)). At 2 h after DMNs were removed, the microholes were naturally resealed and faded from the skin (Figure 48 (c)). Therefore, AA- and Res- loaded DMNs were considered a safe cosmetic product for skin depigmentation.
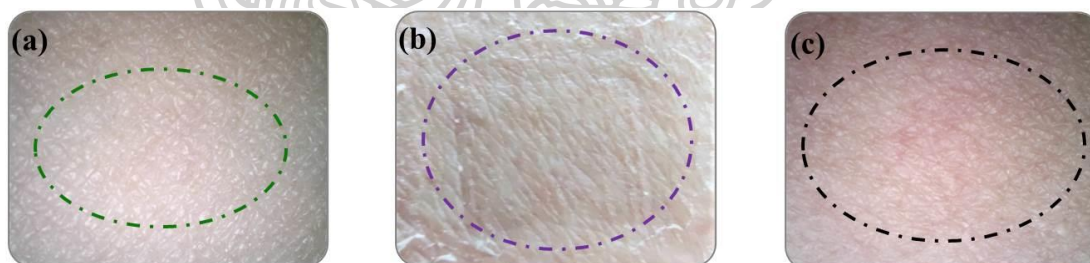
Figure 48. Safety assessment of the combination of 10 % AA and 2 % Res-loaded DMNs patch application (a) before applied DMNs patch, (b) applied area after DMNs patch immediately removed from the skin (c) applied area after DMNs patch removed from the skin for 2 h.

4.11 Stability study

4.11.1 AA-loaded DMNs

The stability of 8 % AA-loaded HPMC/PVP-K90 DMNs revealed good physical and chemical stability for 4 weeks storage under sealed and unsealed conditions at 25±2ºC, 60±5% RH (Figure 49 (a)). The results showed that the recovery amount of AA over 4 weeks in sealed packages was between 98.39±4.04% and 101.86±3.40%, whereas, in unsealed containers, the recovery amount ranged between 97.83±0.66% and 101.86±3.40% when compared with the initial concentration. Moreover, the DMNs patch did not change in color and appearance, which is confirmed good physical stability of DMNs in both sealed and unsealed storage conditions for 4 weeks. Therefore, 8 % AA-loaded HPMC/PVP-K90 DMNs showed good physical and chemical stability in both sealed and unsealed packages at 25ºC with 60±5% RH over 4 weeks. The percentage recovery of AA from 8 % AA-loaded PAMA/PVA DMNs was also analyzed by HPLC as presented in Figure 49 (b). The stability time was designed for 6 months in sealed and unsealed conditions. There was no significant difference in the recovery amount of AA and physical stability between the sealed and unsealed packages. The percentage recovery of the 8 % AA-loaded PAMA/PVA DMNs was found in the range between 96.40±2.16% to 101.06±2.09% for sealed and 95.87±4.94% to 101.06 ± 2.09% for unsealed packages, depending on the storage time. These results confirmed that 8 % AA-loaded PAMA/PVA DMNs formulation was chemically and physically stable to those in sealed and unsealed containers at 25±2ºC with 60±5% RH for 6 months.
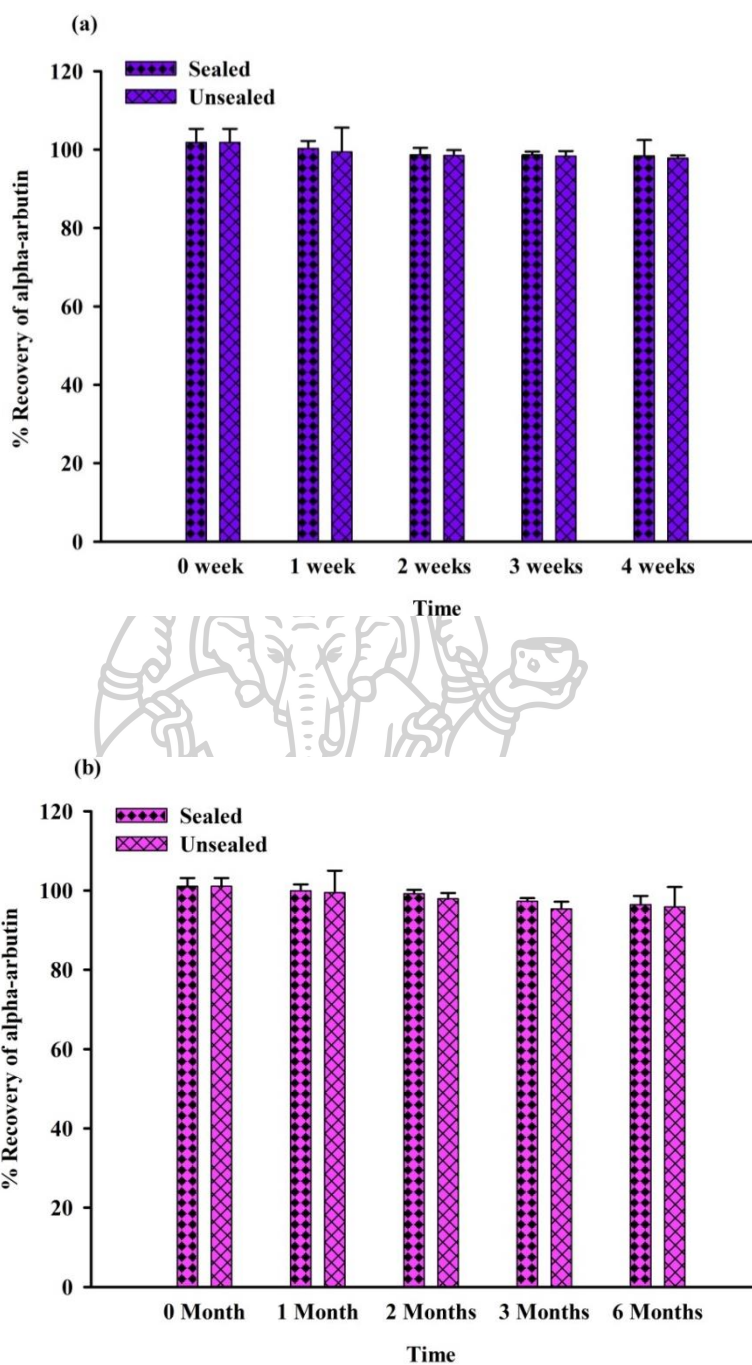
Figure 49. The percentage recovery of AA under sealed and unsealed conditions at 25±2°C with 60±5% RH from (a) 8% AA-loaded HPMC/PVP-K90 DMNs at 0, 1, 2, 3, and 4 weeks and (b) 8% AA-loaded PAMA/PVA DMNs at 0, 1, 2, 3, and 6 months (means ± SD, n = 3)

4.11.2 Res-loaded DMNs

The 5% Res loaded into Eudragit E/PVP-K90 DMNs and Eudragit RS/PVP-K90 DMNs were kept in sealed and unsealed conditions at 25 ± 2°C with 60 ± 5% RH to assess their physical and chemical stability at 0, 1, 2, 3 and 4 weeks (Figure 50 (a) and (b)). Both types of Res-loaded Eudragit E/PVP-K90 DMNs and Eudragit RS/PVP-K90 DMNs showed a good physical appearance at all designated times under sealed and unsealed packages. The percentage recovery of Res from 5% Res-loaded Eudragit E/PVP-K90 DMNs was ranged between 101.88 ± 5.68% to 107.62 ± 3.03% under sealed packages and 101.65 ± 3.12 to 107.62 ± 3.03% for unsealed packages, whereas 5% Res-loaded Eudragit RS/PVP-K90 DMNs were between 103.98 ± 1.49% to 107.28 ± 1.22% for sealed packages and 102.79 ± 6.72 to 107.28 ± 1.22% for unsealed containers when compared with the initial concentration. According to these results, the excellent stability of Res from Eudragit E/VP-K90 DMNs and Eudragit RS/PVP-K90 DMNs were observed and indicated that no drug-polymers interaction affected the stability of DMNs patches.
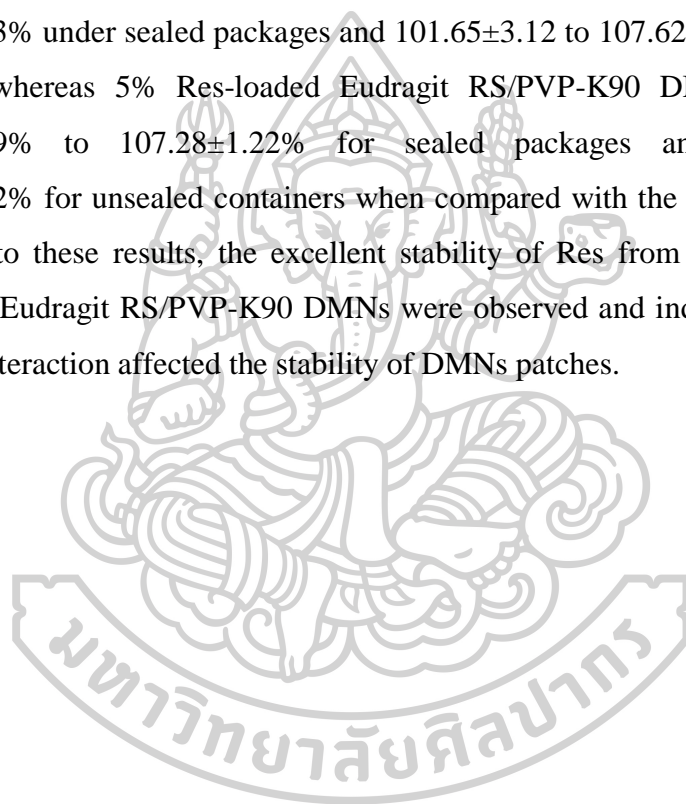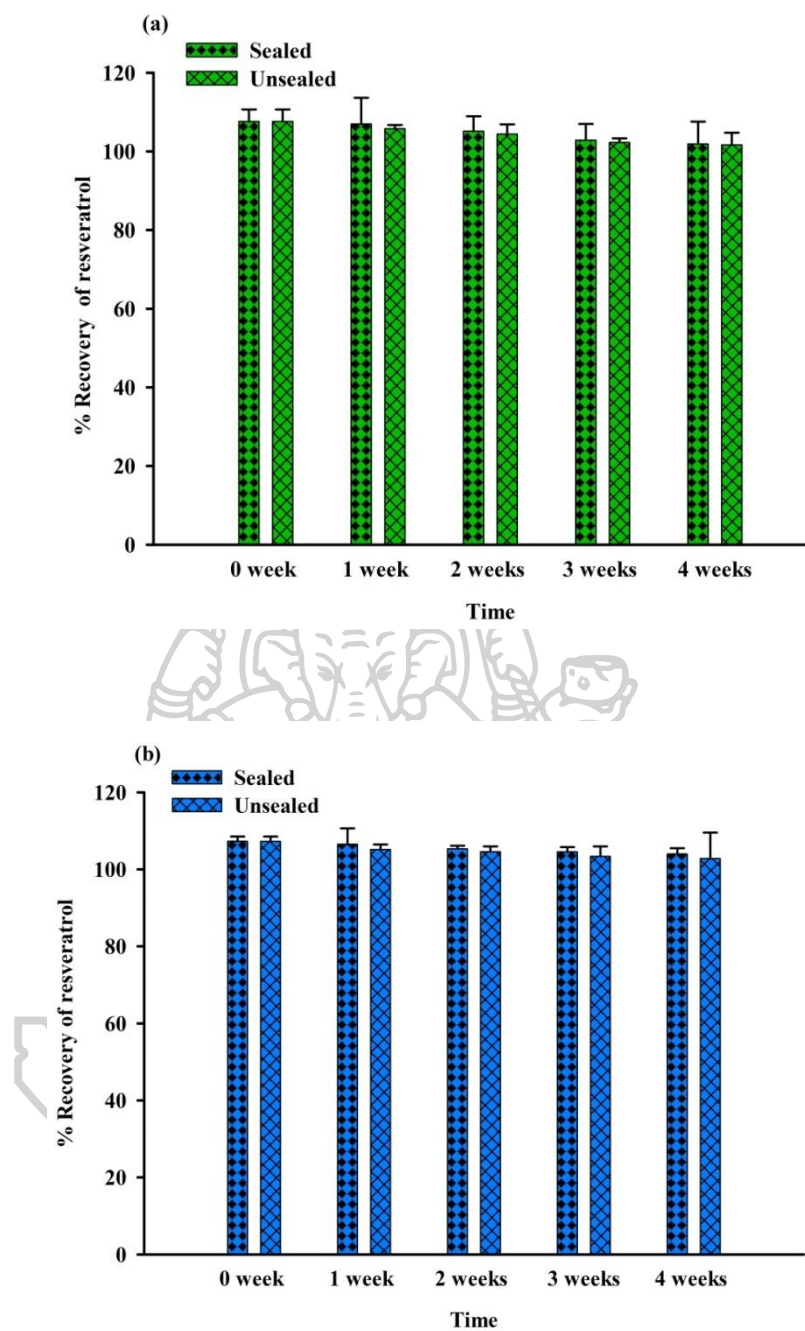
Figure 50. The percentage recovery of Res under sealed and unsealed storage conditions at 25±2°C with 60±5% RH from (a) 5% Res-loaded Eudragit E/PVP-K90 DMNs and (b) 5% Res-loaded Eudragit RS/PVP-K90 DMNs at 0, 1, 2, 3 and 4 weeks (means ± SD, n = 3)

4.11.3 The combination of AA- and Res-loaded DMNs

To evaluate the stability of AA and Res from DMNs, 10% AA and 2% Res-loaded Eudragit RL/PVP-K90 DMNs were stored under sealed and unsealed packages at 25 ± 2ºC with 60 ± 5% RH for 6 months. On the other hand, the same DMNs formulation was kept at 5 ± 3ºC by wrapping with aluminium foil over sealed packages. Figure 51 (a) illustrates the percentage recovery of AA and Res at 25 ± 2ºC with 60 ± 5% RH for 6 months. The results revealed that there was no significant change in physical stability in both sealed and unsealed storage conditions. The amount of AA over 6 months was observed approximately 95.77 ± 7.12% (13.17% reduced compared to initial) in sealed packages and 95.96 ± 7.44% (13% reduced compared to initial) in unsealed packages compared with initial concentration (110.29 ± 4.54%). In the case of Res, percentage recovery from DMNs was found to be 96.02 ± 1.62% for sealed packages and 98.65 ± 2.37% for unsealed packages compared to the initial concentration (107.23 ± 3.25%).

The percentage recovery amount of AA from 10% AA and 2% Res-loaded Eudragit RL/PVP-K90 DMNs stored at 5 ± 3ºC was found in ranged 98.39 ± 6.66% to 110.29 ± 11.47%. Moreover, the percentage recovery of Res was 100.85 ± 2.15% compared with the initial concentration (114.95 ± 9.33%) (Figure 51 (b)). However, the DMNs patch was observed that all arrays were soft under 5ºC storage periods. These arrays were physically unstable and could not pierce the skin. Therefore, the results revealed that both physically and chemically stable AA and Res from Eudragit RL/PVP-K90 DMNs were observed at 25ºC.
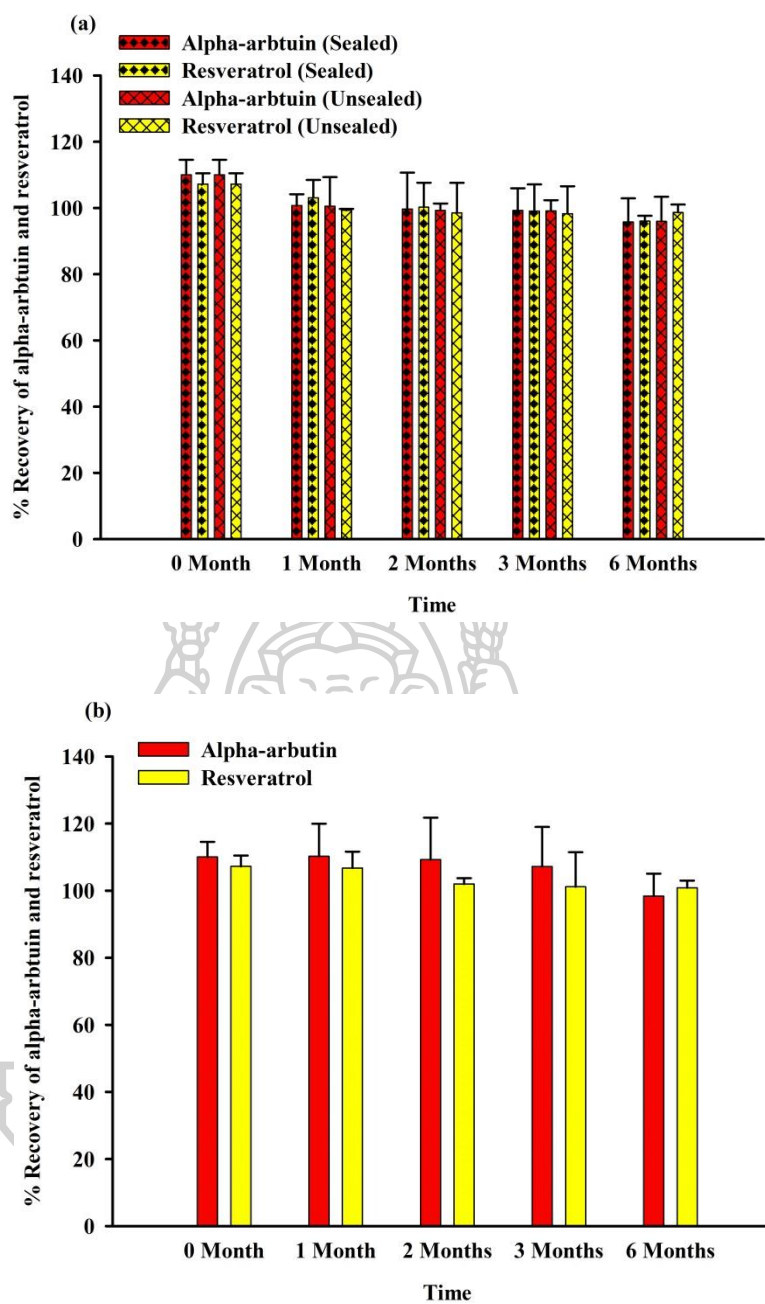
Figure 51. The percentage recovery of AA and Res from the combination of 10 % AA and 2% Res-loaded Eudragit RL/PVP-K90 DMNs at 0, 1, 2, 3 and 6 months, (a) storage at 25±2ºC with 60±5% RH under sealed and unsealed packages and (b) storage at 5±3ºC under sealed packages (means ± SD, n = 3)

CHAPTER 5
CONCLUSION

In this study, alpha-arbutin (AA) and resveratrol (Res) were selected as depigmentation agents because of their effective melanogenesis inhibition and antioxidant activities. However, AA has poor skin permeation, and Res has poor solubility and chemical instability. Therefore, AA was loaded into two types of DMNs which were fabricated using HPMC/PVP-K90 (1:1) and PAMA/PVA (1:4). Res-loaded DMNs were also developed using Eudragit E100/PVP-K90 (1:2) and Eudragit RS100/PVP-K90 (1:2). Moreover, the synergism combination of AA and Res at the weight ratios of 5:1 was incorporated into Eudragit RL100/PVP-K90 (1:2) to fabricate DMNs. AA- and/or Res-loaded DMNs were fabricated by micromolding method, and their morphology, mechanical strength, skin penetration, loading efficiency, and loading capacity were characterized. *In vitro* and *in vivo* dissolution times, skin permeation, skin resealing ability in mice, and stability were also evaluated. Finally, AA and Res-loaded DMNs were applied to human volunteers for safety and clinical assessment. The results of this study could be concluded as follows:

5.1 Development of AA-loaded DMNs

Eight percent AA-loaded HPMC/PVP-K90 DMNs and PAMA/PVA DMNs were successfully fabricated. All arrays were strong, sharp, and had an elegant appearance. In addition, both 8% AA-loaded HPMC/PVP-K90 and PAMA/PVA DMNs exhibited considerable ability to resist compression forces, and approximately 100% of MNs were penetrated through neonatal porcine skin after removal of the DMNs. The loading efficiency and loading capacity of 8% AA-loaded HPMC/PVP-K90 DMNs were higher than 8% AA-loaded PAMA/PVA DMNs. All MNs arrays from both DMNs formulations were dissolved entirely within 45 min *in vitro* dissolution studies. Compared to their gel formulations and 5% AA commercial cream, both types of AA-loaded DMNs showed significantly delivered more AA into the epidermis of neonatal porcine skin. Based on *in vivo* permeation and skin accumulation studies, a plasma concentration of AA was found in the blood of mice

applied by 8% AA-loaded PAMA/PVADMNs and 5% AA commercial cream over 24 h. In contrast, any AA was not found in mice's blood from 8% AA-loaded HPMC/PVP-K90 DMNs. However, the accumulated amount of AA in the mice's skin using both DMNs was significantly higher than the commercial cream formulation. Furthermore, the mice skins were resealed naturally without damaging the skin after removing all AA-loaded DMNs. AA was physically and chemically highly stable in sealed and unsealed packages at 25ºC for 1 month of HPMC/PVP-K90 DMNs and 6 months of PAMA/PVA DMNs.

5.2 Development of Res-loaded DMNs

The arrays of 5% Res-loaded Eudragit E/PVP-K90 DMNs and 5% Res-loaded Eudragit RS/PVP-K90 DMNs showed promising results with an elegant appearance and ability to resist the different compression forces. Both types of DMNs were successfully inserted into the neonatal porcine skin. All MNs tips were entirely dissolved within 30 min. In the case of loading efficiency and loading capacity, Res was successfully loaded, and similar results were found between the two types of DMNs. *In vitro* skin permeation studies proved that after applying DMNs, an increase in resveratrol was delivered into the neonatal porcine skin compared with their gel formulations over 24 h. Moreover, the accumulated amount of Res in the neonatal porcine skin following 24 h application of DMNs had a higher level of Res than their gel formulations. The stability study showed good recovery of Res from both DMNs with an excellent physical appearance at 25ºC for 1 month.

5.3 Development of AA and Res-loaded DMNs

The synergism combination of AA and Res at the weight ratios of 5:1 was successfully encapsulated into the Eudragit RL/PVP-K90 DMNs. The morphology showed that all arrays were fully formed and sharp with a strong baseplate. DMNs also possessed high mechanical resistant property and created 100% microholes on the neonatal porcine skin after applying the DMNs. For the percentage loading efficiency and loading capacity, a significant amount AA and resveratrol was successfully loaded into the Eudragit RL/PVP-K90 polymer mixture. According to the results of *in vitro* and *in vivo* dissolution studies, all needles were dissolved entirely within 15 min in neonatal porcine skin and mice. The higher permeated

amount of AA and Res through the neonatal porcine skins was also found in the DMNs formulation compared with gel and cream formulation. *In vivo* study also proved that AA and Res loaded DMNs was able to bypass the SC and delivered a higher amount of AA into the blood of mice than cream formulation. In contrast, Res was not found in mice blood. However, the increased amount of AA and Res accumulated in mice skin at 24 h was also found in DMNs. The skin's microholes were naturally resealed within a reasonable duration without defect the skin after withdrawal of DMNs. There was no significant change in physical appearance, and AA and Res remained stable in DMNs within 6 months stability at 5±3ºC or 25±2ºC with 60±5% RH. To determine the depigmentation effect of AA and Res in human volunteers, the application skin site was measured by DermaLab and compared with the control. In clinical studies, the results showed a slightly decreased in skin melanin ($p>0.05$), which improved the skin depigmentation effect without inducing skin erythema. Although the skin elasticity showed improvement, the skin hydration value was slightly decreased after DMNs application, this is due to epidermal loss some water contents from the skin. The elevated TEWL proved that DMNs exhibited sufficient human skin puncturability. Furthermore, the developed DMNs containing AA and Res did not cause any skin hypersensitivity in human volunteers.

All the results indicated that developed AA- and/or Res-loaded DMNs could be an excellent promising platform for transdermal delivery of skin depigmentation agents.

REFERENCES

1. Park K, Kwon H, Lee C, Kim D, Yoon J, Kim M, et al. Efficacy and safety of a new microneedle patch for skin brightening: A Randomized, split-face, single-blind study. Journal of cosmetic dermatology. 2017;16.

2. Ebanks JP, Wickett RR, Boissy RE. Mechanisms regulating skin pigmentation: the rise and fall of complexion coloration. International journal of molecular sciences. 2009;10(9):4066-87.

3. Solano F, Briganti S, Picardo M, Ghanem G. Hypopigmenting agents: an updated review on biological, chemical and clinical aspects. Pigment cell research. 2006;19(6):550-71.

4. Lee TH, Seo J, Baek S-H, Kim S. Inhibitory Effects of Resveratrol on Melanin Synthesis in Ultraviolet B-Induced Pigmentation in Guinea Pig Skin. Biomolecules & therapeutics. 2014;22:35-40.

5. Arbab A, Eltahir M. Review on Skin Whitening Agents. Khartoum Pharmacy Journal. 2010;13:5-7.

6. Shin J, Park K. Current clinical use of depigmenting agents. Dermatologica Sinica. 2014;32.

7. Ebanks JP, Wickett RR, Boissy RE. Mechanisms regulating skin pigmentation: the rise and fall of complexion coloration. International journal of molecular sciences. 2009;10(9):4066-87.

8. Gillbro JM, Olsson MJ. The melanogenesis and mechanisms of skin-lightening agents – existing and new approaches. International Journal of Cosmetic Science. 2011;33(3):210-21.

9. Desmedt B, Courselle P, De Beer JO, Rogiers V, Grosber M, Deconinck E, et al. Overview of skin whitening agents with an insight into the illegal cosmetic market in Europe. Journal of the European Academy of Dermatology and Venereology : JEADV. 2016;30(6):943-50.

10. Lee H-J, Kim K-W. Anti-inflammatory effects of arbutin in lipopolysaccharide-stimulated BV2 microglial cells. Inflammation research : official journal of the European Histamine Research Society [et al]. 2012;61:817-25.

11. Couteau C, Coiffard L. Overview of Skin Whitening Agents: Drugs and Cosmetic Products. Cosmetics. 2016;3(3):27.

12. Migas P, Krauze-Baranowska M. The significance of arbutin and its derivatives in therapy and cosmetics. Phytochemistry Letters. 2015;13:35-40.

13. Lin J-W, Chiang H-M, Lin Y-C, Wen K-C. Natural Products with Skin – Whitening Effects. Journal of Food and Drug Analysis. 2008;16.

14. Sccs, Degen GH. Opinion of the Scientific Committee on Consumer safety (SCCS) – Opinion on the safety of the use of α-arbutin in cosmetic products. Regulatory Toxicology and Pharmacology. 2016;74:75-6.

15. Won J, Park J. Improvement of Arbutin Trans-Epidermal Delivery Using Radiofrequency Microporation2014. 1775-81 p.

16. Gülçin I. Antioxidant properties of resveratrol: A structure-activity insight. Innovative Food Science & Emerging Technologies. 2010;11:210-8.

17. Elshaer M, Chen Y, Wang X, Tang X. Resveratrol: An overview of its anti-cancer mechanisms. Life Sciences. 2018;207.

18. Li J, Zhang C-X, Liu Y-M, Chen K-L, Chen G. A comparative study of anti-aging properties and mechanism: resveratrol and caloric restriction. Oncotarget. 2017;8(39):65717-29.

19. Gatson J, Liu M-M, Abdelfattah K, Wigginton J, Smith S, Wolf S, et al. Resveratrol decreases inflammation in the brain of mice with mild traumatic brain injury. The journal of trauma and acute care surgery. 2013;74:470-5.

20. Osman a-m, Al-HarthI S, Alarabi O, Elshal M, Ramadan W, Alaama M, et al. Chemosensetizing and cardioprotective effects of resveratrol in doxorubicin-treated animals. Cancer cell international. 2013;13:52.

21. Campagna M, Rivas C. Antiviral activity of resveratrol. Biochem Soc Trans. 2010;38(Pt 1):50-3.

22. Na J-I, Shin J-W, Choi H-R, Kwon S-H, Park K-C. Resveratrol as a Multifunctional Topical Hypopigmenting Agent. International journal of molecular sciences. 2019;20(4):956.

23. Pentek T, Newenhouse E, O'Brien B, Chauhan AS. Development of a Topical Resveratrol Formulation for Commercial Applications Using Dendrimer Nanotechnology. Molecules (Basel, Switzerland). 2017;22(1).

24. Allan K, Lenehan C, Ellis A. UV Light Stability of α-Cyclodextrin/Resveratrol Host–Guest Complexes and Isomer Stability at Varying pH. Australian Journal of Chemistry - AUST J CHEM. 2009;62.

25. Robinson K, Mock C, Liang D. Pre-formulation studies of resveratrol. Drug development and industrial pharmacy. 2014;41:1-6.

26. Devi P, Sharma P, Rathore C, Negi P. Novel Drug Delivery Systems of Resveratrol to Bioavailability and Therapeutic Effects. 2019.

27. Davidov-Pardo G, McClements D. Resveratrol Encapsulation: Designing Delivery Systems To Overcome Solubility, Stability And Bioavailability Issues. Trends in Food Science & Technology. 2014;38.

28. Caddeo C, Teskac K, Sinico C, Kristl J. Effect of resveratrol incorporated in liposomes on proliferation and UV-B protection of cells. International journal of pharmaceutics. 2008;363(1-2):183-91.

29. Shao J, Li X, Lu X, Jiang C, Hu Y, Li Q, et al. Enhanced growth inhibition effect of resveratrol incorporated into biodegradable nanoparticles against glioma cells is mediated by the induction of intracellular reactive oxygen species levels. Colloids and surfaces B, Biointerfaces. 2009;72(1):40-7.

30. Dillon C, Hughes H, O'Reilly N, McLoughlin P. Formulation and characterisation of dissolving Microneedles for the transdermal delivery of therapeutic peptides. International journal of pharmaceutics. 2017;526.

31. Lee KJ, Jeong SS, Roh DH, Kim DY, Choi H-K, Lee EH. A practical guide to the development of microneedle systems – In clinical trials or on the market. International journal of pharmaceutics. 2020;573:118778.

32. van der Maaden K, Jiskoot W, Bouwstra J. Microneedle Technologies for (Trans) Dermal Drug and Vaccine Delivery. Journal of controlled release : official journal of the Controlled Release Society. 2012;161:645-55.

33. Larrañeta E, Lutton REM, Woolfson A, Donnelly R. Microneedle arrays as transdermal and intradermal drug delivery systems: Materials science, manufacture and commercial development. Materials Science & Engineering R-reports. 2016;104:1-32.

34. Bhatnagar S, Gadeela PR, Thathireddy P, Venuganti VVK. Microneedle-based drug delivery: materials of construction. Journal of Chemical Sciences. 2019;131(9):90.

35. Kim Y-C, Park J-H, Prausnitz MR. Microneedles for drug and vaccine delivery. Advanced Drug Delivery Reviews. 2012;64(14):1547-68.

36. Guillot A, Cordeiro A, Donnelly R, Montesinos C, Garrigues T, Melero A. Microneedle-Based Delivery: An Overview of Current Applications and Trends. Pharmaceutics. 2020;12:569.

37. Hong X, Wei L, Wu F, Wu Z, Chen L, Liu Z, et al. Dissolving and biodegradable microneedle technologies for transdermal sustained delivery of drug and vaccine. Drug design, development and therapy. 2013;7:945-52.

38. Kim S, Yang H, Kim M, Baek J, Kim S, An S, et al. 4-n-butylresorcinol dissolving microneedle patch for skin depigmentation: A randomized, double-blind, placebo-controlled trial. Journal of cosmetic dermatology. 2015;15.

39. Nguyen H, Bozorg BD, Kim Y, Wieber A, Birk G, Lubda D, et al. Poly (vinyl alcohol) microneedles: Fabrication, characterization, and application for transdermal drug delivery of doxorubicin. European Journal of Pharmaceutics and Biopharmaceutics. 2018;129.

40. Yao G, Quan G, Lin S, Peng T, Wang Q, Ran H, et al. Novel dissolving microneedles for enhanced transdermal delivery of levonorgestrel: In vitro and in vivo characterization. International journal of pharmaceutics. 2017;534(1):378-86.

41. Cheng J, Chen G, Zhu Y. Fe3O4/Polycaprolactone Microneedles with Controlled Drug Delivery and Magnetic Hyperthermia. Nano Advances. 2017;2:29-35.

42. Li W, Terry RN, Tang J, Feng MR, Schwendeman SP, Prausnitz MR. Rapidly separable microneedle patch for the sustained release of a contraceptive. Nature biomedical engineering. 2019;3(3):220-9.

43. Hutton A, Quinn H, McCague P, Jarrahian C, Rein-Weston A, Coffey P, et al. Transdermal delivery of vitamin K using dissolving microneedles for the prevention of vitamin K deficiency bleeding. International journal of pharmaceutics. 2018;541.

44. Chen M-C, Ling M-H, Lai K-Y, Pramudityo E. Chitosan Microneedle Patches for Sustained Transdermal Delivery of Macromolecules. Biomacromolecules. 2012;13.

45. Park Y-H, Ha SK, Choi I, Kim KS, Park J, Choi N, et al. Fabrication of degradable carboxymethyl cellulose (CMC) microneedle with laser writing and replica molding process for enhancement of transdermal drug delivery. Biotechnology and Bioprocess Engineering. 2016;21(1):110-8.

46. McCrudden MTC, Alkilani AZ, McCrudden CM, McAlister E, McCarthy HO, Woolfson AD, et al. Design and physicochemical characterisation of novel dissolving polymeric microneedle arrays for transdermal delivery of high dose, low molecular weight drugs. Journal of controlled release : official journal of the Controlled Release Society. 2014;180(100):71-80.

47. Ling M-H, Chen M-C. Dissolving Polymer Microneedle Patches for Rapid and Efficient Transdermal Delivery of Insulin to Diabetic Rats. Acta biomaterialia. 2013;9.

48. Ghosal K, Chakrabarty S, Nanda A. Hydroxypropyl methylcellulose in drug delivery. Der Pharmacia Sinica. 2011;2:152-68.

49. Gaaz T, Bakar A, Akhtar M, Kadhum A, Kadhum H, Mohamad AB, et al. Properties and Applications of Polyvinyl Alcohol, Halloysite Nanotubes and Their Nanocomposites. Molecules (Basel, Switzerland). 2016;20.

50. Gibas I, Janik H. Review: Synthetic Polymer Hydrogels for Biomedical Applications. Chem Chem Technol. 2010;4:297-304.

51. Maitra J, Shukla V. Cross-linking in hydrogels - a review. Am J Polym Sci. 2014;4:25-31.

52. Adeli E. Irbesartan-loaded electrospun nanofibers-based PVP K90 for the drug dissolution improvement: Fabrication, in vitro performance assessment, and in vivo evaluation. Journal of Applied Polymer Science. 2015;132.

53. Saharan P, Bahmani K, Saharan S. Preparation, Optimization and In vitro Evaluation of Glipizide Nanoparticles Integrated with Eudragit RS-100. Pharmaceutical Nanotechnology. 2019;07.

54. Wang Y, Hao M-M, Sun Y, Wang L-F, Wang H, Zhang Y-J, et al. Synergistic Promotion on Tyrosinase Inhibition by Antioxidants. Molecules (Basel, Switzerland). 2018;23:106.

55. Moon E, Kim AJ, Kim SY. Sarsasapogenin Increases Melanin Synthesis via Induction of Tyrosinase and Microphthalmia-Associated Transcription Factor Expression in Melan-a Cells. Biomol Ther (Seoul). 2012;20(3):340-5.

56. Parvez S, Kang M, Chung HS, Cho C, Hong MC, Shin MK, et al. Survey and mechanism of skin depigmenting and lightening agents. Phytotherapy research : PTR. 2006;20(11):921-34.

57. Arbab A, Mudawi M. Review on Skin Whitening Agents. Khartoum Pharmacy Journal. 2010;13:5-7.

58. Ebrahimi B, Naeini FF. Topical tranexamic acid as a promising treatment for melasma. J Res Med Sci. 2014;19(8):753-7.

59. Briganti S, Camera E, Picardo M. Chemical and Instrumental Approaches to Treat Hyperpigmentation. Pigment cell research / sponsored by the European Society for Pigment Cell Research and the International Pigment Cell Society. 2003;16:101-10.

60. Shankar K, Godse K, Aurangabadkar S, Lahiri K, Mysore V, Ganjoo A, et al. Evidence-Based Treatment for Melasma: Expert Opinion and a Review. Dermatology and therapy. 2014;4.

61. Gupta A. A validated UV spectrophotometric method for simultaneous estimation of tretinoin and benzoyl peroxide in bulk and semisolid dosage form. Rasayan J Chem. 2009.

62. Bala HR, Lee S, Wong C, Pandya AG, Rodrigues M. Oral Tranexamic Acid for the Treatment of Melasma: A Review. Dermatologic surgery : official publication for American Society for Dermatologic Surgery [et al]. 2018;44(6):814-25.

63. Sher N, Fatima N, Perveen S, Siddiqui F, Sial AW. Pregabalin and Tranexamic Acid Evaluation by Two Simple and Sensitive Spectrophotometric Methods. International Journal of Analytical Chemistry. 2015;2015.

64. Sang S, Hou Z, Lambert JD, Yang CS. Redox properties of tea polyphenols and related biological activities. Antioxidants & redox signaling. 2005;7(11-12):1704-14.

65. Navarrete-Solís J, Castanedo-Cazares J, Torres-Álvarez B, Oros-Ovalle C, Fuentes-Ahumada C, Gonzalez F, et al. A Double-Blind, Randomized Clinical Trial of Niacinamide 4% versus Hydroquinone 4% in the Treatment of Melasma. Dermatology research and practice. 2011;2011:379173.

66. Burdock G, Soni M, Carabin I. Evaluation of Health Aspects of Kojic Acid in Food. Regulatory toxicology and pharmacology : RTP. 2001;33:80-101.

67. Eslmifar M, Khezri K, Saeedi M. Kojic acid applications in cosmetic and pharmaceutical preparations. Biomedicine & Pharmacotherapy. 2019;110:582-93.

68. Anil K, Rekha R, Poonam Y. Azelaic Acid: A Promising Agent for Dermatological Applications. Current Drug Therapy. 2020;15(3):181-93.

69. Ito S, Nishigaki A, Ishii-Osai Y, Ojika M, Wakamatsu K, Yamashita T, et al. Mechanism of putative neo-antigen formation from N-propionyl-4-S-cysteaminylphenol, a tyrosinase substrate, in melanoma models. Biochemical Pharmacology. 2012;84(5):646-53.

70. Ali S, Galgut J, Choudhary R. On The Novel Action of Melanolysis by a Leaf Extract of Aloe vera and Its Active Ingredient Aloin, Potent Skin Depigmenting Agents. Planta medica. 2012;78:767-71.

71. Jones K, Hughes J, Hong M, Jia Q, Orndorff S. Modulation of Melanogenesis by Aloesin: A Competitive Inhibitor of Tyrosinase. Pigment cell research. 2002;15(5):335-40.

72. Park K-C, Huh S, Choi H-R, Kim D-S. Biology of melanogenesis and the search for hypopigmenting agents. Dermatologica Sinica - DERMATOL SIN. 2010;28:53-8.

73. Amer M, Metwalli M. Topical Liquiritin improves melasma. International journal of dermatology. 2000;39:299-301.

74. YOKOTA T, NISHIO H, KUBOTA Y, MIZOGUCHI M. The Inhibitory Effect of Glabridin from Licorice Extracts on Melanogenesis and Inflammation. Pigment cell research. 1998;11(6):355-61.

75. Badreshia-Bansal S, Draelos Z. Insight into skin lightening cosmeceuticals for women of color. Journal of drugs in dermatology : JDD. 2007;6:32-9.

76. Draelos Z. Skin lightening preparations and the hydroquinone controversy. Dermatologic therapy. 2007;20:308-13.

77. Ando H, Ryu A, Hashimoto A, Oka M, Ichihashi M. Linoleic acid and alpha-linolenic acid lightens ultraviolet-induced hyperpigmentation of the skin. Archives of dermatological research. 1998;290(7):375-81.

78. Hakozaki T, Minwalla L, Zhuang J, Chhoa M, Matsubara A, Miyamoto K, et al. The effect of niacinamide on reducing cutaneous pigmentation and suppression of melanosome transfer. The British journal of dermatology. 2002;147:20-31.

79. Greatens A, Hakozaki T, Koshoffer A, Epstein H, Schwemberger S, Babcock G, et al. Effective inhibition of melanosome transfer to keratinocytes by lectins and niacinamide is reversible. Experimental dermatology. 2005;14:498-508.

80. Zhang Y, Kung C-P, Sil BC, Lane ME, Hadgraft J, Heinrich M, et al. Topical Delivery of Niacinamide: Influence of Binary and Ternary Solvent Systems. Pharmaceutics. 2019;11(12):668.

81. Farris PK. Topical Vitamin C: A Useful Agent for Treating Photoaging and Other Dermatologic Conditions. Dermatologic Surgery. 2005;31(s1):814-8.

82. Barrita J, Snchez M. Antioxidant Role of Ascorbic Acid and His Protective Effects on Chronic Diseases. 2013.

83. Nukala U, Thakkar S, Krager KJ, Breen PJ, Compadre CM, Aykin-Burns N. Antioxidant Tocols as Radiation Countermeasures (Challenges to be Addressed to Use Tocols as Radiation Countermeasures in Humans). Antioxidants. 2018;7(2):33.

84. Lukas B, Schmiderer C, Mitteregger U, Novak J. Arbutin in marjoram and oregano. Food Chemistry - FOOD CHEM. 2010;121:185-90.

85. Yu S, Wang Y, Tian Y, Xu W, Bai Y, Zhang T, et al. Highly efficient biosynthesis of#±-arbutin from hydroquinone by an amylosucrase from Cellulomonas carboniz. Process Biochemistry. 2018;68:93-9.

86. Funayama M, Arakawa H, Yamamoto R, Nishino T, Shin T, Murao S. Effects of α- and β-Arbutin on Activity of Tyrosinases from Mushroom and Mouse Melanoma. Bioscience, Biotechnology, and Biochemistry. 1995;59(1):143-4.

87. Sugimoto K, Nishimura T, Nomura K, Sugimoto K, Kuriki T. Inhibitory effects of alpha-arbutin on melanin synthesis in cultured human melanoma cells and a three-dimensional human skin model. Biol Pharm Bull. 2004;27(4):510-4.

88. Garcia-Jimenez A, Teruel-Puche JA, Berna J, Rodriguez-Lopez JN, Tudela J, Garcia-Canovas F. Action of tyrosinase on alpha and beta-arbutin: A kinetic study. PLOS ONE. 2017;12(5):e0177330.

89. Wang ZX, Shi XX, Chen GR, Ren ZH, Luo L, Yan J. A new synthesis of alpha-arbutin via Lewis acid catalyzed selective glycosylation of tetra-O-benzyl-alpha-D-glucopyranosyl trichloroacetimidate with hydroquinone. Carbohydrate research. 2006;341(11):1945-7.

90. Seo DH, Jung JH, Ha SJ, Cho HK, Jung DH, Kim TJ, et al. High-yield enzymatic bioconversion of hydroquinone to α-arbutin, a powerful skin lightening agent, by amylosucrase. Applied microbiology and biotechnology. 2012;94(5):1189-97.

91. Maeda K, Fukuda M. Arbutin: mechanism of its depigmenting action in human melanocyte culture. The Journal of pharmacology and experimental therapeutics. 1996;276(2):765-9.

92. Polouliakh N, Ludwig V, Meguro A, Kawagoe T, Heeb O, Mizuki N. Alpha-Arbutin Promotes Wound Healing by Lowering ROS and Upregulating Insulin/IGF-1 Pathway in Human Dermal Fibroblast. Frontiers in physiology. 2020;11:586843.

93. Li H, Jeong Y-M, Kim S, Kim M-K, Kim D-S. Arbutin inhibits TCCSUP human bladder cancer cell proliferation via up-regulation of p21. Die Pharmazie. 2011;66:306-9.

94. Liao A-H, Ma W-C, Wang C-H, Yeh M-K. Penetration depth, concentration and efficiency of transdermal α-arbutin delivery after ultrasound treatment with albumin-shelled microbubbles in mice. Drug Delivery. 2014;23.

95.   Liang K, Xu K, Bessarab D, Obaje J, Xu C. Arbutin encapsulated micelles improved transdermal delivery and suppression of cellular melanin production. BMC Research Notes. 2016;9.

96.   Ayumi NS, Sahudin S, Hussain Z, Hussain M, Samah NHA. Polymeric nanoparticles for topical delivery of alpha and beta arbutin: preparation and characterization. Drug delivery and translational research. 2019;9(2):482-96.

97.   Sergides C, Chirilă M, Silvestro L, Pitta D, Pittas A. Bioavailability and safety study of resveratrol 500 mg tablets in healthy male and female volunteers. Experimental and therapeutic medicine. 2016;11(1):164-70.

98.   Baxter R. Anti-aging properties of resveratrol: Review and report of a potent new antioxidant skin care formulation. Journal of cosmetic dermatology. 2008;7:2-7.

99.   Shah P, Patel J. Resveratrol and its biological actions. International Journal of Green Pharmacy. 2010;4.

100.   Wang Y, Hao M-M, Sun Y, Wang L-F, Wang H, Zhang Y-J, et al. Synergistic Promotion on Tyrosinase Inhibition by Antioxidants. Molecules (Basel, Switzerland). 2018;23(1):106.

101.   Newton R, Cook A, Roberts D, Leonard J, Sturm R. Post-Transcriptional Regulation of Melanin Biosynthetic Enzymes by cAMP and Resveratrol in Human Melanocytes. The Journal of investigative dermatology. 2007;127:2216-27.

102.   Gambini J, Inglés M, Olaso G, Lopez-Grueso R, Bonet-Costa V, Gimeno-Mallench L, et al. Properties of Resveratrol: In Vitro and In Vivo Studies about Metabolism, Bioavailability, and Biological Effects in Animal Models and Humans. Oxidative medicine and cellular longevity. 2015;2015:837042.

103.   Ruivo J, Francisco C, Oliveira R, Figueiras A. The main potentialities of resveratrol for drug delivery systems. Brazilian Journal of Pharmaceutical Sciences. 2015;51.

104.   Leonard S, Xia C, Jiang B-H, Stinefelt B, Klandorf H, Harris G, et al. Resveratrol scavenges reactive oxygen species and effects radical-induced cellular responses. Biochemical and biophysical research communications. 2003;309:1017-26.

105.   Na J-I, Shin J-W, Choi H-R, Kwon S-H, Park K-C. Resveratrol as a Multifunctional Topical Hypopigmenting Agent. International journal of molecular sciences. 2019;20:956.

106.   Meng T, Xiao D, Muhammed A, Deng J, Chen L, He J. Anti-Inflammatory Action and Mechanisms of Resveratrol. Molecules (Basel, Switzerland). 2021;26(1):229.

107.   Ko J-H, Sethi G, Um J-Y, Shanmugam MK, Arfuso F, Kumar AP, et al. The Role of Resveratrol in Cancer Therapy. International journal of molecular sciences. 2017;18(12):2589.

108.   Alonso C, Martí M, Barba C, Carrer V, Rubio L, Coderch L. Skin permeation and antioxidant efficacy of topically applied resveratrol. Archives of dermatological research. 2017;309.

109.   Neves AR, Lúcio M, Lima J, Reis S. Resveratrol in Medicinal Chemistry: A Critical Review of its Pharmacokinetics, Drug-Delivery, and Membrane Interactions. Current medicinal chemistry. 2012;19:1663-81.

110. Nam J-B, Ryu J-H, Kim JW, Chang I-S, Suh K-d. Stabilization of resveratrol immobilized in monodisperse cyano-functionalized porous polymeric microspheres. Polymer. 2005;46:8956-63.

111. Bahuguna A, Khan I, Bajpai VK, Chul S. MTT assay to evaluate the cytotoxic potential of a drug. Bangladesh Journal of Pharmacology. 2017;12:8.

112. Grela E, Kozłowska J, Grabowiecka A. Current methodology of MTT assay in bacteria – A review. Acta Histochemica. 2018;120.

113. Hu DN. Methodology for evaluation of melanin content and production of pigment cells in vitro. Photochemistry and photobiology. 2008;84(3):645-9.

114. Wilkes M, Wright C, Du Plessis J, Reeder A. Fitzpatrick Skin Type, Individual Typology Angle, and Melanin Index in an African Population. JAMA Dermatology. 2015.

115. Tai SS-K, Lin C-G, Wu M-H, Chang T-S. Evaluation of Depigmenting Activity by 8-Hydroxydaidzein in Mouse B16 Melanoma Cells and Human Volunteers. International journal of molecular sciences. 2009;10(10):4257-66.

116. Caffarel-Salvador E, Tuan-Mahmood TM, McElnay JC, McCarthy HO, Mooney K, Woolfson AD, et al. Potential of hydrogel-forming and dissolving microneedles for use in paediatric populations. International journal of pharmaceutics. 2015;489(1-2):158-69.

117. Lee K, Kumar, Kim J, Seong, Jung, Yang. Odorless Glutathione Microneedle Patches for Skin Whitening. Pharmaceutics. 2020;12:100.

118. Ono A, Ito S, Sakagami S, Asada H, Saito M, Quan Y-S, et al. Development of Novel Faster-Dissolving Microneedle Patches for Transcutaneous Vaccine Delivery. Pharmaceutics. 2017;9:27.

119. Madden J, O'Mahony C, Thompson M, O'Riordan A, Galvin P. Biosensing in dermal interstitial fluid using microneedle based electrochemical devices. Sensing and Bio-Sensing Research. 2020;29:100348.

120. Li CG, Lee K, Lee CY, Dangol M, Jung H. A Minimally Invasive Blood-Extraction System: Elastic Self-Recovery Actuator Integrated with an Ultrahigh-Aspect-Ratio Microneedle. Advanced Materials. 2012;24(33):4583-6.

121. Mahato R. Chapter 13 - Microneedles in Drug Delivery. In: Mitra AK, Cholkar K, Mandal A, editors. Emerging Nanotechnologies for Diagnostics, Drug Delivery and Medical Devices. Boston: Elsevier; 2017. p. 331-53.

122. Nagarkar R, Singh M, Nguyen H, Jonnalagadda K. A review of recent advances in Microneedle technology for transdermal drug delivery. Journal of Drug Delivery Science and Technology. 2020;59:101923.

123. Guillot AJ, Cordeiro AS, Donnelly RF, Montesinos MC, Garrigues TM, Melero A. Microneedle-Based Delivery: An Overview of Current Applications and Trends. Pharmaceutics. 2020;12(6).

124. Turner J, White L, Estrela P, Leese H. Hydrogel-Forming Microneedles: Current Advancements and Future Trends. Macromolecular Bioscience. 2020;21:2000307.

125. Bhatnagar S, Gadeela PR, Thathireddy P, Venuganti VV. Microneedle-based drug delivery: materials of construction. Journal of Chemical Sciences. 2019;131.

126. Hoang M, Ita K, Bair D. Solid Microneedles for Transdermal Delivery of Amantadine Hydrochloride and Pramipexole Dihydrochloride. Pharmaceutics. 2015;7.

127. Badrana M, Kuntschea J, Fahra A, editors. kin penetration enhancement by a microneedle device Dermaroller ®) in vitro : Dependency on needle size and pplied formulation2009.

128. Pamornpathomkul B, Wongkajornsilp A, Laiwattanapaisal W, Rojanarata T, Opanasopit P, Ngawhirunpat T. A combined approach of hollow microneedles and nanocarriers for skin immunization with plasmid DNA encoding ovalbumin. International journal of nanomedicine. 2017;12:885-98.

129. Tarbox TN, Watts AB, Cui Z, Williams RO. An update on coating/manufacturing techniques of microneedles. Drug delivery and translational research. 2018;8(6):1828-43.

130. Pradeep Narayanan S, Raghavan S. Fabrication and characterization of gold-coated solid silicon microneedles with improved biocompatibility. The International Journal of Advanced Manufacturing Technology. 2019;104(9):3327-33.

131. Lee kJ, Jeong S, Roh D, Kim D, Choi H-K, Lee E. A Practical Guide to the Development of Microneedle Systems – in Clinical Trials or on the Market. International journal of pharmaceutics. 2019;573:118778.

132. González-Vázquez P, Larrañeta E, McCrudden MTC, Jarrahian C, Rein-Weston A, Quintanar-Solares M, et al. Transdermal delivery of gentamicin using dissolving microneedle arrays for potential treatment of neonatal sepsis. Journal of controlled release : official journal of the Controlled Release Society. 2017;265:30-40.

133. Park Y, Kim KS, Chung M, Sung JH, Kim B. Fabrication and characterization of dissolving microneedle arrays for improving skin permeability of cosmetic ingredients. Journal of Industrial and Engineering Chemistry. 2016;39:121-6.

134. Ita K. Dissolving Microneedles for Transdermal Drug Delivery: Advances and Challenges. Biomedicine & Pharmacotherapy. 2017;93.

135. Chen Y, Chen B, Wang Q, Jin X, Guo XD. Fabrication of coated polymer microneedles for transdermal drug delivery. Journal of Controlled Release. 2017;265.

136. Cao Y, Tao Y, Zhou Y, Gui S. Development of sinomenine hydrochloride-loaded polyvinylalcohol/maltose microneedle for transdermal delivery. Journal of Drug Delivery Science and Technology. 2016;35:1-7.

137. Ito Y, Kobuchi S, Inoue G, Kakumu E, Aoki M, Sakaeda T, et al. Dissolving microneedles for enhanced local delivery of capsaicin to rat skin tissue. Journal of Drug Targeting. 2016;25:1-26.

138. Pamornpathomkul B, Ngawhirunpat T, Tekko IA, Vora L, McCarthy HO, Donnelly RF. Dissolving polymeric microneedle arrays for enhanced site-specific acyclovir delivery. European Journal of Pharmaceutical Sciences. 2018;121:200-9.

139. Ronnander P, Simon L, Spilgies H, Koch A, Scherr S. Dissolving polyvinylpyrrolidone-based microneedle systems for in-vitro delivery of sumatriptan succinate. European Journal of Pharmaceutical Sciences. 2017;114.

140. Qiu Y, Li C, Zhang S, Yang G, Meilin H, Gao Y. Systemic Delivery of Artemether by Dissolving Microneedles. International journal of pharmaceutics. 2016;508.

141. Hirobe S, Azukizawa H, Hanafusa T, Matsuo K, Quan Y-S, Kamiyama F, et al. Clinical study and stability assessment of a novel transcutaneous influenza vaccination using a dissolving microneedle patch. Biomaterials. 2015;57.

142. Qiu Y, Guo L, Zhang S, Xu B, Gao Y, Yan H, et al. DNA-based vaccination against hepatitis B virus using dissolving microneedle arrays adjuvanted by cationic liposomes and CpG ODN. Drug delivery. 2015;30:1-8.

143. Matsuo K, Hirobe S, Yokota Y, Ayabe Y, Seto M, Quan Y-S, et al. Transcutaneous immunization using a dissolving microneedle array protects against tetanus, diphtheria, malaria, and influenza. Journal of controlled release : official journal of the Controlled Release Society. 2012;160:495-501.

144. Edens C, Dybdahl-Sissoko N, Weldon W, Oberste M, Prausnitz M. Inactivated polio vaccination using a microneedle patch is immunogenic in the rhesus macaque. Vaccine. 2015;33.

145. Edens C, Collins M, Goodson J, Rota P, Prausnitz M. A Microneedle Patch Containing Measles Vaccine is Immunogenic in Non-human Primates. Vaccine. 2015;33.

146. Pattani A, McKay P, Garland M, Curran R, Migalska K, Cassidy C, et al. Microneedle Mediated Intradermal Delivery of Adjuvanted Recombinant HIV-1 CN54gp140 Effectively Primes Mucosal Boost Inoculations. Journal of controlled release : official journal of the Controlled Release Society. 2012;162:529-37.

147. Ito Y, Hagiwara E, Saeki A, Sugioka N, Takada K. Feasibility of microneedles for percutaneous absorption of insulin. European journal of pharmaceutical sciences : official journal of the European Federation for Pharmaceutical Sciences. 2006;29:82-8.

148. Fukushima K, Ise A, Morita H, Hasegawa R, Ito Y, Sugioka N, et al. Two-Layered Dissolving Microneedles for Percutaneous Delivery of Peptide/Protein Drugs in Rats. Pharmaceutical research. 2010;28:7-21.

149. Ito Y, Taniguchi M, Hayashi A, Anai M, Morita S, Ko E, et al. Application of dissolving microneedles to glucose monitoring through dermal interstitial fluid. Biol Pharm Bull. 2014;37(11):1776-81.

150. Ito Y, Inagaki Y, Kobuchi S, Takada K, Sakaeda T. Therapeutic Drug Monitoring of Vancomycin in Dermal Interstitial Fluid Using Dissolving Microneedles. International Journal of Medical Sciences. 2016;13(4):271-6.

151. Park KY, Kwon HJ, Lee C, Kim D, Yoon JJ, Kim MN, et al. Efficacy and safety of a new microneedle patch for skin brightening: A Randomized, split-face, single-blind study. Journal of cosmetic dermatology. 2017;16(3):382-7.

152. Azizi Machekposhti S, Soltani M, Najafizadeh P, Ebrahimi S, Chen P. Biocompatible polymer microneedle for transdermal delivery of tranexamic acid. Journal of Controlled Release. 2017;261.

153. Kang G, Tu TNT, Kim S, Yang H, Jang M, Jo D, et al. Adenosine-loaded dissolving microneedle patches to improve skin wrinkles, dermal density, elasticity and hydration. International Journal of Cosmetic Science. 2018;40(2):199-206.

154. Pamornpathomkul B, Ngawhirunpat T, Tekko I, Vora L, McCarthy H, Donnelly R. Dissolving polymeric microneedle arrays for enhanced site-specific acyclovir delivery. European Journal of Pharmaceutical Sciences. 2018;121.

155. Kathuria H, Kochhar JS, Fong MHM, Hashimoto M, Iliescu C, Yu H, et al. Polymeric Microneedle Array Fabrication by Photolithography. J Vis Exp. 2015(105):52914.

156. Kim JD, Kim M, Yang H, Lee K, Jung H. Droplet-born air blowing: novel dissolving microneedle fabrication. Journal of controlled release : official journal of the Controlled Release Society. 2013;170(3):430-6.

157. Singh P, Carrier A, Chen Y, Lin S, Wang J, Cui S, et al. Polymeric microneedles for controlled transdermal drug delivery. Journal of Controlled Release. 2019;315.

158. Larrañeta E, Lutton REM, Woolfson AD, Donnelly RF. Microneedle arrays as transdermal and intradermal drug delivery systems: Materials science, manufacture and commercial development. Materials Science and Engineering: R: Reports. 2016;104:1-32.

159. Tuan-Mahmood TM, McCrudden MT, Torrisi BM, McAlister E, Garland MJ, Singh TR, et al. Microneedles for intradermal and transdermal drug delivery. European journal of pharmaceutical sciences : official journal of the European Federation for Pharmaceutical Sciences. 2013;50(5):623-37.

160. Xie L, Zeng H, Sun J, Qian W. Engineering Microneedles for Therapy and Diagnosis: A Survey. Micromachines. 2020;11(3):271.

161. Rzhevskiy AS, Singh TRR, Donnelly RF, Anissimov YG. Microneedles as the technique of drug delivery enhancement in diverse organs and tissues. Journal of Controlled Release. 2018;270:184-202.

162. Migdadi E, Courtenay A, Tekko I, McCrudden M, Kearney M-C, McAlister E, et al. Hydrogel-forming microneedles enhance transdermal delivery of metformin hydrochloride. Journal of Controlled Release. 2018;285.

163. Lim D-J, Vines J, Park H, Lee S-H. Microneedles: A Versatile Strategy for Transdermal Delivery of Biological Molecules. International Journal of Biological Macromolecules. 2017;110.

164. Ita K. Ceramic Microneedles and Hollow Microneedles for Transdermal Drug Delivery: Two Decades of Research. Journal of Drug Delivery Science and Technology. 2018;44.

165. Roy Biswas G. Hydroxy Propyl Methyl Cellulose: Different Aspects in Drug Delivery. Journal of Pharmacy and Pharmacology. 2016;4:381-5.

166. Zarmpi N, Flanagan T, Meehan L, Mann J, Fotaki N. Biopharmaceutical Understanding of Excipient Variability on Drug Apparent Solubility Based on Drug Physicochemical Properties: Case Study-Hypromellose (HPMC). The AAPS journal. 2020;22:49.

167. Muppalaneni S. Polyvinyl Alcohol in Medicine and Pharmacy: A Perspective. Journal of Developing Drugs. 2013;02.

168. Teodorescu M, Bercea M. Poly(vinylpyrrolidone) – A Versatile Polymer for Biomedical and Beyond Medical Applications. Polymer-Plastics Technology and Engineering. 2015;54:923–43.

169. Guzmán ML, Manzo RH, Olivera ME. Eudragit E100 as a Drug Carrier: The Remarkable Affinity of Phosphate Ester for Dimethylamine. Molecular pharmaceutics. 2012;9(9):2424-33.

170. Saharan P, Bahmani K, Saharan SP. Preparation, Optimization and In vitro Evaluation of Glipizide Nanoparticles Integrated with Eudragit RS-100. Pharm Nanotechnol. 2019;7(1):72-85.

171. Larrañeta E, Moore J, Vicente-Pérez E, Gonzalez Vazquez P, Lutton R, Woolfson A, et al. A Proposed Model Membrane and Test Method for Microneedle Insertion Studies. International journal of pharmaceutics. 2014;472.

172. Donnelly R, Majithiya R, Singh T, Morrow D, Garland M, Demir YK, et al. Design, Optimization and Characterisation of Polymeric Microneedle Arrays Prepared by a Novel Laser-Based Micromoulding Technique. Pharmaceutical research. 2011;28:41-57.

173. Cilurzo F, Minghetti P, Sinico C. Newborn pig skin as model membrane in in vitro drug permeation studies: a technical note. AAPS PharmSciTech. 2007;8(4):E94-E.

174. Lee J, Park J-H, Prausnitz M. Lee, JW, Park, JH and Prausnitz, MR. Dissolving microneedles for transdermal drug delivery. Biomaterials 29: 2113-2124. Biomaterials. 2008;29:2113-24.

175. Ng S-F, Rouse J, Sanderson F, Meidan V, Eccleston G. Validation of a Static Franz Diffusion Cell System for In Vitro Permeation Studies. AAPS PharmSciTech. 2010;11:1432-41.

176. Zsikó S, Csányi, Kovács A, Budai S, Gácsi A, Berkó S. Methods to Evaluate Skin Penetration In Vitro. Scientia Pharmaceutica. 2019;87:19.

177. Salamanca CH, Barrera-Ocampo A, Lasso JC, Camacho N, Yarce CJ. Franz Diffusion Cell Approach for Pre-Formulation Characterisation of Ketoprofen Semi-Solid Dosage Forms. Pharmaceutics. 2018;10(3):148.

178. Todo H. Transdermal Permeation of Drugs in Various Animal Species. Pharmaceutics. 2017;9(3):33.

179. Makvandi P, Kirby M, Hutton A, Shabani M, Yiu C, Baghbantaraghdari Z, et al. Engineering Microneedle Patches for Improved Penetration: Analysis, Skin Models and Factors Afecting Needle Insertion. Nano-Micro Letters. 2021;13.

180. Gupta J, Gill H, Andrews S, Prausnitz M. Kinetics of Skin Resealing After Insertion of Microneedles in Human Subjects. Journal of controlled release : official journal of the Controlled Release Society. 2011;154:148-55.

181. Yuan X-H, Yao C, Oh J-H, Park C-H, Tian Y-D, Han M, et al. Vasoactive intestinal peptide stimulates melanogenesis in B16F10 mouse melanoma cells via CREB/MITF/tyrosinase signaling. Biochemical and Biophysical Research Communications. 2016;477.

182. Lim YJ, Lee EH, Kang TH, Ha SK, Oh MS, Kim SM, et al. Inhibitory effects of arbutin on melanin biosynthesis of alpha-melanocyte stimulating hormone-induced hyperpigmentation in cultured brownish guinea pig skin tissues. Archives of pharmacal research. 2009;32(3):367-73.

183. Chou T-C. Drug Combination Studies and Their Synergy Quantification Using the Chou-Talalay Method. Cancer Research. 2010;70(2):440.

184. Xu W, Ma WW, Zeng HH. Synergistic effect of ethaselen and selenite treatment against A549 human non-small cell lung cancer cells. Asian Pacific journal of cancer prevention : APJCP. 2014;15(17):7129-35.

185. Shin SH, Srivilai J, Ibrahim S, Strasinger C, Hammell D, Hassan H, et al. The Sensitivity of In Vitro Permeation Tests to Chemical Penetration Enhancer Concentration Changes in Fentanyl Transdermal Delivery Systems. AAPS PharmSciTech. 2018;19.

186. Rodgers AM, McCrudden MTC, Vincente-Perez EM, Dubois AV, Ingram RJ, Larrañeta E, et al. Design and characterisation of a dissolving microneedle patch for intradermal vaccination with heat-inactivated bacteria: A proof of concept study. International journal of pharmaceutics. 2018;549(1):87-95.

187. Susanne M, Erdfelder E, Buchner A, Faul F. A short tutorial of GPower. Tutorials in Quantitative Methods for Psychology. 2007;3.

188. Tansathien K, Suriyaaumporn P, Charoenputtakhun P, Ngawhirunpat T, Opanasopit P, Rangsimawong W. Development of Sponge Microspicule Cream as a Transdermal Delivery System for Protein and Growth Factors from Deer Antler Velvet Extract. Biol Pharm Bull. 2019;42(7):1207-15.

189. Zhang M, Ma Y, Wang Z, Han Z, Gao W, Gu Y. Optimizing molecular weight of octyl chitosan as drug carrier for improving tumor therapeutic efficacy. Oncotarget. 2017;8(38):64237-49.

190. Çalış S, Öztürk Atar K, Arslan FB, Eroğlu H, Çapan Y. Chapter 4 - Nanopharmaceuticals as Drug-Delivery Systems: For, Against, and Current Applications. In: Mohapatra SS, Ranjan S, Dasgupta N, Mishra RK, Thomas S, editors. Nanocarriers for Drug Delivery: Elsevier; 2019. p. 133-54.

191. Kalepu S, Nekkanti V. Insoluble drug delivery strategies: review of recent advances and business prospects. Acta Pharmaceutica Sinica B. 2015;5(5):442-53.

192. Patra C, Priya R, Swain DS, Jena G, Panigrahi K, Ghose D. Pharmaceutical significance of Eudragit: A review. Future Journal of Pharmaceutical Sciences. 2017;3.

193. Chantasart D, Tocanitchart P, Wongrakpanich A, Teeranachaideekul V, Junyaprasert V. Fabrication and Evaluation of Eudragit® Polymeric Films for Transdermal Delivery of Piroxicam. Pharmaceutical development and technology. 2017;23:1-27.

194. Donnelly RF, Raj Singh TR, Woolfson AD. Microneedle-based drug delivery systems: microfabrication, drug delivery, and safety. Drug delivery. 2010;17(4):187-207.

195. Makvandi P, Kirkby M, Hutton ARJ, Shabani M, Yiu CKY, Baghbantaraghdari Z, et al. Engineering Microneedle Patches for Improved Penetration: Analysis, Skin Models and Factors Affecting Needle Insertion. Nano-Micro Letters. 2021;13(1):93.

196. Gupta J, Gill HS, Andrews SN, Prausnitz MR. Kinetics of skin resealing after insertion of microneedles in human subjects. Journal of controlled release : official journal of the Controlled Release Society. 2011;154(2):148-55.

197. Grubauer G, Elias PM, Feingold KR. Transepidermal water loss: the signal for recovery of barrier structure and function. Journal of lipid research. 1989;30(3):323-33.

198. Firooz A, Sadr B, Babakoohi S, Sarraf-Yazdy M, Fanian F, Kazerouni-Timsar A, et al. Variation of biophysical parameters of the skin with age, gender, and body region. TheScientificWorldJournal. 2012;2012:386936.

199. Abdlaty R, Fang Q. Skin Erythema Assessment Techniques: Review Article. 2018.

200. Milani M, Sparavigna A. The 24-hour skin hydration and barrier function effects of a hyaluronic 1%, glycerin 5%, and Centella asiatica stem cells extract moisturizing fluid: an intra-subject, randomized, assessor-blinded study. Clin Cosmet Investig Dermatol. 2017;10:311-5.

201. Kalra A, Lowe A. An Overview of Factors Affecting the Skins Youngs Modulus. Journal of Aging Science. 2016;4.

202. Christ C, Brenke R, Sattler G, Siems W, Novak P, Daser A. Improvement in Skin Elasticity in the Treatment of Cellulite and Connective Tissue Weakness by Means of Extracorporeal Pulse Activation Therapy. Aesthetic Surgery Journal. 2008;28(5):538-44.

203. Park AC, Baddiel C, editors. Rheology of stratum corneum-I: A molecular interpretation of the stress-strain curve1972.

204. Marrakchi S, Maibach H. Biophysical parameters of skin: Map of human face, regional, and age-related differences. Contact dermatitis. 2007;57:28-34.

205. Lim Y-J, Lee E, Kang T, Ha SK, Oh M, Kim S, et al. Inhibitory effects of arbutin on melanin biosynthesis of alpha-melanocyte stimulating hormone-induced hyperpigmentation in cultured brownish guinea pig skin tissues. Archives of pharmacal research. 2009;32:367-73.

206. Jo D, Seok J, Kim S, Park W, Baek J, Kim YM, et al. Human skin-depigmenting effects of resveratryl triglycolate, a hybrid compound of resveratrol and glycolic acid. International Journal of Cosmetic Science. 2018;40.

VITA

NAME

Nway Nway Aung

DATE OF BIRTH

23 February 1985

PLACE OF BIRTH

Mandalay, Myanmar

INSTITUTIONS ATTENDED

2021-Present: Doctor of Philosophy, Ph.D. in Pharmaceutical Technology, Faculty of Pharmacy, Silpakorn University, Thailand.
2015: Master of Pharmacy, University of Pharmacy, Mandalay, Myanmar.
2006: Bachelor of Pharmacy, University of Pharmacy, Mandalay, Myanmar.

HOME ADDRESS

Tampawaddy, Chanmyatharzi Township, Mandalay City, Myanmar

PUBLICATION

1. Nway Nway Aung, Yin Yin Myat, Tanasait Ngawhirunpat, Theerasak Rojanarata, Prasopchai Patrojanasophon, Praneet Opanasopit and Boonnada Pamornpathomkul. Evaluation of Thermally Crosslinked Poly(Acrylic Acid-Co-Maleic Acid) (PAMA)/Poly(Vinyl Alcohol) (PVA) Microneedle Arrays, Key Eng. Mater, 819, 2019, 45-50.
2. Nway Nway Aung, Tanasait Ngawhirunpat, Theerasak Rojanarata, Prasopchai Patrojanasophon, Praneet Opanasopit and Boonnada Pamornpathomkul. HPMC/PVP Dissolving Microneedles: a Promising Delivery Platform to Promote Trans-Epidermal Delivery of Alpha-Arbutin for Skin Lightening, AAPS PharmSciTech, 21, 2019, 25.
3. Nway Nway Aung, Tanasait Ngawhirunpat, Theerasak Rojanarata, Prasopchai Patrojanasophon, Boonnada Pamornpathomkul and Praneet Opanasopit. Fabrication, characterization and comparison of α-arbutin loaded dissolving and hydrogel forming microneedles, Int J Pharm, 586, 2020, 119508.
4. Nway Nway Aung, Tanasait Ngawhirunpat, Theerasak Rojanarata, Prasopchai Patrojanasophon, Praneet Opanasopit and Boonnada Pamornpathomkul. Enhancement of transdermal delivery of resveratrol using Eudragit and polyvinyl pyrrolidone-based dissolving microneedle patches, Journal of Drug Delivery Science and Technology, 61, 2021, 102284.